Title

Identification and Characterization of Key Regulatory Factors Mediating Ribosomal Ubiquitylation and Quality Control during Translation

Author

Garshott, Danielle Marie

Publication Date

2021

Peer reviewed|Thesis/dissertation

UNIVERSITY OF CALIFORNIA SAN DIEGO

Identification and Characterization of Key Regulatory Factors Mediating Ribosomal Ubiquitylation and Quality Control during Translation

A dissertation submitted in partial satisfaction of the requirements for the degree Doctor of Philosophy

in

Biology

by

Danielle Marie Garshott

Committee in charge:

Professor Eric Bennett, Chair
Professor Shannon Lauberth
Professor Jens Lykke-Andersen
Professor Eugene Yeo
Professor Brian Zid

2021

The dissertation of Danielle Marie Garshott is approved, and it is acceptable in quality and form for publication on microfilm and electronically.

University of California San Diego

2021

DEDICATION

To my beloved parents John and Denise Garshott, who have guided me through the highs and lows of this journey. Thank you for your invaluable words of advice, constant encouragement, and for teaching me the true meaning of hard work and perseverance.

I love you dearly.

TABLE OF CONTENTS

LIST OF FIGURES

ACKNOWLEDGMENTS

I would like to express my sincerest thanks and heartfelt gratitude to my graduate advisor Dr. Eric J. Bennett, whose unwavering enthusiasm and passion for science continually inspires me to push beyond my boundaries and pursue new challenges. Because of your immense support, unyielding guidance, and patience over these past years, I can finally fulfill my dream of being a scientist. It is an absolute privilege to call you, my mentor. I would also like to thank the other members of my thesis committee: Dr. Shannon Lauberth, Dr. Jens Lykke-Andersen, Dr. Brian Zid and Dr. Gene Yeo. Your insight, advice and encouragement were influential throughout this journey.

Thank you to my esteemed lab mates without whom this would not have been possible. I am forever grateful for your inspiring intellectual contributions, daily encouragement to keep striving for excellence, and your boundless friendships. A special thanks to Nambi, for all the insightful discussions, never-ending wisdom, and patience while teaching me new techniques. You have helped me grow as both a scientist and as a human being. To the one and only superhuman Marilyn, thank you for always being a constant source of understanding and early morning laughter. You are truly wonderful and have helped guide me through so much. To Amit, the man with the most generous soul and contagious laughter, thank you for your continual generosity, enthusiasm to teach me new things, and for always being available to listen. To an amazing friend and colleague Julie, for always being so excited to talk science or just chat, for answering my endless number of questions, and for always being a shoulder to lean on. You inspire me every day to keep pushing forward and strive to be a better person. And finally, to my wonderful friend Adi, for always understanding my situation and being a source of comfort and truth. Thank you for never allowing me to feel alone in this process, and constantly putting a smile on my face. You are one of a kind.

Lastly, thank you to my family for their constant supply of love and reassurance. To my parents whose unconditional love and sacrifices have provided me with the foundation on which to build my dreams. To my siblings Jillian, Dominic and Jordanne, for providing me with endless hours of TikToks and Memes to lift my spirits. And a special thanks to my grandmother Delphine, your spiritual guidance and uplifting words of advice helped me push through the difficult times. I could not have accomplished this without any of you.

Chapter 2, in full, is a reprint of the material as it occurs in eLife, Garshott, D.M.; Sundaramoorthy, E.; Leonard, M.; Bennett, E.J.; eLife Sciences Publications Ltd, 2020. I am the primary author.

Chapter 3, in full, is a reprint of the material as it occurs in Cell Reports, Garshott, D.M.; An, H.; Sundaramoorthy, E.; Leonard, M.; Vicary, A.; Harper, J.W.; Bennett, E.J.; Cell Press, 2021. I am the primary author.

VITA

2006 – 2011	Bachelor of Science in Biochemistry and Minor in Philosophy University of Detroit Mercy
2011 – 2012	Research Technician, Wayne State University
2012 – 2016	Research Assistant/ Lab Manager, Wayne State University
2016 – 2021	Doctor of Philosophy in Biology University of California San Diego

PUBLICATIONS

Garshott DM, An H, Sundaramoorthy E, Leonard M, Vicary A, Harper, JW and Bennett EJ. iRQC, a surveillance pathway for 40S ribosomal quality control during mRNA translation initiation. Cell Reports. 2021 Aug 36;9:109642. PMID: 34469731

Sinha NK, Ordureau A, Best K, Saba JA, Zinshteyn B, Sundaramoorthy E, Fulzele A, **Garshott DM**, Denk T, Thoms M, Paulo JA, Harper JW, Bennett EJ, Beckmann R, Green R. EDF1 coordinates cellular responses to ribosome collisions. Elife. 2020 Aug 3;9:e58828. PMID: 32744497

Garshott DM, Sundaramoorthy E, Leonard M, and Bennett EJ. Distinct regulatory ribosomal ubiquitylation events are reversible and hierarchically organized. Elife. 2020 Feb 3;9:e54023. PMID:32011234

AWARDS

2020	Founding Faculty Award for Graduate Excellence
2020	David V. Goeddel Chancellor's Fellowship
2018	National Science Foundation Graduate Research Fellowship (DGE1650112)
2017	Ray Thomas Edwards Award (for scholarly excellence in graduate studies)
2017	NIH-T32 UCSD Cell and Molecular Genetics Training Program (T32GM007240)

FIELDS OF STUDY

Major Field: Molecular and Cell Biology

ABSTRACT OF THE DISSERTATION

Identification and Characterization of Key Regulatory Factors Mediating Ribosomal Ubiquitylation and Quality Control during Translation

by

Danielle Marie Garshott

Doctor of Philosophy in Biology

University of California San Diego, 2021

Professor Eric J. Bennett, Chair

Protein ubiquitylation plays a critical role in shaping proteome dynamics and responding to proteostasis dysfunction. Activation of the integrated stress response (ISR) or the ribosome-associated quality control (RQC) pathway stimulates regulatory ribosomal ubiquitylation (RRub) on distinct 40S ribosomal proteins, yet the cellular role for these ubiquitylation events remains unclear. We previously demonstrated that conserved monoubiquitylation events are required for downstream RQC events following the translation of poly(A) sequences. We identified the E3 ubiquitin ligase, ZNF598, which is responsible for initiating RQC by catalyzing the ubiquitylation of eS10 and uS10. An additional set of ubiquitylation events on uS5 and uS3 are triggered upon activation of the ISR and appear to function outside of the RQC pathway, however the critical regulators remained unknown.

In this dissertation I establish that RRub events diminish over time following exposure to UV stress, implicating a role for deubiquitylating enzymes (Dubs) within the RQC pathway. I identified the Dubs OTUD3 and USP21 that, when overexpressed, result in read-through of poly(A)-mediated stalls, and directly antagonize ZNF598. USP21 or OTUD3 knockout cell lines revealed that loss of expression for either Dub results in enhanced stalling on poly(A) sequences and prolonged site-specific RRub following UV exposure. Additionally, I establish a hierarchical structure for the ribosome ubiquitin code by demonstrating that eS10 and uS3 ubiquitylation is necessary for subsequent uS10 and uS5 ubiquitylation, respectively, suggesting a specific order of ribosome ubiquitylation events occurs to ensure optimal resolution of RQC nucleating events. These results demonstrate that Dubs can constrain RQC activation and may serve to remove ubiquitin from 40S subunits to allow for subunit recycling.

uS5 and uS3 ubiquitylation events operate outside of the canonical RQC pathway. Here I demonstrate that translation initiation inhibition, either through moderate ISR activation which produces low levels of eIF2α phosphorylation, or overt pharmacological inhibition of translation initiation trigger these site-specific modifications. I identify the E3 ubiquitin ligase RNF10 and the Dub USP10 as the regulators of uS3 and uS5 ubiquitylation. Additionally, I show that prolonged ubiquitylation results in 40S but not 60S ribosomal protein degradation in an autophagy-independent manner. This study identifies and characterizes a discrete ribosome-associated quality control pathway that surveys preinitiation complex status during mRNA translation initiation.

Chapter 1

Introduction

1.1 Protein Homeostasis

Proteins serve as the arbiter of cellular function, regulating highly diverse physiological processes ranging from tissue formation to responding to viral infections. The proteome comprises the entire complement of all expressed proteins encoded by an organism's genome. It is through the construction of elaborate proteomes that cells perform their countless tasks each second. The protein homeostasis (proteostasis) network is comprised of various interconnected signaling pathways that regulate critical cellular functions ranging from protein biogenesis, molecular chaperone assisted protein folding, and protein degradation through the ubiquitin-proteosome or the autophagy pathway (Balch et al., 2008; Taylor et al., 2014). Cells are constantly assaulted with diverse forms of stress which can lead to erroneous translation, improper folding, or unregulated protein accumulation. Maintaining proteostasis within the cell is a challenging process, especially when cells are faced with signals that increase the demand for protein biogenesis or are exposed to extrinsic stressors that challenge protein folding capacities leading to cellular toxicity. In response to increasing levels of misfolded or aggregated proteins the cell also activates a number of cellular stress response pathways which include the integrated stress response (ISR), the heat shock response (HSR) and the mitochondrial and endoplasmic reticulum unfolded protein response ($Mito^{UPR}$, ER^{UPR}) (Taylor et al., 2014). It is critical to the survival and functionality of both cells and tissues that proteostasis balance is continuously maintained.

1.2 Proteostasis dysregulation in human disease

Errors during transcription or mRNA processing can often result in translation of defective or truncated substrates, which can potentially lead to the accumulation of defective nascent protein products (Brandman and Hegde, 2016; Schuller and Green, 2018). Failure to clear these deleterious proteins can have catastrophic consequences for an organism, including proteotoxic stress and a wide range of protein misfolding diseases, like neurodegeneration (Gregersen, 2006; Gregersen et al., 2006). Destabilization of the proteome inevitably escalates over the lifespan of the organism, placing increasing pressure on quality control pathways primarily due to failures in translational machinery and a decline of fail-safe mechanisms (Taylor and Dillin, 2011). Proteotoxic aggregates often arise from translational errors that happen as a result of cellular stress or aging (Vendruscolo, 2012). When proteins fail to properly fold into their tertiary structures, accumulations of these misfolded proteins form and are characteristic of many neurodegenerative diseases, including Parkinson's and Alzheimer's disease (Douglas and Dillin, 2010). The inability to maintain proteins in their functional conformation results in a cell with a heightened proteostasis burden but without the means to clear excess and pathogenic translational products. Protein aggregation studies in *c. elegans* models demonstrated that expression of pathogenic aggregation-prone proteins can further destabilize metastable endogenous proteins like temperature sensitive mutant proteins.(Gidalevitz et al., 2006). Genetic perturbations that increase synthesis error rates or deplete quality control factors have been shown to lead to neurodegeneration in mice (Lee et al., 2006), which further underscores the importance of proteome fidelity mechanisms.

1.3 The role of the ubiquitin-proteosome pathway in protein degradation

Regulating the levels of intercellular proteins is critical to controlling physiological processes. Once thought to be controlled entirely by changes in transcription or translation, protein levels can be tuned via degradation mediated in large part by a small 76 residue regulatory protein, ubiquitin, which is covalently linked to proteins targeted for degradation (Varshavsky, 2005). One of the major proteolytic systems within the cell is the ubiquitin-

proteasome system (UPS) (Hershko et al., 1983). Ubiquitin-dependent proteolysis regulates many biological functions ranging from regulating signal transduction, cellular growth and differentiation, to immune responses and cell death (Pickart, 2004; Varshavsky, 2005). To guard against proteome instability, cells have evolved quality control (QC) mechanisms that oversee protein biogenesis and initiate tightly controlled responses to aberrant protein products or failures within the translation machinery.

The post-translational modification of a substrate by ubiquitin can have numerous effects on protein function, including altering protein localization, nucleating protein-protein interactions, or altering protein abundance through degradation (Hershko and Ciechanover, 1998). These effects are facilitated by the addition of either multiple ubiquitin molecules linked through various lysine linkages to form different polyubiquitin chains, or a single ubiquitin attachment (monoubiquitylation). Ubiquitin conjugation to a lysine residue within a target substrate is catalyzed by three concerted enzymes (Komander and Rape, 2012). E1 ubiquitin activating-enzymes activate ubiquitin by formation of a ubiquitin adenylate utilizing two molecules of ATP. Activated ubiquitin is then transferred, through a thioester bond, to one of several E2 ubiquitin-conjugating enzymes. The ubiquitin-charged E2 is recruited by an E3 ubiquitin ligase to the targeted substrate where it facilitates the transfer of ubiquitin by formation of an isopeptide bond between a lysine residue on the substrate and the carboxy-terminal glycine of ubiquitin (Ciechanover, 2015; Hershko et al., 1983) (Figure 1.1). The downstream impact of protein ubiquitylation is dependent upon the type and degree of the ubiquitin modification. Proteomic studies have argued that monoubiquitylation events are more prevalent in the cell than polyubiquitylation (Kaiser et al., 2011). The formation of polymeric chains results from subsequent ubiquitylation of ubiquitin itself via linkages to the first N-terminal methionine or one of seven internal lysine residues (Lys^{6}, Lys^{11}, Lys^{27}, Lys^{29}, Lys^{33}, Lys^{48}, and Lys^{63}) on the proximal ubiquitin (Akutsu et al., 2016). Canonically, Lys^{48} linked polyubiquitylation targets

proteins to the proteolytic 26S proteasome to be degraded while recycling ubiquitin back into the free cytosolic pool (Hershko and Ciechanover, 1998).

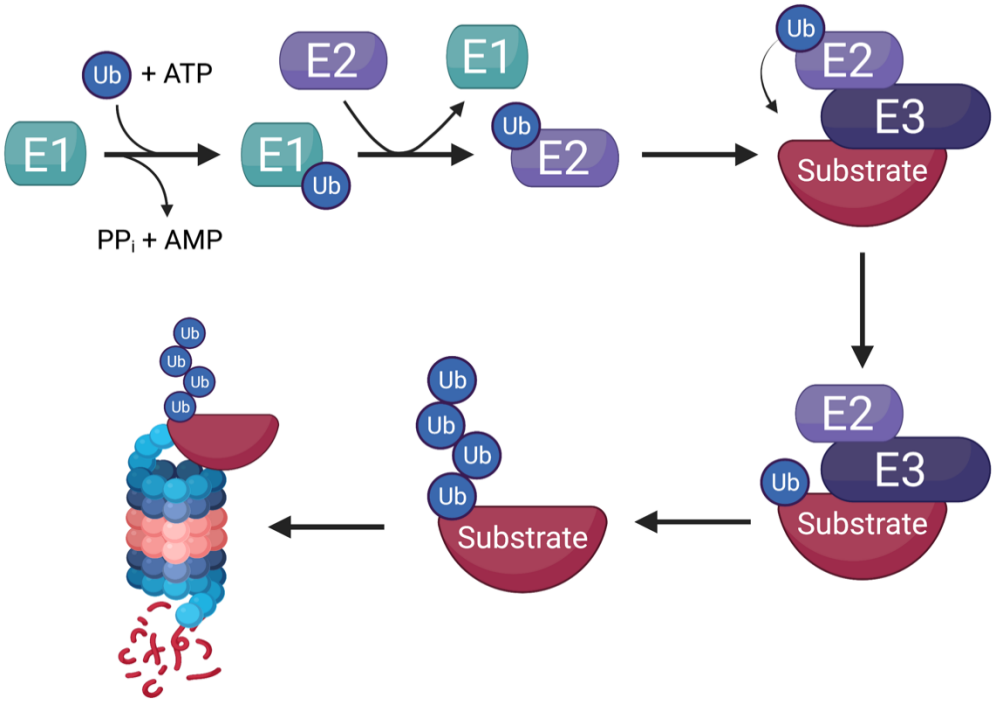

Figure 1.1. The ubiquitylation cascade.
Schematic of the attachment of ubiquitin onto a substrate protein bound for degradation by the 26S proteasome.

1.4 The role of E3 ubiquitin ligases and deubiquitylating enzymes during proteostasis

Ubiquitin-ligases (E3) are a critical component of the ubiquitin cascade due to their strict substrate specificity and versatility. This specificity is imparted by the large number (500-1,000) E3 ligases expressed in mammals. Ubiquitin ligases are broadly composed of two structural classes containing either a HECT (homologous to the E6AP carboxyl terminus)-domain or a RING (really interesting new gene)-finger-domain (Deshaies and Joazeiro, 2009; Nakayama and Nakayama, 2006; Zheng and Shabek, 2017). Distinct from RING-domain E3s HECT-domain ligases catalyze substrate ubiquitylation via an intermediate formation of a ubiquitin

thioester bond on an internal cysteine residue within the HECT domain prior to transferring the ubiquitin to the target substrate (Scheffner et al., 1995). The majority of mammalian E3s contain a RING-domain which utilize cysteine and histidine residues to coordinate zinc ions to bring the activated E2 into close proximity for direct transfer of ubiquitin onto the substrate (Ye and Rape, 2009). The coordination and recruitment of ubiquitin ligases, and preservation of high substrate specificity is crucial for protein ubiquitylation. Failure to recognize and tag misfolded or mislocalized proteins with ubiquitin may result in collapse of critical cellular pathways.

While the modification of a protein with ubiquitin canonically serves to target the protein for degradation, this is by no means always the circumstance. Ubiquitin hydrolases (deubiquitylating enzymes or Dubs) function to remove the distal ubiquitin from proximal ubiquitin, or substrates often antagonizing protein degradation and facilitating the reversal of spurious ubiquitylation events (Heideker and Wertz, 2015; Komander et al., 2009). Humans express roughly 100 Dubs that fall into two distinct superfamilies characterized by their catalytic domains. The cysteine isopeptidase (cysteine-protease) superfamily is comprised of four subclasses: USP (ubiquitin-specific protease), OTU (ovarian tumor), UCH (ubiquitin C-terminal hydrolase) and Machado-Joseph disease domain. This superfamily of Dubs is defined by the active cysteine residue residing within a catalytic diad or triad that form transient covalent enzyme-substrate arrangements (Heideker and Wertz, 2015; Komander, 2010; Komander et al., 2009). The JAMM/MPN+ Dubs are metalloproteases that facilitate ubiquitin hydrolysis through coordination of a zinc and water molecule. Deubiquitylation is mediated both locally and temporally by an ensemble of mechanisms. Association with co-factors, or E2/E3 enzymes, post-translational modifications and integration into larger protein complexes are just a few of the ways Dub activity can be regulated (Heideker and Wertz, 2015).

1.5 Translational regulation

The average HeLa cell has roughly 10^7 ribosomes translating at a speed of about five amino acids per second which results in $3x10^6$ proteins synthesized per minute (Yewdell, 2001).

That speed combined with such a tremendous protein output, it's no surprise that protein synthesis doesn't always go perfectly. It's been suggested that more than 10% of the proteome is degraded immediately after synthesis (Kim et al., 2011). These proteosome targets are nascent polypeptides that due to mistranslation or errors in post-translational processing never acquire their native configuration. Utilizing a monoclonal antibody that recognizes the tryptic remnant of ubiquitylated peptides (K-GG or diGly residue of ubiquitylated proteins), Kim et al. metabolically labeled HCT116 cells with heavy lysine (K8) followed by proteasome inhibition (bortezomib, Btz) either with or without the translational inhibitor cycloheximide (CHX). They showed that inhibition of translation resulted in almost complete loss of all measurable diGly peptides (Kim et al., 2011). To further substantiate the degree to which newly synthesized polypeptides are ubiquitylated, Kim et al. employed SILAC-switch experiments. HCT116 cells were switched from light to heavy labeling followed by continued growth, or treatment with Btz in the presence or absence of CHX. DiGly proteomics data showed an increase incorporation of heavy labeled lysines in cells treated with Btz, in a synthesis dependent manner. Together these findings suggest that the majority of ubiquitylated substrates come from the newly synthesized population of polypeptides.

The synthesis of proteins is an energetically consuming undertaking that involves the precise coordination of many protein factors. Translation is the process by which messenger RNA (mRNA) is decoded into newly synthesized proteins. It is comprised of three phases: initiation, elongation, and termination. Eukaryotic cap-dependent translation initiation begins with scanning of the 5' leader sequence (5'UTR- untranslated region) of a messenger RNA to identify the AUG start codon. This process starts with the formation of the 43S preinitiation complex (PIC) which is comprised of the small 40S ribosomal subunit along with the ternary complex (TC): GTP-bound form of eukaryotic initiation factor 2 (eIF2) and the methionyl initiator transfer RNA (Met-tRNA$_i$). This assembly is stimulated by organization of eukaryotic initiation factors 1, 1A, and 5, and the multi-subunit complex eIF3, which bind directly to the 40S subunit

(Hinnebusch, 2011). Recruitment of the 43S PIC to the 7-methylguanosine capped end of an mRNA is facilitated by the eIF4F complex which includes the cap-binding protein eIF4E, the scaffolding protein eIF4G, the RNA helicase eIF4A, and the poly(A)-binding protein (PABP), thereby forming a 'closed loop' structure (Hinnebusch, 2011). The ATP-dependent RNA helicase eIF4A mediates the unwinding of the transcript while resolving any secondary structures that may have formed, facilitating ribosome scanning along the 5'UTR. During 5'UTR scanning, the 43S PIC moves in the 5'-to-3' direction along the transcript sampling base-by-base to identify the AUG start codon. Upon complementarity with the anticodon of the Met-$tRNA_i$ in the P-site of the 40S subunit, scanning concludes. At this point the GTPase-activating protein eIF5 hydrolyses the GTP bound TC resulting in the formation of the 48S complex. eIF2-GDP and the remaining initiation factors are released from the 48S permitting joining of the 60S subunit thus forming an elongation competent 80S.

The fully formed 80S ribosome can now commence with polypeptide chain synthesis with the initiator methionyl tRNA seated in the ribosomal P-site. Subsequently, cognate and noncognate aminoacyl tRNAs (aa-tRNA) are delivered to the A-site in complex with the elongation factor 1A (eEF1A) and GTP. Upon recognition of the correct codon-anticodon base pairing, conformational changes in the 40S subunit's rRNA to allow for three bases to directly interact with the mRNA-tRNA complex (Kapp and Lorsch, 2004; Ogle et al., 2001). Peptide bond formation proceeds in the ribosomal peptidyl transferase center following the release of the aa-tRNA into the A-site by the GDP bound eEF1A. At this point the formation of the peptidyl-tRNA duplex is in a A/P hybrid state where in the anticodon is located in the A-site of the 40S while the acceptor end is situated in the P-site of the 60S. Additionally, the deacylated tRNA takes on a P/E hybrid state with the anticodon in the 40S P-site and the acceptor end seated in the E-site of the 60S (Green and Noller, 1997). Movement of the tRNA, or translocation, is facilitated by elongation factor 2 (eEF2) and the hydrolysis of GTP, permitting the deacylated tRNA to be seated in the E-site, while the peptidyl tRNA is situated in the P-site. Translocation

will further advance the ribosome three nucleotides in the 3' direction positioning the next codon in the A-site. This sequence of events will continue until one of three stop codons (UAA, UAG, or UGA) enter the A-site, thus initiating termination (Kapp and Lorsch, 2004).

A single class 1 release factor (eRF1) is responsible for decoding all stop codons presented in the ribosomal A-site thus initiating the termination phase which results in hydrolysis of the peptidyl-tRNA and release of the fully formed polypeptide chain. Additionally, a GTPase class 2 release factor (eRF3) is required to stimulate the activity of eRF1, however the mechanism by which this stimulation occurs is still unclear (Kapp and Lorsch, 2004). Furthermore, it has been shown that both the ribosome and eRF1 are necessary for eRF3 GTPase activity, but the presence of a stop codon is not (Frolova et al., 1996). Following peptide release, the GDP-bound eRF3 dissociates, leaving behind eRF1 still bound to the post-termination ribosomal complex (Shoemaker and Green, 2011). The ribosome is now poised for splitting to allow for recycling of the individual subunits back into the translation cycle. Following the release of eRF3, the ATP binding cassette (ABC) protein ABCE1 is recruited to the ribosome. Utilizing ATP hydrolysis and a power stroke upon nucleotide-binding domain closure, ABCE1 splits the ribosome into its individual subunits (Becker et al., 2012). With the close connection between recycling and re-initiation, it has been proposed that initiation factors like eIF3, eIF1, eIF1A and eIF3j can also stimulate ribosome splitting post-termination (Pisarev et al., 2007).

Translation is highly regulated during protein homeostasis stress to both turn down the rate of protein synthesis and activate protein degradation pathways. While regulation of protein synthesis can occur during any stage of the translation cycle, the initiation phase is most often targeted. Stressors such as defects in protein homeostasis, amino acid deprivation, viral infection, and oxidative stress can trigger activation of specialized response mechanisms in attempt to restore cellular homeostasis. The integrated stress response (ISR) is one such pathway that attenuates global translation through translation initiation inhibition through the

reduction of ternary complex concentrations within the cell. As discussed previously, the eukaryotic initiation factor eIF2 is an integral part of the ternary complex. eIF2 is a heterotrimeric complex comprised of an α, β and γ subunit. ISR activating stress signals are sensed by four specific kinases: PERK (PKR-like ER kinase), HRI (Heme-regulated eIF2α kinase), PKR (Double-stranded RNA-dependent protein kinase) and GCN2 (General control non-depressible protein 2) which culminate in the phosphorylation of Ser^{51} on the alpha subunit of eIF2 (Costa-Mattioli and Walter, 2020a; Pakos-Zebrucka et al., 2016b). eIF2α phosphorylation ultimately inhibits TC formation through noncompetitive inhibition of eIF2B. eIF2B is a heterodecamer composed of two copies of five different subunits (α, β, δ, γ, and ε) and serves as the guanine nucleotide exchange factor (GEF) for eIF2. Upon phosphorylation, eIF2α undergoes structural rearrangements that form a hydrophobic patch with increased affinity for eIF2Bε binding(Kashiwagi et al., 2019; Kenner et al., 2019). This interaction blocks the exchange of GDP for GTP resulting in failure to form the 43S PIC thereby reducing overall cap-dependent protein synthesis.

Although eIF2α phosphorylation facilitates the repression of translation for the majority of transcripts, there are some transcripts that are translationally upregulated in response to ISR activation. Transcripts encoding ATF4, CHOP, or GADD34 escape ISR-mediate translational repression by utilizing alternative translation initiation mechanisms including IRES (internal ribosome entry sites)-mediated cap-independent recruitment or re-initiation. One mechanism utilized to repress translation is the placement of upstream open reading frames (uORFs) within the 5'UTRs of transcripts, upstream of the main open reading frame, referred to as the coding sequence (CDS). A single transcript can contain one or more uORFs, of which downstream uORFs can overlap with the CDS. uORFs are translated when the scanning ribosome recognizes a suitable AUG codon, at which point that ribosome has several different fates for decoding the various ORFs. The ribosome can translate the first uORF, followed by dissociation

resulting in an inability to translation the main ORF (CDS). Alternatively, the termination codon in the uORF could be interpreted as premature thus eliciting a nonsense-mediated mRNA decay response (Wittmann et al., 2006). Another possibility is that translation of the uORF proceeds followed by termination, but the 40S remains engaged with the mRNA allowing for it reinitiate at additional downstream uORFs or the main open reading frame (Barbosa et al., 2013). One of the most studied examples of uORFs inhibiting translation of the main coding sequence until induced by stress conditions is GCN4 (or ATF4 in vertebrates) (Mueller and Hinnebusch, 1986). As in the case of ATF4 (activating transcription factor 4), under normal growth conditions, when the level of ternary complex is high, scanning ribosomes on the ATF4 transcript will initiate translation at the first uORF (uORF1) where it will proceed with elongation and synthesis of a short polypeptide before encountering a stop codon. The ribosome will then re-initiate at uORF2. For this mRNA the second upstream open reading frame (uORF2) partially overlaps with the CDS for ATF4, thereby preventing the translation of functional full-length ATF4. Under cellular stress conditions, when eIF2α phosphorylation is high, ribosomes will still initiate translation of uORF1 however due to the lower abundance of TC, ribosomes will scan through uORF2 and have a higher likelihood of reinitiating at the start of the main coding sequence (Bond et al., 2020). Bioinformatic analysis predicts that approximately 35-49% of human transcripts contain uORFs, implicating the role of eIF2α phosphorylation in regulating many cellular functions (Wethmar et al., 2010).

Although the ubiquitin-dependent regulation of misfolded protein degradation is well characterized, how ubiquitin plays a regulatory role during the translation cycle is still unclear. A global quantitative ubiquitin proteomics study revealed that both activation of the unfolded protein response (UPR) and translation inhibition stimulated regulatory ribosomal ubiquitylation on site-specific 40S ribosomal proteins (Higgins et al., 2015). Additionally, Higgins et al. demonstrated that some of these ubiquitylation events were concurrent with the phosphorylation

of eIF2α, in a PERK dependent-manner. These findings suggest a direct role for ubiquitin in mediating translational control during protein homeostasis stress. The question then remains, what is the functional role of these ubiquitylated ribosomal proteins during translation?

1.6 Ribosome-associated quality control pathway

The ribosome is the macromolecular complex tasked with translating mRNAs into functional proteins. When ribosomes stall along an mRNA this can lead to the production of potentially toxic truncated protein products, and it is imperative to the health of the cell that these polypeptides be eliminated. During translation elongation there are a number of situations that can induce ribosome stalling events, including, but not limited to, variability in tRNA levels, decoding of suboptimal codons, strong secondary structures within mRNA coding sequence, premature stop codons, the presence of polyA sequence within the coding sequence, or damage to the mRNA (Brandman and Hegde, 2016). The length of these stalling events can range from transient, in the case of slowly decoded codons, to irreversible blocks, such as truncations within the mRNA. It is the job of a highly conserved ribosome-associated quality control (RQC) pathway to differentiate between these types of pausing events to mitigate the accumulation of potentially toxic, defective translation products. This pathway is responsible for identifying stalled ribosomal complexes and initiating a quality control mechanism that results in degradation of the nascent polypeptide chains, followed by recycling of the ribosomal subunits (Figure 1.2). RQC failure results in the production of aberrant protein products and an eventual accumulation of protein aggregates (Choe et al., 2016).

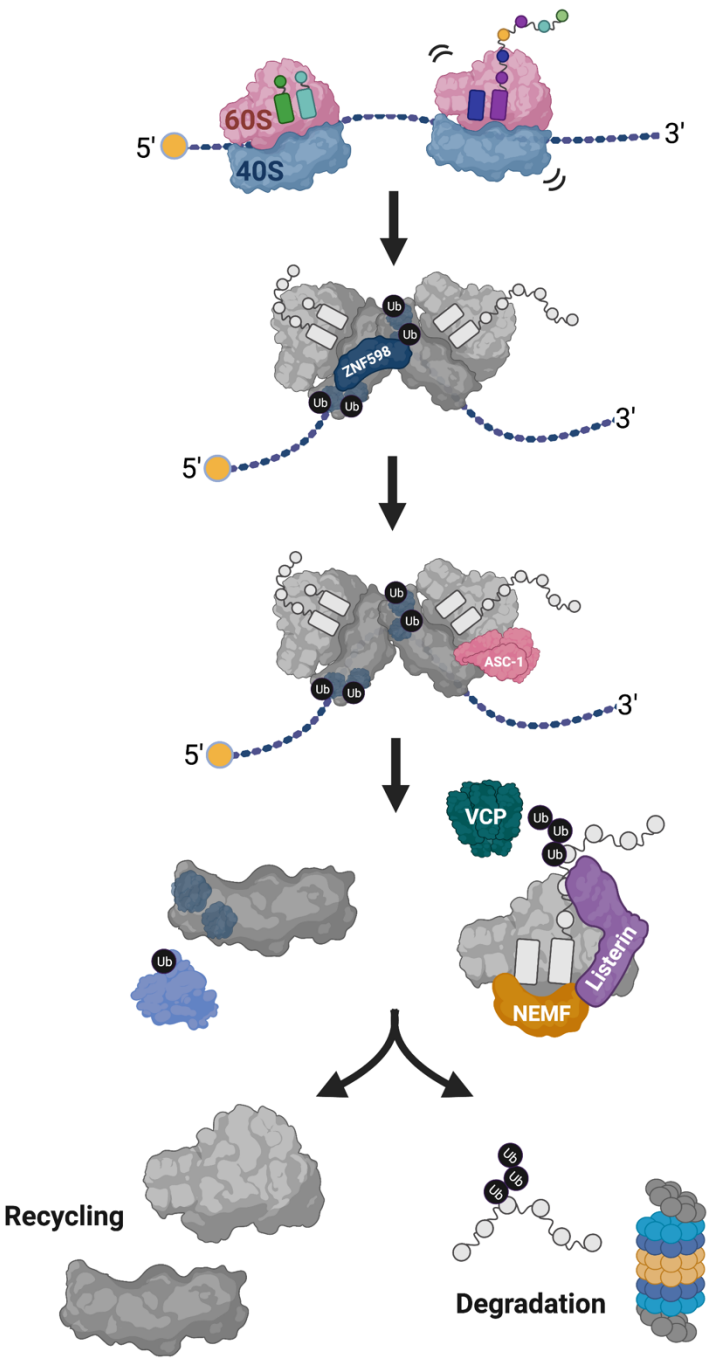

Figure 1.2. Ribosome-associated quality control of collided ribosomes.
A stalled leading ribosome is first recognized following collision with the trailing ribosome. The E3 ligase ZNF598 to recruited to the collision interface to ubiquitylate specific ribosomal proteins on the 40S subunit. Ribosomal splitting factors (ASC-1 complex) then engage the leading ribosome to dissociate the two subunits. Exposure of the peptidyl-tRNA is recognized by the E3 ligase Listerin and RQC factor NEMF which work to ubiquitylated the nascent polypeptide chain, followed by VCP extraction. The polyubiquitylated chain is degraded by the proteasome while the ribosomal subunits are recycled back into the translation cycle.

When an elongating ribosome stalls during translation long enough for a trailing ribosome to collide with it, a unique 40S-40S collision interface is formed (Ikeuchi et al., 2019; Juszkiewicz et al., 2018a). The E3 ubiquitin ligase ZNF598 (Hel2 in yeast) is believed to be the first factor recruited to the collision site where it ubiquitylates site-specific 40S ribosomal proteins eS10 (RPS10) and uS10 (RPS20) in mammals, thus initiating downstream mRNA and protein quality control (Garzia et al., 2017; Ikeuchi et al., 2019; Juszkiewicz et al., 2018a; Juszkiewicz and Hegde, 2017; Matsuo et al., 2017; Sundaramoorthy et al., 2017). Early work from our lab established that translation elongation inhibition stimulates site-specific regulatory ubiquitylation of 40S ribosomal proteins (RRub) (Higgins et al., 2015). Interestingly, these monoubiquitylation events do not target ribosomal proteins for degradation but rather regulate ribosomal function that is important during RQC. Additionally, we showed that the small subunit protein RACK1 along with ZNF598 catalyzed RRub events in response to translation elongation inhibition. RACK1 is required for uS5 (RPS2), uS3 (RPS3), eS10 and uS10 regulatory ubiquitylation, while ZNF598 explicitly facilitated RRub of eS10 and uS10 (Sundaramoorthy et al., 2017).

The RQC pathways have been genetically well-characterized in *S. cerevisiae*, however, much still remains to be elucidated for the mammalian RQC pathway. Following subunit disassociation, the nascent peptidyl-tRNA linked polypeptide will remain associated with the 60S, thereby exposing the P-site localized tRNA at its interface. The E3 ligase Ltn1 (Listerin in mammals) is recruited to the large subunit with Rqc2 (NEMF), a co-factor that stabilizes Ltn1 and precludes ribosomal subunit re-association (Shao et al., 2013). Ltn1 catalyzes ubiquitylation of the nascent chain at the polypeptide exit tunnel. Extraction of the ubiquitylated nascent chain and delivery to the proteasome for degradation is facilitated by the AAA+ ATPase cdc48 (VCP) (Brandman et al., 2012; Verma et al., 2013). Release of the ribosomal subunits results in recycling back into the translation cycle. Additionally, the mRNA can then be degraded by both

the exosome complex and Xrn1 to prevent further rounds of aberrant translation (Shoemaker and Green, 2012). We know that RRub is pervasive and highly conserved, the question remains as to how RRub events are dynamically regulated, or the mechanism by which RRub is needed for downstream RQC events.

To identify additional effector proteins associated with ZNF598, quantitative proteomics studies utilizing sucrose gradient and translation elongation inhibition identified EDF1 and GIGYF2 to be selectively recruited to collided ribosomes (Juszkiewicz et al., 2020a; Sinha et al., 2020). While the RACK1 dependent recruitment of EDF1 to the collision interface proved to be ZNF598-independent, it does facilitate the recruitment of the translational repression complex, GIGYF2 and 4EHP (eIF4E2). 4EHP will out compete eIF4E 5'-cap binding and thus inhibit 43S recruitment. These results suggest that defective mRNAs that result in continuous ribosome collisions (increased ribosome density) will activate a negative-feedback loop through EDF1 to selectively inhibit further translation of these mRNAs (Juszkiewicz et al., 2020a; Sinha et al., 2020). The question then is when does ZNF598 ubiquitylation come into play? Juszkiewicz et al. suggest that ZNF598 ubiquitylates its target proteins only when the collisions become pathological. If a collision occurs due to a physiological reaction, such as pausing due to a rare codon, once elongation resumes repression of initiation by 4EHP is relieved. However, in the case of a perpetual response, like persistent stalling on an internal poly(A)-sequence, ZNF598 will ubiquitylate the ribosome thus recruiting the ASC-1 complex to disassociate the leading stalled ribosome (Juszkiewicz et al., 2020a).

Genetic studies in yeast demonstrated how ribosome splitting ensued through coordination of Dom34 (Pelota in mammals), Hbs1 (HBS1L) and the ATPase Rli1 (ABCE1) (Shoemaker et al., 2010) following a stalling event at or near the 3'-end of mRNAs. Hbs1, a GTP hydrolase, catalyzes the transfer of Dom34 into the ribosome A site. Dom34 subsequently recruits Rli1 to coordinate the separation of the 40S and 60S subunits. Unlike stalling events that take place at or near the 3'-end of a transcript, internal stalls require the ASC-1 complex to

disassemble the leading stalled ribosome. The ASC-1 complex (ASCC) is made up of four proteins: the ATP-dependent helicase ASCC3 (Slh1 in yeast), ASCC2 (related to Cue3 in yeast), ASC-1 (related to Rqt4 in yeast) and ASCC1 (no yeast homology) (Juszkiewicz et al., 2020b). Although the mechanism remains to be elucidated, ASCC disassembles the lead ribosome thereby releasing a peptidyl-tRNA bound 60S subunit to be targeted by the RQC (Juszkiewicz et al., 2020b; Matsuo et al., 2020). While ZNF598-mediated ubiquitylation is required for the clearance of stalled ribosomes, the exact role that ubiquitin plays remain unclear. While ubiquitin was first thought to be the recruiting mark for ASCC engagement, subsequent studies demonstrated that the ASCC complex can be detected in polysome-containing sucrose gradient fractions in ZNF598 knockout cells. Additionally, other ubiquitylated ribosomal proteins are also unlikely involved as ASCC was found to be functional only in the presence of eS10 and uS10 ubiquitylation (Juszkiewicz et al., 2020b). This begs the questions: What is the ubiquitin doing, and what role does it play in downstream recruitment of splitting factors? Are these events reversible? And what role do other ubiquitylated ribosomal proteins play in the canonical RQC pathway?

In chapter 2 I will address the questions regarding the cellular role and fate of ubiquitylated ribosomal proteins. I will demonstrate that a ubiquitin code exists on ribosomes, with the ubiquitylation of uS10 and uS5 being dependent upon eS10 and uS3 ubiquitylation, respectively. Additionally, I will show using a dual-fluorescent optical RQC reporter that two deubiquitylating enzymes, USP21 and OTUD3, are responsible for antagonizing ZNF598-mediated ubiquitylation of eS10 and uS10 and can thus limit RQC activation. In chapter 3 I will begin to tackle the question regarding the role of additional ribosomal ubiquitylation sites on uS3 and uS5. I will demonstrate that uS3 and uS5 ubiquitylation is mediated by the E3 ligase RNF10 in response to translation initiation inhibition and activation of the integrated stress response. I will also describe studies that demonstrate that enhanced uS5 and uS3 ubiquitylation, be it

through overexpression of the ligase or loss of the Dub USP10, results in degradation of 40S ribosomal subunits to regulate translation activity and capacity.

Chapter 2

Distinct regulatory ribosomal ubiquitylation events are reversible and hierarchically organized

2.1 Abstract

Activation of the integrated stress response (ISR) or the ribosome-associated quality control (RQC) pathway stimulates regulatory ribosomal ubiquitylation (RRub) on distinct 40S ribosomal proteins, yet the cellular role and fate of ubiquitylated proteins remain unclear. We demonstrate that uS10 and uS5 ubiquitylation are dependent upon eS10 or uS3 ubiquitylation, respectively, suggesting that a hierarchical relationship exists among RRub events establishing a ubiquitin code on ribosomes. We show that stress dependent RRub events diminish after initial stimuli and that RRub loss is the result of demodification by deubiquitylating enzymes rather than protein degradation. Utilizing an optical RQC reporter we identify OTUD3 and USP21 as deubiquitylating enzymes that antagonize ZNF598-mediated 40S ubiquitylation and can limit RQC activation. Critically, cells lacking USP21 or OTUD3 have altered RQC activity and delayed eS10 deubiquitylation indicating a functional role for deubiquitylating enzymes within the RQC pathway.

2.2 Introduction

The proteome must continuously adapt to changing environmental conditions and exposure to extrinsic proteotoxic stressors that challenge cellular, tissue, and organismal health. A prominent source of proteotoxic stress arises during translation where transcriptional or mRNA processing errors can result in the translation of defective or truncated proteins and lead to the accumulation of toxic nascent protein products (Brandman and Hegde, 2016; Schuller and Green, 2018). Failure to remove these deleterious proteins can lead to aggregation and

contribute to human pathologies including a wide range of neurodegenerative disorders (Gestwicki and Garza, 2012). A variety of cellular quality control and stress response pathways have evolved to guard against the accumulation of these aberrant nascent polypeptides and maintain cellular homeostasis (Dubnikov et al., 2017; Lykke-Andersen and Bennett, 2014; Sontag et al., 2017). One prominent example is the integrated stress response (ISR) which is activated by a variety of protein homeostasis stressors. ISR activation results in rapid global protein synthesis attenuation while also stimulating the translation of critical stress response factors, including protein chaperones and ubiquitin ligases, that assist in rebalancing homeostasis (Guan et al., 2017; Pakos-Zebrucka et al., 2016a). Quality control pathways safeguard against the accumulation of potentially toxic misfolded or otherwise aberrant proteins. The ribosome-associated quality control (RQC) pathway is one such quality control system that identifies elongating ribosomal complexes whose progression is halted due to a defect in the translating mRNA or emerging nascent chain (Brandman and Hegde, 2016). After the initial recognition event, RQC pathway components catalyze the degradation of both the mRNA and nascent polypeptide, followed by ribosome subunit recycling (Ikeuchi et al., 2018). Defects within the RQC pathway result in the production of aberrant protein products and an eventual accumulation of protein aggregates (Choe et al., 2016; Defenouillere et al., 2016; Yonashiro et al., 2016).

Protein ubiquitylation plays a key role during these stress response and quality control pathways to facilitate the degradation of misfolded or damaged proteins (Bengtson and Joazeiro, 2010; Brandman et al., 2012; Joazeiro, 2017, 2019; Pilla et al., 2017). Monoubiquitylation, which typically does not target proteins for degradation, of distinct ribosomal proteins is also stimulated in response to ISR activation and conditions that stimulate RQC suggesting that ubiquitylation regulates these pathways beyond protein degradation (Garzia et al., 2017; Higgins et al., 2015; Ikeuchi et al., 2019; Juszkiewicz et al., 2018a; Matsuo et al., 2017; Simms et al., 2017; Sugiyama et al., 2019; Sundaramoorthy et al., 2017). Studies in both

S. cerevisiae and mammalian systems have identified a list of RQC factors and have delineated a series of events that occur when ribosome progression is slowed enough to initiate a QC response (Joazeiro, 2019). Regulatory ribosomal ubiquitylation (RRub) has emerged as a conserved critical initiating signal during RQC events (Ikeuchi et al., 2019; Juszkiewicz and Hegde, 2017; Matsuo et al., 2017; Simms et al., 2017; Sundaramoorthy et al., 2017). In mammals, the ubiquitin ligase ZNF598 catalyzes site-specific ubiquitylation of eS10 (RPS10) and uS10 (RPS20) to resolve ribosomes that have stalled during decoding of polyA sequences (Juszkiewicz and Hegde, 2017; Sundaramoorthy et al., 2017). Ablation of ZNF598 or the ribosomal protein RACK1, as well as conserved ubiquitylated target lysines in uS10 or eS10 results in RQC failure and subsequent readthrough of stall inducing sequences (Juszkiewicz and Hegde, 2017; Sundaramoorthy et al., 2017). Similar, yet distinct ubiquitylation events regulate RQC in yeast (Matsuo et al., 2017). Current models suggest that ribosome collisions are the key initiation signal which recruits critical ubiquitin ligases to facilitate RRub allowing for subsequent nascent chain ubiquitylation, mRNA degradation, and ribosome recycling (Ikeuchi et al., 2019; Juszkiewicz et al., 2018a; Simms et al., 2017). The observation that both uS10 and eS10 ubiquitylation are required for mammalian RQC suggest a potential structured order of ubiquitylation events may be needed to specifically mark collided ribosomes. While it is clear that RRub is required for downstream RQC events, the precise mechanistic role the 40S ubiquitylation plays during RQC and the consequence of ubiquitylation on target ribosomal proteins remain open questions.

Activation of the integrated stress response (ISR) in mammalian cells triggers an additional set of RRub events on uS3 (RPS3) and uS5 (RPS2) that do not require ZNF598 and do not function within the RQC pathway and whose function remains uncharacterized (Higgins et al., 2015). The presence of two separate ubiquitylation events on neighboring ribosomal proteins again suggests a possible hierarchical relationship among distinct RRub events that likely impart separate functions. Studies in mammalian cells have demonstrated that the extent

of ISR-stimulated uS3 and uS5 monoubiquitylation diminished upon removal of ISR agonists (Higgins et al., 2015). This observation suggests that either RRub events are reversed by the action of deubiquitylating enzymes (Dubs) or that ubiquitin-modified ribosomal proteins are degraded after RQC events.

Here, we establish that regulatory ribosomal ubiquitylation events are reversible and mediated by deubiquitylating enzymes following activation of the ISR or RQC pathways. We utilized an overexpression screen to identify two Dubs, USP21 and OTUD3, whose expression stimulates readthrough of poly(A)-mediated ribosome stalls. We demonstrate that USP21 and OTUD3 can directly antagonize ZNF598-mediated eS10 and uS10 ubiquitylation events. Further, we show that USP21 and OTUD3 expression results in augmented removal of ubiquitin from eS10 and uS10 following UV-induced RQC. USP21 expression also represses ISR-stimulated uS3 and uS5 ubiquitylation. Importantly, cells lacking USP21 or OTUD3 display reduced levels of poly(A)-mediated stall readthrough and a delay in eS10 demodification following UV-induced RQC activation. Expression of OTUD3 results in enhanced stall readthrough compared to knock-in cell lines engineered to lack either eS10 or uS10 RRub sites indicating that combinatorial ribosomal ubiquitylation is required for optimal RQC function. Interestingly, we demonstrate that uS10 ubiquitylation is dependent upon eS10 ubiquitylation and that uS5 ubiquitylation requires uS3 ubiquitylation further suggesting a hierarchical relationship upon RRub events. Taken together, our results establish that RRub events are reversible by deubiquitylating enzymes and that RRub represents a combinational post-translational code that imparts distinct functional outcomes on ribosomes.

2.3 Results

2.3.1 Regulatory ribosomal ubiquitylation is reversible

Previous studies demonstrated that the integrated stress response (ISR)-stimulated regulatory ubiquitylation of uS5 (RPS2) and uS3 (RPS3) is diminished upon cessation of the

ISR (Higgins et al., 2015). The reduced levels of ubiquitylated uS5 or uS3 after ISR stimulation could be the result of demodification by a deubiquitylating enzyme (Dub) or turnover of ribosomal proteins. We also reasoned that the ZNF598-catalyzed ubiquitylation of uS10 (RPS20) and eS10 (RPS10), a critical initiating signal within the ribosome associated quality control (RQC) pathway, may also be reversible. To examine the reversibility of RRub events, HCT116 cells were treated with the translation elongation inhibitor anisomycin (ANS) to induce both ribosome stalling, as well as inhibit global protein synthesis (Juszkiewicz et al., 2018a). This allowed us to simultaneously observe the timing of RRub demodification relative to total protein turnover in the absence of new protein synthesis. Consistent with previous studies, ANS induced ubiquitylation of both eS10 and uS10 (Figure 2.1A) (Juszkiewicz et al., 2018a; Matsuo et al., 2017). While eS10 ubiquitylation diminished and uS10 ubiquitylation persisted over time, there was no discernable reduction in the relative amount of the unmodified form of each protein (Figure 2.1A,B). Further no accumulation of unmodified or ubiquitylated eS10 or uS10 was observed in combined treatment of proteasome inhibitors and ANS over 12 hours indicating that ribosomal proteins are not rapidly degraded when ribosome stalling is stimulated. To address whether deubiquitylation is observed with uS5 and uS3 RRub events, we transiently exposed HCT116 cells with the ISR agonist dithiotheritol (DTT) alone or in combination with the protein synthesis inhibitor cycloheximide (CHX) followed by DTT washout with and without cycloheximide. DTT stimulated uS5 and uS3 ubiquitylation which subsequently diminished to pre-treatment levels over time (Figure 2.1C). Further, the relative amount of the unmodified protein remained stable despite global protein synthesis attenuation (Figure 2.1C,D). The varying kinetics of demodification observed with CHX treatment as compared to DTT alone correlates with heightened ISR activation and prolonged phosphorylation of eIF2α which results in sustained uS3 and uS5 ubiquitylation. Together these results suggest that the loss in the amount of ubiquitylated ribosomal proteins likely results from demodification by deubiquitylating enzymes rather than protein turnover.

To further examine the reversibility and timing of distinct RRub events, we utilized UV-induced ISR activation which stimulates uS5, uS3, eS10 and uS10 regulatory ubiquitylation (Elia et al., 2015; Higgins et al., 2015). We exposed 293T cells to UV and allowed cells to recover for increasing periods of time. All observed RRub events diminished over time further indicating the RRub events are reversible (Figure 2.1E,F). Interestingly, eS10 and uS10 ubiquitylation preceded uS5 and uS3 ubiquitylation after UV exposure (Figure 2.1E,F). Consistent with previous studies demonstrating that ISR-stimulated uS5 and uS3 RRub events require eIF2α phosphorylation, uS5 and uS3 ubiquitylation occurred coincidently with eIF2α phosphorylation (Higgins et al., 2015). This timing offset between RRub events and the demonstration that uS10 and eS10 ubiquitylation is catalyzed by ZNF598 whereas uS5 and uS3 ubiquitylation does not require ZNF598 suggests that uS5 and uS3 RRub events are functionally distinct from the more immediate eS10 and uS10 ubiquitylation that likely occur as a direct result of UV-induced ribosomal stalls.

2.3.2 Distinct sets of RRub events are hierarchically organized

To investigate the importance of individual RRub events, we generated point mutant knock-in HCT116 cell lines in which the endogenous eS10, uS10, uS3 or uS5 loci were modified by CRISPR/Cas9 approaches to replace previously identified ubiquitylated lysine residues with arginine. We first examined if mutating RRub lysine residues resulted in altered protein stability. We observed no appreciable change in total protein abundance in the eS10 K138R/K139R knock-in (eS10-KI) and uS10 K4R/K8R knock-in (uS10-KI) cells following ANS treatment (Figure 2.2A,B and 2.8A,B). Similarly the inability to ubiquitylate uS5 K54R/K58R (uS5-KI) and uS3 K214R (uS3-KI) did not change the steady-state abundance or the turnover of uS5 or uS3 (Figure 2.2C,D and 2.8C,D). Interestingly in the course of this experiment and validation of these cell lines we noticed a hierarchal relationship among the ubiquitylation events (Figure 2.8E,F). As expected, eS10-KI cell lines completely lack ANS-induced eS10 ubiquitylation.

However, loss of eS10 ubiquitylation substantially reduces uS10 ubiquitylation (Figure 2.2A and 2.8F) as compared to control cell lines. The inability to ubiquitylate eS10 had a negligible impact on the levels of UV-induced uS5 and uS3 ubiquitylation (Figure 2.8F). In contrast, uS10-KI cells maintained their ability to ubiquitylate eS10, uS5, and uS3 despite the expected loss of uS10 ubiquitylation (Figure 2.2B and 2.8E). These results indicate that eS10 ubiquitylation may be required for optimal uS10 ubiquitylation upon induction of RQC events. Similar to the hierarchy of eS10 and uS10, the lack of DTT-induced uS3 ubiquitylation in the uS3-KI cells results in complete ablation of uS5 modification while loss of uS5 ubiquitylation did not effect uS3 DTT-stimulated RRub (Figure 2.2C,D). Combined, these results suggest that hierarchical relationships exist within distinct classes of RRub events and imply a specific order of ubiquitylation events.

2.3.3 Identification of deubiquitylating enzymes that antagonize eS10 and uS10 regulatory ubiquitylation

Our results implicate the direct involvement of deubiquitylating enzymes in regulating RRub and RQC function. To identify and characterize deubiquitylating enzymes (Dubs) that operate within the RQC pathway, we utilized a previously established dual-fluorescence RQC reporter assay in which a stall-inducing poly(A) sequence placed between GFP and cherry fluorescent protein (ChFP) coding sequences results in the repression of downstream ChFP fluorescence as compared to GFP, indicative of an RQC event initiating upon translation of the poly(A) sequence. (Juszkiewicz and Hegde, 2017; Sundaramoorthy et al., 2017). Previous studies demonstrated that loss of ZNF598 function and the resulting decrease in eS10 and uS10 ubiquitylation results in readthrough of poly(A) sequences and a subsequent increase in the ChFP:GFP ratio of the stall reporter (Juszkiewicz and Hegde, 2017; Sundaramoorthy et al., 2017). Overexpression of a deubiquitylating enzyme that mediates deubiquitylation of eS10 and uS10 RRub events would phenocopy ZNF598 loss-of-function and enhance the amount of poly(A) readthrough. Based on this rationale, a panel of 60 human Dub expression plasmids

were individually co-transfected with the poly(A) stall reporter plasmid into 293T cells and the corresponding ChFP:GFP ratio was measured by flow cytometry. Immunoblotting confirmed the expression of 58 Dubs albeit to varying expression levels (Figure 2.9). A Z-score analysis of the ChFP:GFP ratio for the stall reporter identified six candidate Dubs whose expression resulted in the largest enhancement of poly(A) readthrough above the population mean (Figure 2.3A). We validated that expression of the six candidate Dubs resulted in a reproducible enhancement of poly(A)-stall readthrough and a subsequent increase in ChFP:GFP values using the stall-reporter assay (Figure 2.3B). To directly validate that the resulting increase in the ChFP:GFP ratio was specific to the poly(A) reporter, each candidate Dub was expressed with a control plasmid lacking the internal poly(A) sequence (Figure 2.3B). OTUB2, OTUD3, USP10 and UCHL1 expression did not alter the ChFP:GFP ratio of the control reporter while OTUD1 and USP21 only modestly elevated the ChFP:GFP ratio indicating that the identified Dubs specifically alter the ability of ribosomes to progress through a poly(A)-induced ribosomal stall (Figure 2.3B).

2.3.4 Overexpression of candidate RQC-Dubs results in poly(A) stall-sequence readthrough in an activity-dependent manner

To examine whether the overexpression-induced increase in poly(A)-mediated stall readthrough was dependent on the catalytic activity of each of the identified Dubs, catalytically inactive versions of each Dub were generated by site-directed mutagenesis to convert the critical catalytic cysteine residue to serine. Each Dub and the respective catalytically inactive mutant (CS) were co-expressed with the poly(A)-stall reporter (Figure 2.3C). Expression of OTUB2 and OTUD1 inactive mutants resulted in an equivalent degree of poly(A)-stall readthrough as compared to the respective wild type enzymes (Figure 2.3C). Additionally, expression of inactive UCHL1 resulted in enhanced readthrough of the poly(A)-sequence compared to wild type UCHL1. This result suggests that the observed increase in ChFP fluorescence does not require the catalytic activity of OTUB2 or OTUD1. In contrast, expression

of the inactive mutants for the deubiquitylating enzymes USP21, OTUD3, and USP10 resulted in a substantial reduction of the ChFP:GFP ratios compared to wild type versions. Expression of inactive OTUD3 or USP21 resulted in elevated stall readthrough compared to control transfections indicating a possible alternative role for OTUD3 and USP21 within the RQC pathway that is ZNF598 independent. Together, these results indicate that USP21, OTUD3, and USP10 expression results in elevated poly(A)-mediated stall readthrough in an activity-dependent manner.

2.3.5 USP21 and OTUD3 antagonize ZNF598-mediated RRub events

Having demonstrated that exogenous expression of USP21, OTUD3, and USP10 enhanced poly(A) stall-induced readthrough, we wanted to examine the ability of the Dubs to directly antagonize ZNF598-mediated translational stalling of the poly(A) reporter. As expected, exogenous expression of wild type ZNF598 resulted in decreased ChFP:GFP ratios as compared to control transfections (Figure 2.3D). Next, the poly(A) reporter and candidate Dubs were expressed along with exogenous ZNF598. Both USP21 and OTUD3, when co-expressed with ZNF598, resulted in a greater than 2.5 fold increase in the ChFP:GFP poly(A) reporter ratio relative to what was observed when ZNF598 was expressed in isolation (Figure 2.3D). Antagonism with ZNF598 was not observed for USP10 which suggests its role within the RQC operates independently of ZNF598. Combined expression of OTUD3 and USP21 did not further enhance poly(A)-mediated stall readthrough events or result in enhanced antagonism of ZNF598 (Figure 2.10A). These results are consistent with the hypothesis that USP21 and OTUD3 directly antagonize ZNF598-mediated RRub events. Immunoblot analysis revealed that cells solely overexpressing ZNF598 displayed a 5-fold increase in the abundance of ubiquitylated eS10 compared to untransfected cells (Figure 2.3E). Exogenous expression of USP21 substantially reduced the ZNF598-stimulated eS10 and uS10 ubiquitylation in an activity-dependent manner (Figure 2.3E). The same result was observed upon expression of OTUD3 and ZNF598 (Figure 2.3E). These results demonstrate the ability of USP21 and OTUD3

to remove ubiquitin from eS10 and uS10 following ZNF598-mediated RRub events. Because USP21 and OTUD3 were the only Dubs to show activity dependent antagonism of ZNF598 in our stall readthrough assay, these Dubs were selected for subsequent analyses.

To further examine the antagonism between ZNF598 and OTUD3 and USP21, parental HCT116 cells and ZNF598 knock-out (ZNF598-KO) cells were transfected with either USP21 or OTUD3 expressing plasmids and the poly(A) stall-inducing reporter. We reasoned that expression of these Dubs in the absence of ZNF598 would not impact the amount of poly(A)-stall readthrough beyond that observed with loss of ZNF598 expression. As expected, expression of either Dub along with the poly(A)-reporter in parental HCT116 cells markedly increased the ChFP:GFP ratio of the stall reporter (Figure 2.4A,B). ZNF598-KO cells displayed the expected elevated ChFP:GFP ratio of the stall reporter which was modestly enhanced upon further expression of either Dub (Figure 2.4A,B). This modest enhancement was also observed upon expression of either the wild type or inactive versions of other Dubs, OTUB2, OTUD1, and UCHL1 in the ZNF598-KO cell line suggesting that the increased readthrough is possibly non-specific and does not require Dub activity (Figure 2.10B). However, the observation that USP21 or OTUD3 expression modestly augments readthrough of poly(A) sequences in cells lacking ZNF598 suggests that USP21 and OTUD3 may function within the RQC in a ZNF598 independent manner while also directly antagonizing ZNF598 ribosomal ubiquitylation.

2.3.6 USP21 and OTUD3 deubiquitylate ZNF598 substrates eS10 and uS10

To investigate the role of individual RRub events during RQC, we utilized the uS10-KI and eS10-KI HCT116 cell lines to examine if the enhanced readthrough of poly(A) stall-inducing sequences observed upon USP21 or OTUD3 overexpression required uS10 or eS10 ubiquitylation. Consistent with our previous results, eS10-KI and uS10-KI cell lines allowed for enhanced readthrough of poly(A)-mediated stall events using our stall reporter FACS assay whereas uS3-KI and uS5-KI cell lines did not appreciably alter reporter levels compared to parental cells (Figure 2.8G) (Sundaramoorthy et al., 2017). We expressed OTUD3 or USP21 in

uS10 or eS10 knock-in cell lines along with the poly(A) stall reporter. USP21 or OTUD3 overexpression in either eS10-KI or uS10-KI cells resulted in a further enhancement of the ChFP:GFP ratio above the respective transfection controls (Figure 2.4C,D). This enhancement was largely activity-dependent as expression of inactive OTUD3 reduced the extent of readthrough compared to wild type in both eS10 and uS10 knock-in cell lines (Figure 2.4D). Expression of inactive USP21 resulted in reduced readthrough compared to wild type in uS10-KI cells but not eS10-KI cells (Figure 2.4C). These results indicate that OTUD3 and USP21 can demodify both uS10 and eS10, consistent with our immunoblotting data (Figure 2.3E). Further, these results indicate that the combined loss of uS10 and eS10 RRub events results in a stronger RQC defect than loss of either uS10 or eS10 ubiquitylation events alone.

To validate the poly(A)-reporter results, we immunoblotted cell lysates in which we expressed either wild type or inactive USP21 or OTUD3 in parental or eS10-KI or uS10-KI cell lines to visualize eS10 and uS10 ubiquitylation. As expected, ZNF598 expression stimulated eS10 and uS10 ubiquitylation in parental HCT116 cells (Figure 2.4E). ZNF598 expression in uS10-KI cells failed to induce uS10 ubiquitylation without impacting the ability of ZNF598 to ubiquitylate eS10. Conversely, ZNF598 expression failed to ubiquitylate eS10 in eS10-KI cells, and uS10 ubiquitylation was substantially reduced compared to ZNF598 expression in parental cells. This is consistent with a model in which eS10 ubiquitylation is needed prior to uS10 ubiquitylation. While expression of wild type USP21 or OTUD3 reduced the abundance of both monoubiquitylated eS10 and uS10 in parental HCT116 cells, expression of the inactive variants restored ubiquitylation to steady-state levels (Figure 2.4E). Expression of either Dub in the eS10-KI cell line could further demodify the small amount of uS10 ubiquitylation observed upon ZNF598 expression (Figure 2.4E). Similarly, USP21 and OTUD3 antagonized the ZNF598-dependent eS10 ubiquitylation in uS10-KI cells in an activity dependent manner. Taken together, these results indicate that USP21 or OTUD3 can deubiquitylate both eS10 and uS10, resulting in enhanced readthrough of poly(A)-mediated stall events. Further, these results

demonstrate that the combined ubiquitylation of eS10 and uS10 is required for optimal resolution of RQC events.

2.3.7 The abundance of ZNF598 in relation to USP21 or OTUD3 governs RQC events

Examination of quantitative proteomic datasets from human cell lines revealed that ZNF598 protein levels are 19-fold in excess of OTUD3 while USP21 levels were undetectable indicating that ZNF598 protein levels are in vast excess of either RRub Dub at steady state (Itzhak et al., 2016). Given the relative excess of ZNF598 compared to its antagonizing Dubs, we set out to examine how varying the levels of the Dubs relative to ZNF598 would impact RQC events. We transfected increasing amounts of a ZNF598 expressing plasmid in ZNF598-KO cell lines and examined poly(A)-mediated stall readthrough events using the stall reporter assay. Expression of the poly(A)-reporter with increasing concentrations of exogenous ZNF598 in isolation did not result in a dose-dependent decrease in the ChFP:GFP ratio suggesting that ZNF598 expression at the lowest levels tested were sufficient to fully restore RQC function and that elevated ZNF598 levels do not further enhance ribosomal stall resolution (Figure 2.4F,G and 2.10C,D). We then varied the relative ZNF598 expression levels compared to either USP21 or OTUD3 and examined the impact on the ChFP:GFP ratio of the stall reporter. When equal amounts of USP21 or OTUD3 and ZNF598 expression plasmids were transfected, a substantial increase in the ChFP:GFP ratio was observed as compared to ZNF598 expressed alone which further verified the direct antagonism observed previously (Figure 2.4F,G and 2.10C,D). The reporter ChFP:GFP ratio declined as ZNF598 plasmid transfections were doubled and tripled with respect to USP21 or OTUD3 plasmid DNA (Figure 2.4F,G and 2.10C,D). Conversely, doubling and tripling the expression of USP21 while holding ZNF598 expression levels constant revealed additional readthrough of the poly(A) stall-inducing sequence with increasing ChFP:GFP ratios, suggesting further antagonism of the ligase. This result suggests that maintaining ZNF598 expression levels high relative to USP21 and OTUD3 is a feature that may be required to enable rapid 40S ribosomal ubiquitylation upon RQC-triggering events that are

not immediately removed by antagonistic Dubs. These results also indicate that OTUD3 or USP21 overexpression (40-fold and 100-fold above endogenous, respectively) is required to compete with endogenous ZNF598 activity.

2.3.8 OTUD3 and USP21 deubiquitylate 40S ribosomal proteins following RRub induction

To examine the ability of USP21 and OTUD3 to catalyze deubiquitylation of RRub events, we generated doxycycline (Dox)-inducible 293 cell lines that conditionally express either the wild type or inactive version of each Dub. To observe the reversal of RRub events, we induced ribosome stalling and subsequent RRub using UV exposure. To test the impact of Dub expression, cells were either treated with or without Dox for 16 hours prior to UV exposure. Cells were then UV irradiated and allowed to recover for increasing periods of time. Based on our previously established reversibility of RRub events, we suspected that overexpression of wild type USP21 or OTUD3 would induce a more rapid removal of eS10 and uS10 ubiquitylation during recovery from UV-induced stress. Control cells without induction of Dub overexpression displayed induced eS10 and uS10 ubiquitylation immediately following UV treatment, followed by rapid demodification 4 hours after UV exposure (Figure 2.5A-D and 2.11). Interestingly, in cells overexpressing exogenous wild type USP21, the amount of detectable eS10 ubiquitylation rapidly declined 1-hour post UV exposure, while uS10 ubiquitylation was completely ablated (Figure 2.5A and 2.11). These observations suggest that USP21 can demodify eS10 and uS10 following UV-induced stress. To substantiate these observations, we induced the expression of inactive USP21 and determined the dynamicity of UV-induced RRub events. Immunoblots confirmed that the dynamics of eS10 and uS10 ubiquitylation following UV treatment in cells expressing inactive USP21 were unaltered compared to cells without Dox-treatment. (Figure 2.5B and 2.11). These findings confirm that USP21 can remove ubiquitin from eS10 and uS10 in an activity-dependent manner. Similar to what was observed upon USP21 expression, OTUD3 expression resulted in substantially reduced eS10 ubiquitylation and complete ablation

of uS10 ubiquitylation following UV treatment compared to uninduced cells (Figure 2.5C and 2.11). This reduction in eS10 and uS10 ubiquitylation was activity dependent as induction of inactive OTUD3 did not alter either eS10 or uS10 ubiquitylation upon UV treatment (Figure 2.5D and 2.11). It was surprising that overexpression of the inactive versions of USP21 or OTUD3 did not result in a dominant negative phenotype with enhanced eS10 or uS10 ubiquitylation at steady state or reduced demodification kinetics following UV exposure. This observation suggests that the dubs do not compete for the same binding surface on the ribosome despite their ability to demodify the same RRub sites.

2.3.9 OTUD3 or USP21 loss-of-function reduces stall readthrough and extends eS10 ubiquitylation following RQC activation

To determine if USP21 or OTUD3 loss of function impacted RRub or RQC activity, we generated USP21 and OTUD3 knock out cell lines and USP21/OTUD3 double knockout cell lines using genome engineering approaches (Figure 2.12A). Two separate knockout clones for both USP21 and OTUD3 displayed reduced poly(A)-mediated stall readthrough which is consistent with our demonstration that overexpression of OTUD3 or USP21 enhances stall readthrough (Figure 2.6A). Combined loss of USP21 and OTUD3 did not further reduce stall readthrough compared to individual knockouts suggesting that the dubs may be acting at distinct points within the RQC pathway (Figure 2.6A). We then evaluated the kinetics of eS10 demodification following UV-induced RQC activation in parental and knockout cell lines. Consistent with previous results, eS10 ubiquitylation was rapidly induced following UV exposure and was fully demodified to pre-exposure levels by 16 hours in parental 293T cells (Figure 2.6B and 2.12B). USP21 or OTUD3 knockout cells displayed reduced demodification kinetics following UV exposure with eS10 ubiquitylation persisting up to 24 hours in OTUD3 knockout cells (Figure 2.6B and 2.12B). OTUD3 and USP21 double knockout cells also displayed sustained eS10 ubiquitylation following UV exposure compared to parental controls (Figure 2.6B and 2.12B). While a delay in eS10 demodification was observed in the knockout cells, the extent

of eS10 ubiquitylation is clearly reduced compared to peak levels in all knockout cells indicating that other Dubs can compensate for the loss of USP21 or OTUD3 and that further redundancy exists in the pathway.

It is notable that we failed to observe an RQC phenotype upon siRNA-mediated knockdown of USP21, OTUD3, or combinations of candidate Dubs (Figure 2.12C-F). We also could not detect reduced stall readthrough upon knockdown of 24 additional Dubs that were not represented in our overexpression library (Figure 2.12G). These results demonstrate that complete genetic ablation of OTUD3 or USP21 expression is required to observe defects with RQC and RRub demodification following RQC activation.

2.3.10 OTUD3 preferentially demodifies RQC RRub sites and is present within ribosome enriched fractions

Stressors that induce the integrated stress response (ISR) also induce RRub events on uS3 and uS5 that function in a distinct manner compared to eS10 or uS10 RQC ubiquitylation events (Higgins et al., 2015). To examine if OTUD3 or USP21 act specifically on eS10 and uS10 RQC RRub events or act more broadly on ubiquitylated ribosomes we utilized the OTUD3 and USP21 inducible cell lines. After induced Dub expression, cells were treated with DTT or harringtonine (HTN) which stimulates uS5 and uS3 RRub events in a distinct manner (Higgins et al., 2015). Interestingly, USP21 expression reduced both HTN and DTT-induced uS5 and uS3 ubiquitylation in an activity-dependent manner (Figure 2.7A). However, OTUD3 expression reduced uS5 ubiquitylation, albeit to a lesser extent than UPS21 expression, and had no impact on HTN or DTT-induced uS3 ubiquitylation (Figure 2.7B). These results indicate that USP21 expression has a larger impact on all RRub events examined and that OTUD3 primarily demodifies ZNF598-catalyzed eS10 and uS10 ubiquitylation events.

Given the ability of USP21 and OTUD3 to remove RRub events, we examined if OTUD3 or USP21 associated with ribosomes. We treated OTUD3 or USP21 inducible cells with ANS in the presence or absence of Dox and then pelleted ribosomes by running whole cell extracts

through a sucrose cushion. As expected, ANS induces eS10 ubiquitylation which is abrogated upon OTUD3 or USP21 expression (Figure 2.7C,D). Importantly, both OTUD3 and USP21 are present in the ribosome pellet fraction suggesting that OTUD3 and USP21 associates with ribosomes. To determine which ribosomal subpopulation is associated with OTUD3 upon RQC stimulation, we treated OTUD3 expressing cells with anisomycin and separated whole cell extracts over a linear sucrose gradient. Subsequent immunoblotting of gradient fractions revealed OTUD3 to be present in 40S containing fractions and largely absent from 80S and polysome containing fractions (Figure 2.7E). These results suggest that OTUD3 may preferentially demodify ubiquitylated 40S proteins that arise after subunit splitting and position OTUD3-mediated deubiquitylation as a putative late step during RQC events. Overall, our observations indicate OTUD3 and USP21 can demodify distinct sets of RRub events and regulate RQC activity.

2.4 Discussion

Proteomics studies have revealed that a substantial portion of the ubiquitin-modified proteome may play a role in regulating cellular processes in a non-degradative capacity rather than targeting substrates for degradation (Kim et al., 2011). Several of these putative regulatory ubiquitylation events appear to be conserved, including many ribosomal monoubiquitylation events. Previous studies have established that conserved site-specific regulatory 40S ubiquitylation (RRub) is among the first signaling events required for proper RQC execution (Garzia et al., 2017; Juszkiewicz and Hegde, 2017; Matsuo et al., 2017; Sundaramoorthy et al., 2017). While the ubiquitin ligase that catalyzes the RQC-specific RRub events has been characterized in both mammals and yeast, whether RRub demodification was a critical step in ultimate resolution of RQC events and the identity of potential RRub Dubs remained unknown.

Here we identify two Dubs, USP21 and OTUD3, that contribute to the removal of ubiquitin from 40S ribosomal proteins. Overexpression of USP21 or OTUD3 results in enhanced

readthrough of a poly(A) stall-inducing sequence. USP21 and OTUD3 have overlapping yet distinct ribosomal protein substrate specificities. The ubiquitin-specific proteases (USP) and the ovarian tumor (OTU) family make up the two largest Dub families. While USP Dubs are typically more promiscuous with regards to the types of polyubiquitin linkages they demodify (Faesen et al., 2011), OTU Dubs have been shown to exhibit ubiquitin-chain linkage specificity (Mevissen et al., 2013). Consistent with these observations, USP21 is more promiscuous than OTUD3 in that USP21 can hydrolyze all four tested RRub events while OTUD3 preferentially demodifies ZNF598-catazlyed eS10 and uS10 ubiquitylation events. These results establish that Dubs can play a regulatory role within the RQC pathway.

The factors that govern the regulation of these Dubs and when RRub events are removed within the RQC pathway remain unclear. We postulate two ways that Dubs may act as regulators of the ISR and RQC pathways. First, USP21 and OTUD3 may limit the activity of ZNF598 and other RRub ligases through direct antagonism to prevent spurious RRub. Unregulated 40S ubiquitylation could result in premature translational attenuation and destruction of properly processed mRNAs. Though plausible, the observed substochiometric ratio of OTUD3 and USP21 relative to ZNF598 suggests that Dubs may not directly limit ZNF598 activity. The low expression levels of USP21 and OTUD3 relative to ZNF598 may ensure that when progression of the ribosome is halted to a degree that requires RQC activity, the forward reaction is favored. A second possibility is that following 80S splitting, Dubs serve to strip the 40S of its ubiquitin in order to recycle unmodified 40S complexes which can reenter the translation cycle. Implicit in this model is that a ubiquitylated 40S may prevent or reshape translation initiation events, a scenario which has not been directly established. More in-depth biochemical studies are required to identify the factors and mechanisms that regulate these reversible ribosomal regulatory ubiquitylation events, and the timing by which OTUD3 and USP21 exert their activity.

The mechanistic role of these regulatory ubiquitylation events remains obscure. One possibility is that ubiquitylation serves as a scaffold for targeting endo- or exoribonucleases responsible for downstream degradation of the mRNA. Recent work has shown that the endonuclease Cue2 is recruited to collided ribosomal complexes and is responsible for cleaving the mRNA within the A site (D'Orazio et al., 2019). With the unique interface formed by collided disomes and the positioning of ubiquitylated eS10 and uS10, it is conceivable that Cue2 uses its two ubiquitin binding domains to latch onto the stalled complex. Another possibility is that ribosome ubiquitylation represents a ubiquitin code that distinguishes ribosomes that are simply paused at a specific codon to allow for proper nascent chain folding or to relocalize translation from those that are terminally stalled due to an irreconcilable defect in the mRNA. A ribosomal ubiquitin code implies a possible order of operations and suggests that individual RRub events may not be occurring simultaneously, but rather in succession. Support for this model comes from the hierarchical relationship we observed among the different sets of RRub events, where the loss of eS10 ubiquitylation results in a reduction in uS10 modification (Figure 2.2A). This observation suggests that eS10 is the first ubiquitylation event required for RQC initiation. Taken together, these results suggest that the combined modification of both eS10 and uS10 is required for robust resolution of stalled ribosomes. This observation is replicated for ISR stimulated uS3 and uS5 ubiquitylation where loss of the ability to ubiquitylate uS3 results in a complete ablation of uS5 modification which suggest that hierarchical RRub events may regulate translation beyond RQC function (Figure 2.2D).

Current models suggest that collided ribosomes trigger ZNF598 mediated eS10 and uS10 ubiquitylation(Ikeuchi et al., 2019; Juszkiewicz et al., 2018a). In this case, it remains conceivable that the individual ubiquitylation events on eS10 and uS10 may not be taking place on the same ribosome, but rather occur on neighboring, collided ribosomes. For example, upon collision with the trailing ribosome, ZNF598 may mediate ubiquitylation of eS10 on the leading ribosome followed by ubiquitylation of uS10 on the trailing ribosome or vice versa. This could

require a specific conformation of ZNF598 in order to traverse both ribosomes, or following addition of the first ubiquitin the ligase moves upstream to the next site. Support for this model comes from studies in yeast that indicate ribosome collisions are critical events to initiate the no-go RNA decay pathway (Simms et al., 2017), and are required for upstream cleavage of the defective mRNA by the endonuclease Cue2 (D'Orazio et al., 2019; Guydosh and Green, 2017). Having shown that modification of both eS10 and uS10 are required to prevent readthrough of polyA-induced stalls, it is probable that the collision with the leading ribosome triggers combinatorial ubiquitylation events that are required for recruitment of downstream RQC factors. Further biochemical analysis is needed to determine the cellular role of RRub events in recruitment of quality control factors and reshaping the translational landscape.

2.5 Materials and Methods

Plasmids

The dual-fluorescence translation stall reporter plasmids were described previously (Juszkiewicz and Hegde, 2017; Sundaramoorthy et al., 2017). All Dub coding regions were cloned into Myc-tagging CMV expression vectors using Gateway cloning system (Invitrogen). QuickChange site-directed mutagenesis was done utilizing PCR-based approaches (primers 5' to 3': OTUD3-C76S, GGGGACGGCAATAGCTTGTTCAGAGC; OTUD1-C320S, CATTCCAGACGGCAACAGCCTCTACCGAGCTG; OTUB2-C15S, GGGGATGGGAACAGCTTCTACAGGG; USP10-C424S, GATCAATAAAGGGAACTGGAGCTACATTAATGCTACACTG; USP21-C250S, CCTGGGAAACACGAGCTTCCTGAATGC), followed by Dpn1 digestion of template DNA and transformation of the mutated plasmids into TOP10 E.coli cells. Plasmids were confirmed by sequencing and screened for expression by immunoblotting.

Cell lines, transfections and siRNA

All reagents utilized in this study can be found in Supplementary File 1: Key Resources Table.

HCT116 and HEK293 cells were grown in DMEM (high glucose, pyruvate and L-Glutamine) containing 10% fetal bovine serum (FBS) and 1% penicillin/streptomycin and maintained in a 5% CO_2 humidified incubator. Where indicated, cells were exposed to 0.02J/cm^2 UV radiation using a Spectorlinker™ XL-1000 (Spectronics) before harvesting or treated with 5mM DTT or 2 μg/mL Haringtonine for 4 hours before harvesting. Ansiomycin was used at final concentration of 5μg/ml.

HCT116 knock-in cells (uS10 K4R/K8R and eS10 K138R/K139R) were generated using CRISPR/Cas9 genome engineering approaches (Biocytogen). Individual clones were first validated by genomic sequencing. Cells containing the desired point mutation were selected for validation by immunoblotting. USP21 and OTUD3 knock out cell lines were generated in the 293T cell background using CRISPR/Cas9 genome engineering utilizing three individual guide RNAs (oligonucleotides 5' to 3': USP21: CAAGTATCGGTGGAGCCCGG, GGTAGCTTGGATCCCACTCG, TATGGAGCACGAGGATTCGA; OTUD3: CGGAATCGGCCGGAGTCTGG, CAACGCTTGAGGCGGACGCT, GCTCTTGGTGATCAATTGGA). 293T cells were transfected with the pSpCas9(BB)-2a-GFP plasmid containing individual guide RNAs using lipofectamine 2000. After 2 days GFP positive cells were single cell sorted on a BD FACSAria Fusion (BD BioSciences) cell sorter. Cells were validated for loss of USP21 and OTUD3 by immunoblotting.

Stable doxycycline inducible cell lines expressing Flag-HA-tagged proteins were generated using the Flp-In™ system (Thermo Fisher) through single locus integration, and Hygromycin selection. Flp-In T-Rex 293 cells were transfected with Flp-In expression vectors for the gene of interest (listed in resource table) using TransIT 293 transfection reagent (Mirus) according to manufacturer guidelines. Cells seeded at 60% confluency were transfected for 24 hours followed by selection of stable expression clones with 100 μg/mL Hygromycin. Protein

expression was induced with 2 μg/mL doxycycline 16 hours prior to UV exposure, drug treatment, or harvesting.

All cellular transient transfections were performed using Lipofectamine 2000 (Thermo Fisher) and siRNA (see Supplementary File 1: Key Resources Table) knockdown transfections were performed using Lipofectamine RNAiMAX (Thermo Fisher) according to manufacturer guidelines.

Dual-fluorescence translational stall reporter assay

All dual-fluorescent reporter plasmid cellular transfections were done using Lipofectamine 2000 according to manufacturer guidelines. Cellular ChFP and GFP fluorescence intensities for 10,000 individual events were measured 48 hours following transfection on a BD LSRFortessa™ X-20 cell analyzer (BD Biosciences). FACS data was analyzed using FlowJo (v10.4.1).

Immunoblotting

Cell pellets were resuspended in denaturing lysis buffer (8 M urea, 50 mM Tris-Cl, pH 8.0, 75 mM NaCl, 1mM β-glycerophosphate, 1 mM NaF, 1 mM NaV, 40 mM NEM and EDTA-free protease inhibitor cocktail (Roche Diagnostics)) and kept on ice throughout preparation. Cell lysates were sonicated for 10s at output of 3 W with a membrane dismembrator model 100 (Fisher Scientific) with a microtip probe followed by centrifugation at 15,000 rpm at 4ºC for 10 min. Supernatant protein concentrations were determined by BCA Protein assay (Thermo Fisher). Laemmli sample buffer with β-mercaptoethanol was added to cell lysates and heated at 95ºC for 10 min. Lysates were resolved on 12 or 15% SDS-PAGE gels then transferred to PVDF membranes (Bio-Rad) using Bjerrum semi-dry transfer buffer (48 mM Tris Base, 39 mM Glycine-free acid, 0.0375% SDS, 20% MeOH, pH 9.2) and a semi-dry transfer apparatus (Bio-Rad Turbo Transfer) at 25V for 30 min. Immunoblots were blocked with 5% blotting grade nonfat dry milk (APEX Bioresearch) in TBST for 1 hour, followed by diluted primary antibody in

5% BSA over-night. Membranes were probed with anti-RPS2 (Cat# A303-794A, Bethyl); anti-RPS3 (Cat# A303-840A, Bethyl); anti-RPS10 (Cat# ab151550, Abcam) (antibody was used in figures 1E, 3E, 4E, 5A-D, 7C,E, S1E,F) ; anti-RPS10 (Cat# A6056, ABclonal, this was used for all other RPS10 (eS10) immunoblots); anti-RPS20 (Cat# ab133776, Abcam); anti-ZNF598 (Cat# HPA041760, Sigma); anti-OTUD3 (Cat# ab107646, Abcam); anti-USP21 (RRID:AB_10603227, Cat# HPA028397, Sigma); anti-USP21 (Cat# ab171028, Abcam) (antibody was used in figure S5C); anti-phospho-eIF2α(Ser51)(D9G8) (Cat# 3398S, Cell Signaling Tech); anti-c-Myc (9E10) (Cat# sc-40, Santa Cruz); anti-ubiquitin (Cat# MAB1510, EMD Millipore); anti-HA (Cat# MMS-101P, Biolegend); anti-tubulin (Cat# 3873S, Cell Signaling Tech); anti-Rabbit IgG, HRP (Cat# W4011, Promega); or anti-Mouse IgG, HRP (Cat# W4021, Promega). Immunoblots were developed with Clarity Western ECL Substrate (Bio-Rad) and imaged on a Bio-Rad Chemi-Doc XRS+ system. Imagelab (Bio-Rad) software was used to process all blots with final images prepared in Adobe Illustrator.

Sucrose cushion

Cells were lysed in 600ul of (50mM Hepes, pH 7.4, 100mM KAc, 2.5mM MgAc2, 0.5% Triton X-100, 1mM DTT, 1 mM NaF, 1 mM NaV, 40 mM NEM and EDTA-free protease inhibitor cocktail) buffer and 500ul of whole cell extracts were pelleted over a 0.5M sucrose cushion (500ul) by spinning whole cell lysate in a TLA120.2 rotor at 100,000rpm at 4ºC for 35 min. Pelleted material was resuspended in Laemmli sample buffer with β-mercaptoethanol and heated at 95ºC for 10 min followed by standard immunoblotting.

Sucrose gradient

Cells were lysed in 600ul of (500mM Tris, pH 7.8, 1.5M NaCl, 150mM MgCl2, 0.5% NP-40, 150ug/ml cycloheximide, 8U/ml SUPERase In RNAse inhibitor, 1 mM NaF, 1 mM NaV, 40 mM NEM and EDTA-free protease inhibitor cocktail) lysis buffer followed by sonication and clarification of lysate at 15,000rpm at 4ºC for 10 min. 500ul of whole cell extract was

fractionated over a 10-50% sucrose gradient (prepared on Gradient Master 108 (Biocomp): 1min 38s, 81.5 degrees, 18rpm) spinning at 41,000rpm at 4ºC for 2 hours in an SW41i rotor. 1ml fractions were collected using a PGFip piston gradient fractionator (Biocomp). Protein fractions were precipitated overnight at 4ºC with 10% Trichloroacetic acid (TCA) followed by three washes with ice-cold acetone. Pellets were dried in Vacufuge plus (Eppendorf) at room temperature for 5min then resuspended in Laemmli sample buffer with β-mercaptoethanol and heated at 95ºC for 10 min followed by standard immunoblotting.

2.6 Quantification and Statistical Analysis

All FACS-based assays, plasmid transfections and siRNA transfections were performed in triplicate (n = 3) as biologically distinct samples. The mean ChFP:GFP ratio and SEM were calculated and compared to K20-reporter transfection alone, parental cell type or control siRNA knockdown. Immunoblot quantification of the relative ubiquitin modification was calculated by normalization of the individual Ub intensities for each time point to that of the no UV control. Significance (p value) was calculated using an unpaired two-tailed Student's t test using GraphPad Prism 7.0.

2.7 Acknowledgments

We thank the Goldrath lab (UCSD) for providing assistance on all FACS-based experiments. We thank Julie Monda for providing a critical reading of this manuscript. This work was supported by a UCSD Cell and Molecular Genetics Training Program (T32GM007240) and a National Science Foundation Graduate Research Fellowship (DGE-1650112) (D.M.G), and the NIH (DP2-GM119132 and PGM085764) (E.J.B).

2.8 Declaration of Interests

The authors declare no competing interests.

Chapter 2, in full, is a reprint of the material as it occurs in eLife, Garshott, D.M.; Sundaramoorthy, E.; Leonard, M.; Bennett, E.J.; eLife Sciences Publications Ltd, 2020. I am the primary author.

2.9 Figures

Figure 2.1. Stress-induced RRub events are reversible.
(A) HCT116 cells were treated with anisomycin (ANS, 5μg/ml) alone or with MG132 (10μM) for the indicated times. Whole-cell extracts were analyzed by SDS-PAGE and immunoblotted with the indicated antibodies. The ubiquitin-modified and unmodified ribosomal protein is indicated by the arrow and asterisk, respectively. S and L denote short and long exposures (n=1).
(B) The amount of ubiquitylated eS10 (red line) and uS10 (blue dashed line) and unmodified eS10 (black column) and uS10 (grey column) after the indicated treatments compared to untreated cells quantified from panel A.
(C) HCT116 cells were treated with DTT (5mM) alone or with cycloheximide (CHX, 100μg/ml) for 4 hours followed by DTT washout in media with or without CHX alone or with MG132 (10μM) for the indicated times. Whole-cell extracts were analyzed by SDS-PAGE and immunoblotted with the indicated antibodies. The ubiquitin-modified and unmodified ribosomal protein is indicated by the arrow and asterisk, respectively. S and L denote short and long exposures (n=1).
(D) The amount of ubiquitylated uS3 (red line) and uS5 (blue dashed line) and unmodified uS3 (black column) and uS5 (grey column) after the indicated treatments compared to untreated cells quantified from panel C.
(E) 293T cells were exposed to UV and allowed to recover for the indicated times. Whole-cell extracts were analyzed by SDS-PAGE and immunoblotted with the indicated antibodies. The ubiquitin-modified ribosomal protein is indicated by the arrow. S and L denote short and long exposures (n=1).
(F) The amount of ubiquitylated eS10 (blue line), uS10 (red line), uS5 (black line) and uS3 (grey line) after UV exposure compared to untreated cells quantified from panel E.

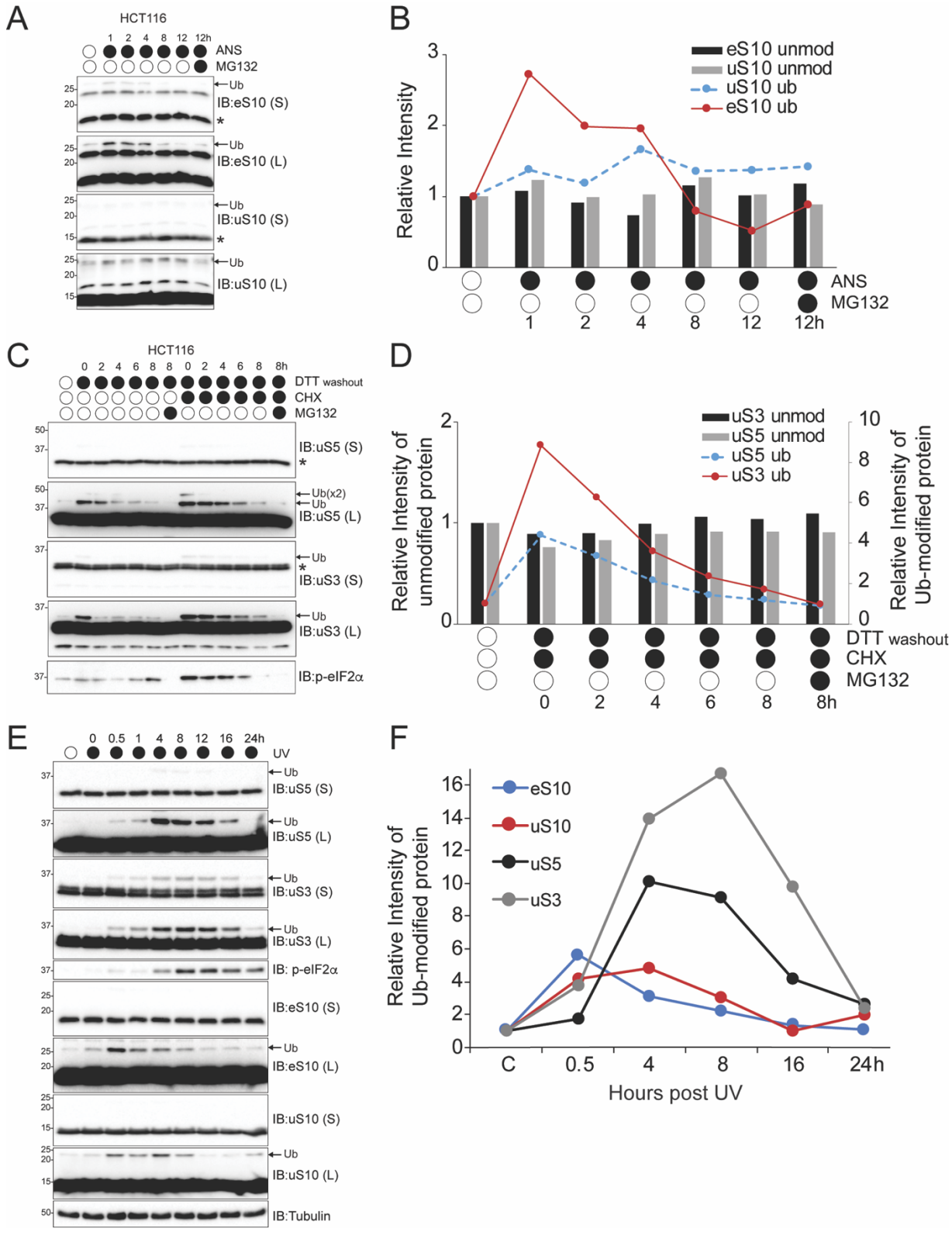
A
HCT116
1 2 4 8 12 12h
ANS
MG132
Ub
IB:eS10 (S)
IB:eS10 (L)
IB:uS10 (S)
IB:uS10 (L)
B
Relative Intensity
eS10 unmod
uS10 unmod
uS10 ub
eS10 ub
ANS
MG132
1 2 4 8 12 12h
C
HCT116
0 2 4 6 8 8 0 2 4 6 8 8h
DTT washout
CHX
MG132
IB:uS5 (S)
Ub(x2)
IB:uS5 (L)
IB:uS3 (S)
IB:uS3 (L)
IB:p-eIF2α
D
Relative Intensity of unmodified protein
Relative Intensity of Ub-modified protein
uS3 unmod
uS5 unmod
uS5 ub
uS3 ub
DTT washout
CHX
MG132
0 2 4 6 8 8h
E
0 0.5 1 4 8 12 16 24h
UV
IB:uS5 (S)
IB:uS5 (L)
IB:uS3 (S)
IB:uS3 (L)
IB: p-eIF2α
IB:eS10 (S)
IB:eS10 (L)
IB:uS10 (S)
IB:uS10 (L)
IB:Tubulin
F
Relative Intensity of Ub-modified protein
eS10
uS10
uS5
uS3
C 0.5 4 8 16 24h
Hours post UV

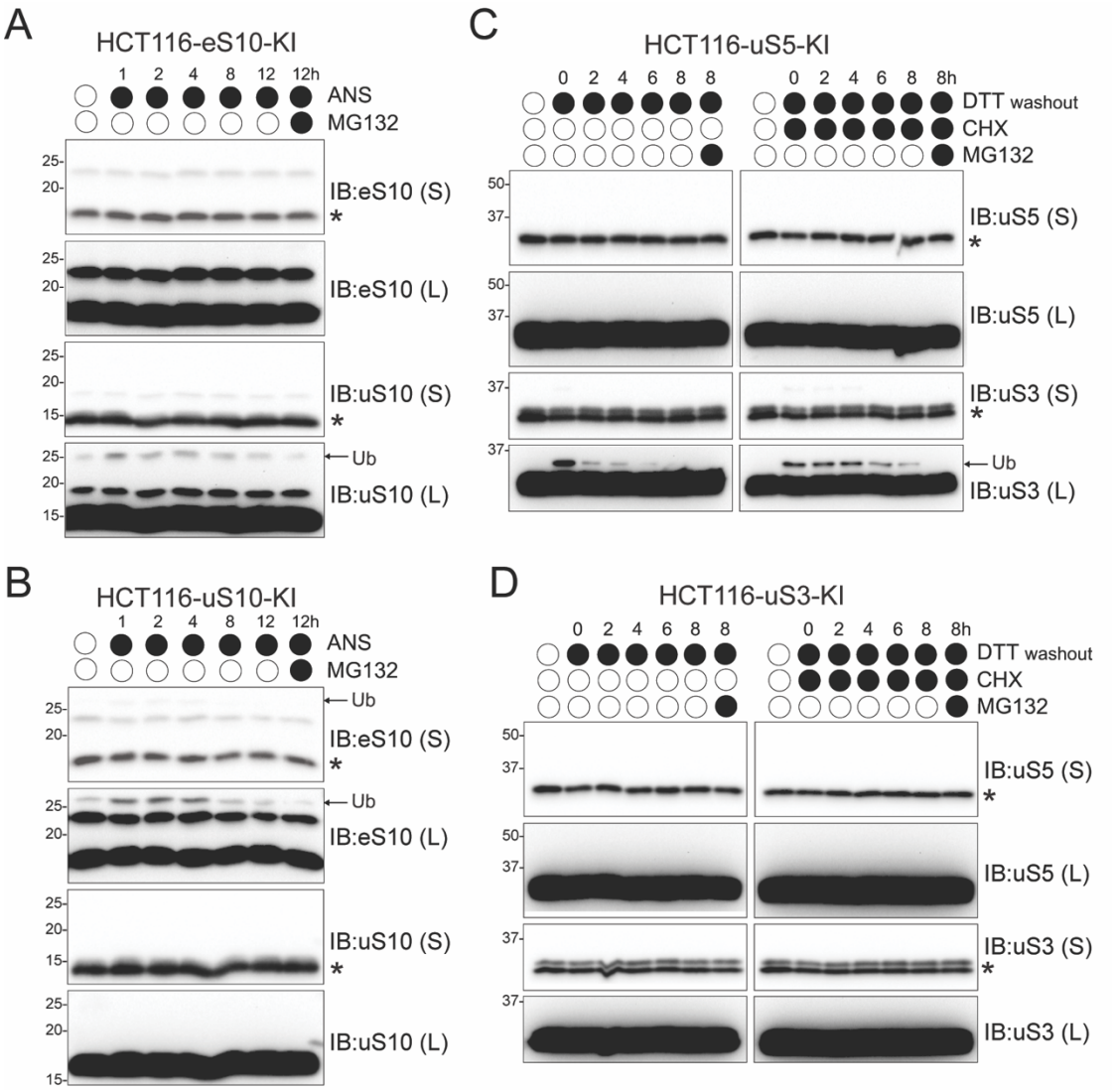

Figure 2.2. Distinct sets of RRub events are hierarchically organized.
(A,B) HCT116 mutant RRub knock-in (KI) cell lines eS10-KI (K138RK139R) or uS10-KI (K4RK8R)(A,B) were treated with ANS (5μg/ml) and MG132 (10μM) continuously for the indicated times. Whole-cell extracts were analyzed by SDS-PAGE and immunoblotted with the indicated antibodies.
(C,D) HCT116 mutant uS5-KI (K54RK58R) or uS3-KI (K214R) were either untreated or pre-treated with DTT (5mM) alone or with CHX (100μg/ml) for 4 hours followed by DTT washout in media with or without CHX (100μg/ml) and MG132 (10μM). Cells were collected at the indicated times post DTT washout. Whole-cell extracts were analyzed by SDS-PAGE and immunoblotted with the indicated antibodies. The ubiquitin-modified and unmodified ribosomal protein is indicated by the arrow and asterisk, respectively. S and L denote short and long exposures (n=1).

Figure 2.3. Identification of deubiquitylating enzymes that allow for readthrough of poly(A)-mediated ribosome stalls.
(A) 60 human deubiquitylating enzyme (Dub) expression plasmids were individually co-transfected with the poly(A)-stall reporter plasmid and the resulting ChFP and GFP fluorescence intensities were measured by flow cytometry. The Z-score value for each Dub is depicted (n=1). The six Dubs with the highest Z-score are boxed to indicate candidate Dubs that induce increased readthrough of poly(A)-stall reporter. Expression of wild type (blue dot) and catalytically inactive (red dot) ZNF598 are shown as controls.
(B) The ChFP:GFP ratio from cells transfected with the poly(A)-stall reporter (solid bars) or a reporter containing no stall sequence (striped bars), along with expression plasmids for the indicated Dubs relative to a control plasmid. Error bars denote SEM for triplicate transfections. **p<0.0001, *p<0.01 using Student's t-test comparing Dub expression to control transfections.
(C) The ChFP:GFP ratio from cells transfected with expression plasmids for either wild type (black circle) or catalytically inactive (grey circle) Dubs and the poly(A)-stall reporter relative to a control plasmid. Control transfections with the poly(A) reporter plasmid alone are indicated by the open circle. Error bars denote SEM for triplicate transfections. **p<0.0001, *p<0.001 using Student's t-test comparing the wild type to the catalytically inactive mutant for each Dub or ZNF598. NS=not significant.
(D) The ChFP:GFP ratio from cells transfected with the poly(A)-stall reporter plasmid and ZNF598 alone or in combination with the indicated wild type Dubs (black circle) relative to a control plasmid. Control transfections with the poly(A) reporter plasmid alone are indicated by the open circle. Error bars denote SEM for triplicate transfections. **p<0.0001, *p<0.01, using Student's t-test comparing wild type ZNF598 alone to samples with ZNF598 and the indicated Dub.
(E) Whole-cell extracts from ZNF598- knock out (KO) cells transfected with expression plasmids for wild type (black circles) ZNF598, USP21, or OTUD3 and their respective inactive mutants (grey circles) were analyzed by SDS-PAGE and immunoblotted using the indicated antibodies. The ubiquitin-modified ribosomal protein is indicated by the arrow. S and L denote short and long exposures (n=1).

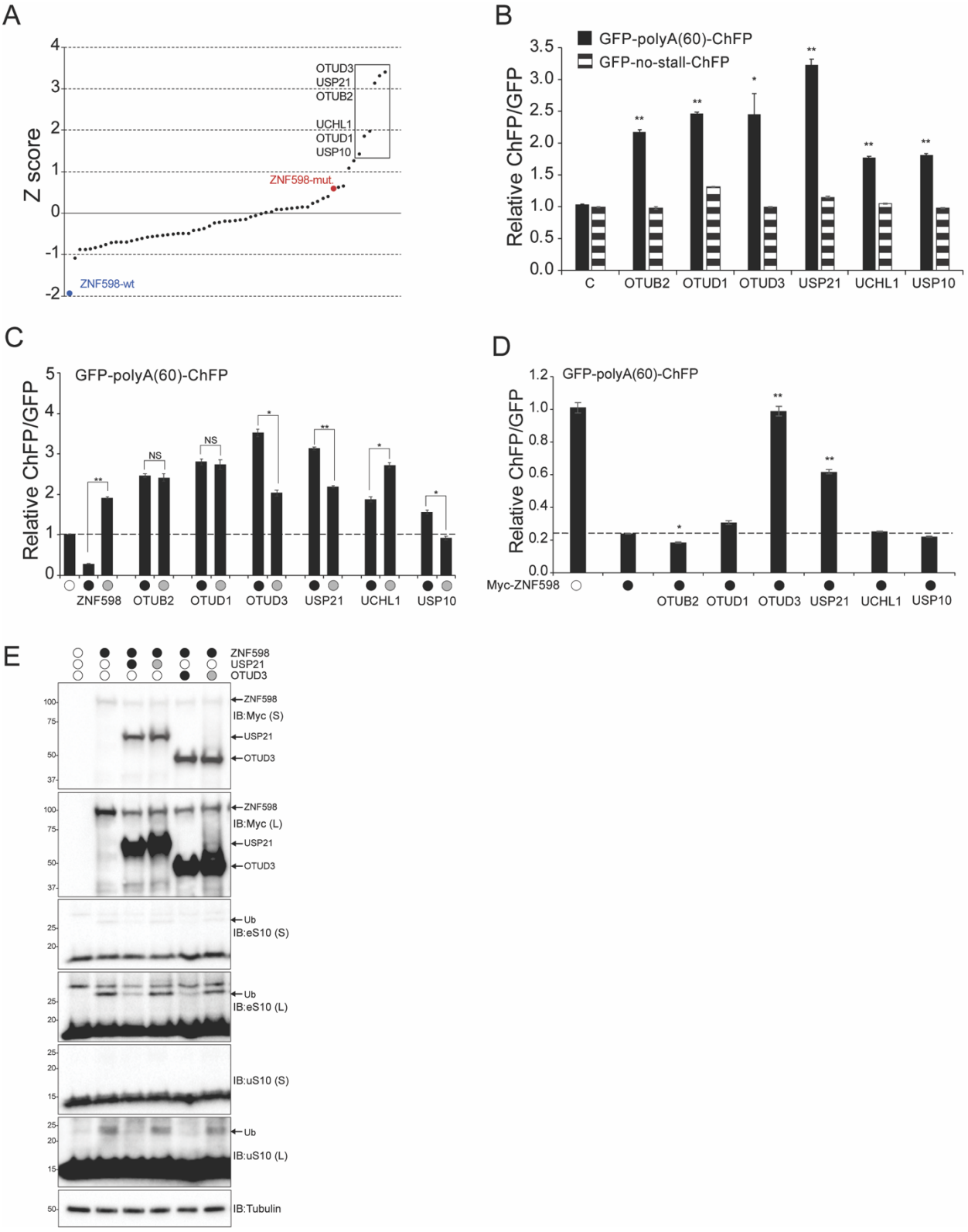
A
Z score
OTUD3
USP21
OTUB2
UCHL1
OTUD1
USP10
ZNF598-mut
ZNF598-wt
B
GFP-polyA(60)-ChFP
GFP-no-stall-ChFP
Relative ChFP/GFP
C
OTUB2
OTUD1
OTUD3
USP21
UCHL1
USP10
C
GFP-polyA(60)-ChFP
Relative ChFP/GFP
NS
ZNF598
OTUB2
OTUD1
OTUD3
USP21
UCHL1
USP10
D
GFP-polyA(60)-ChFP
Relative ChFP/GFP
Myc-ZNF598
OTUB2
OTUD1
OTUD3
USP21
UCHL1
USP10
E
ZNF598
USP21
OTUD3
IB:Myc (S)
IB:Myc (L)
IB:eS10 (S)
IB:eS10 (L)
IB:uS10 (S)
IB:uS10 (L)
IB:Tubulin
Ub

Figure 2.4. USP21 and OTUD3 antagonize ZNF598-mediated RRub events.
(A,B) Parental HCT116 cells and ZNF598 knock-out (KO) cells were transfected with USP21 (A) or OTUD3 (B) expression plasmids and the poly(A)-stall reporter (black circles) or the poly(A)-stall reporter alone (open circles). Fluorescence intensities were measured by flow cytometry and the relative ChFP:GFP ratio is depicted. Error bars denote SEM for triplicate transfections. ***p<0.0001, **p<0.001, *p<0.05, using Student's t-test comparing Dubs to control transfection.
(C,D) The ChFP:GFP ratio from parental HCT116 cells or point mutant knock-in (KI) eS10 or uS10 cell lines transfected with the poly(A)-stall reporter alone (open circles) or with expression plasmids for wild type (black circles) or inactive mutant (grey circles) USP21 (C) or OTUD3 (D) relative to control transfections in the indicated cell lines. Error bars denote SEM for triplicate transfections. *p<0.0001 using Student's t-test comparing wild type Dub transfections to control transfection in the indicated cell lines.
(E) Whole-cell extracts from cells transfected as indicated in panels C and D were analyzed by SDS-PAGE and immunoblotted for the indicated antibodies. Black and grey circles denote expression of wild type or inactive versions, respectively. The ubiquitin-modified ribosomal protein is indicated by the arrow. S and L denote short and long exposures (n=1).
(F,G) The ChFP:GFP ratio from HCT116 ZNF598 knock-out (KO) cells transfected with increasing amounts of plasmid DNA for either wild type ZNF598 and USP21 (F) or OTUD3 (G) and the poly(A)-stall reporter. Numbers indicate the ratio of transfected DNA for each plasmid. Error bars represent SEM of triplicate replicates. ***p<0.0001, **p<0.001, *p<0.05 using Student's t-test comparing the different ZNF598 to Dub DNA ratios as indicated.

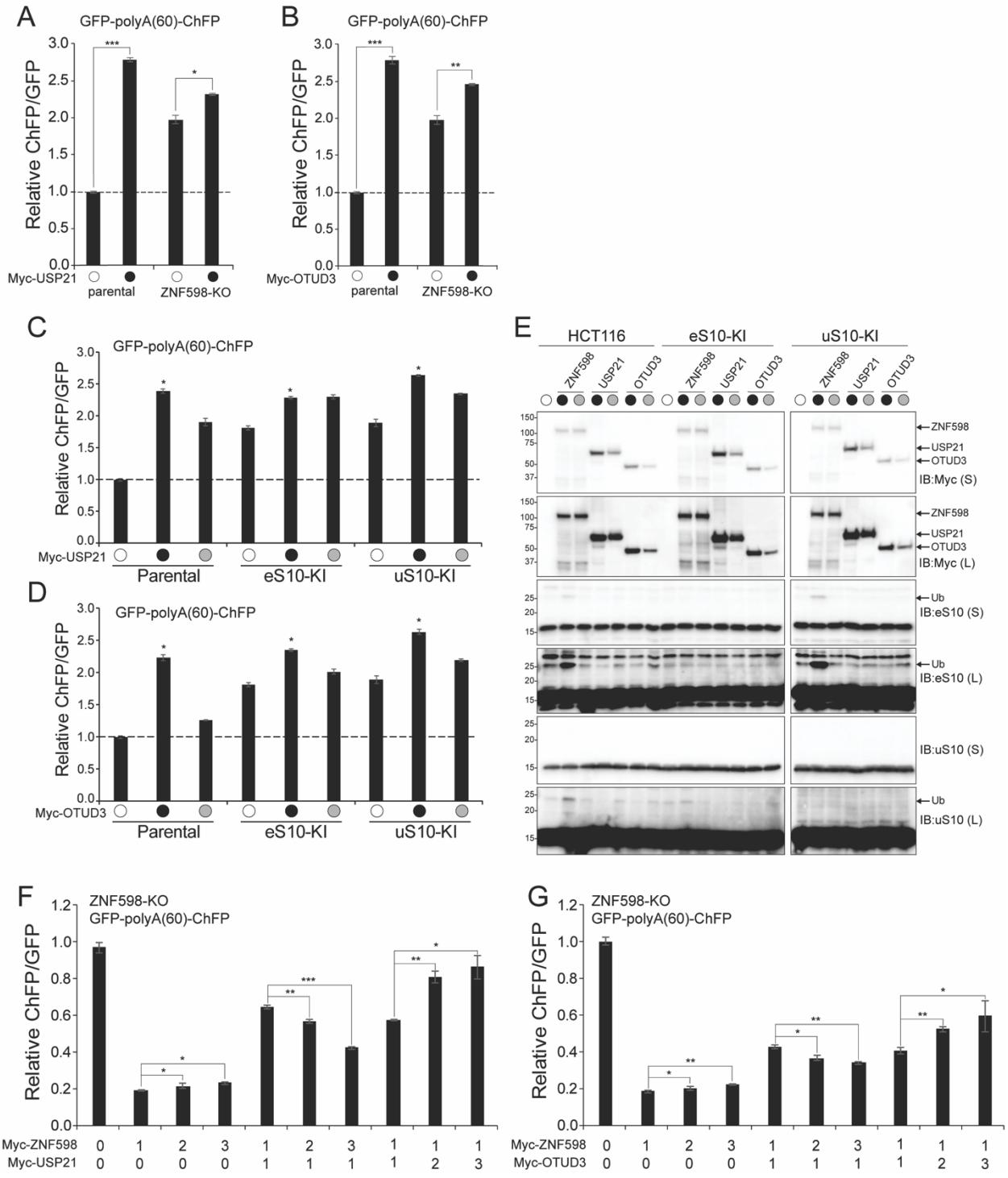
A
GFP-polyA(60)-ChFP
Relative ChFP/GFP
Myc-USP21
parental
ZNF598-KO
B
GFP-polyA(60)-ChFP
Relative ChFP/GFP
Myc-OTUD3
parental
ZNF598-KO
C
GFP-polyA(60)-ChFP
Relative ChFP/GFP
Myc-USP21
Parental
eS10-KI
uS10-KI
D
GFP-polyA(60)-ChFP
Relative ChFP/GFP
Myc-OTUD3
Parental
eS10-KI
uS10-KI
E
HCT116
eS10-KI
uS10-KI
ZNF598
USP21
OTUD3
IB:Myc (S)
IB:Myc (L)
IB:eS10 (S)
IB:eS10 (L)
IB:uS10 (S)
IB:uS10 (L)
Ub
F
ZNF598-KO
GFP-polyA(60)-ChFP
Relative ChFP/GFP
Myc-ZNF598
Myc-USP21
G
ZNF598-KO
GFP-polyA(60)-ChFP
Relative ChFP/GFP
Myc-ZNF598
Myc-OTUD3

Figure 2.5. USP21 and OTUD3 expression accelerates RRub demodification following UV exposure.
(A-D) Cells with stable inducible expression of wild type USP21 (A), OTUD3 (C) or inactive versions (B, D, respectively) were induced or uninduced with doxycycline (Dox, 2μg/ml) for 16 hours followed by UV exposure. Whole cell extracts from cells collected at the indicated times after UV exposure were analyzed by SDS-PAGE and immunoblotted using the indicated antibodies. The ubiquitin-modified ribosomal protein is indicated by the arrow. S and L denote short and long exposures (n=1).

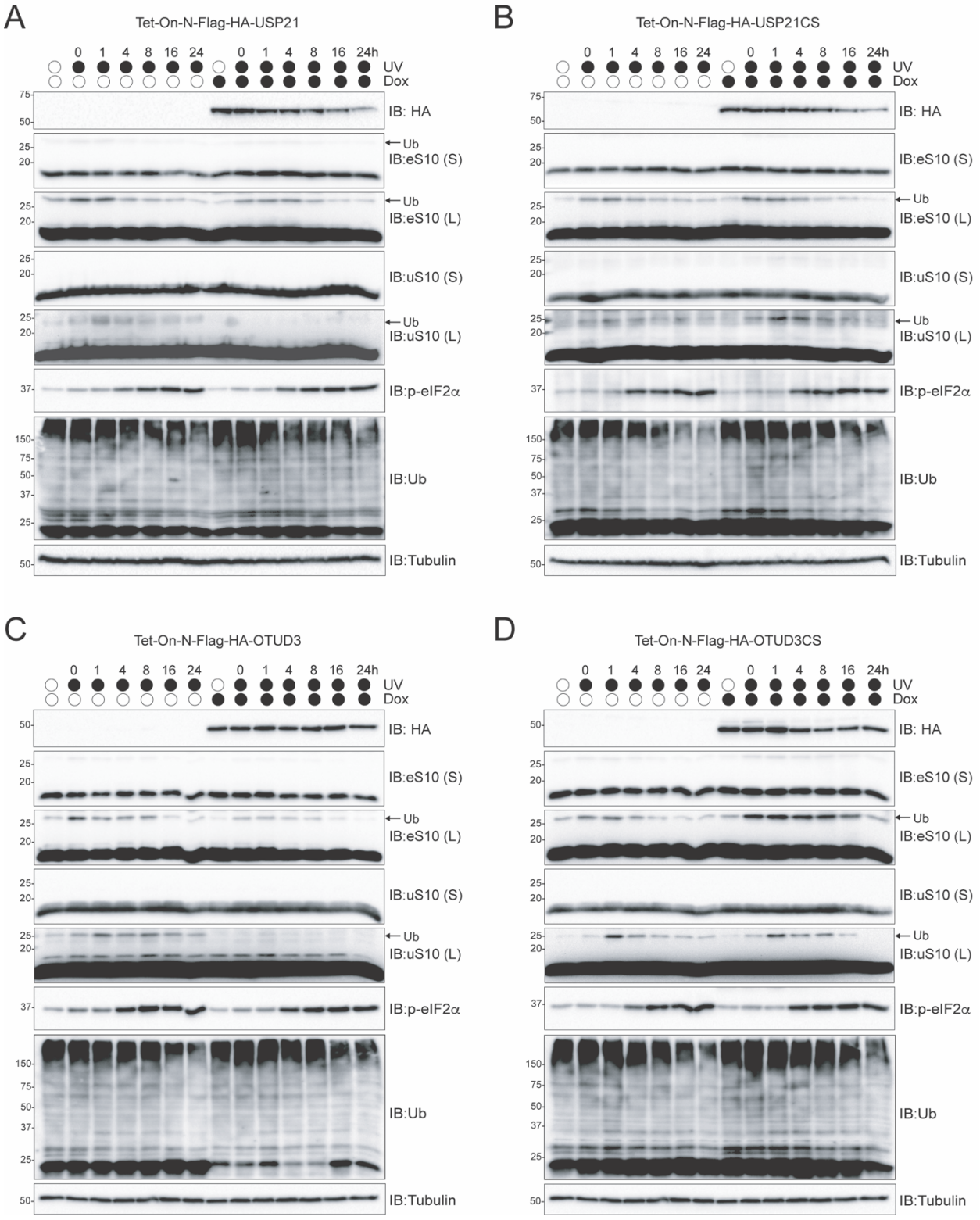
A
Tet-On-N-Flag-HA-USP21
B
Tet-On-N-Flag-HA-USP21CS
C
Tet-On-N-Flag-HA-OTUD3
D
Tet-On-N-Flag-HA-OTUD3CS
0 1 4 8 16 24 0 1 4 8 16 24h
UV
Dox
IB: HA
IB:eS10 (S)
IB:eS10 (L)
IB:uS10 (S)
IB:uS10 (L)
IB:p-eIF2α
IB:Ub
IB:Tubulin
Ub

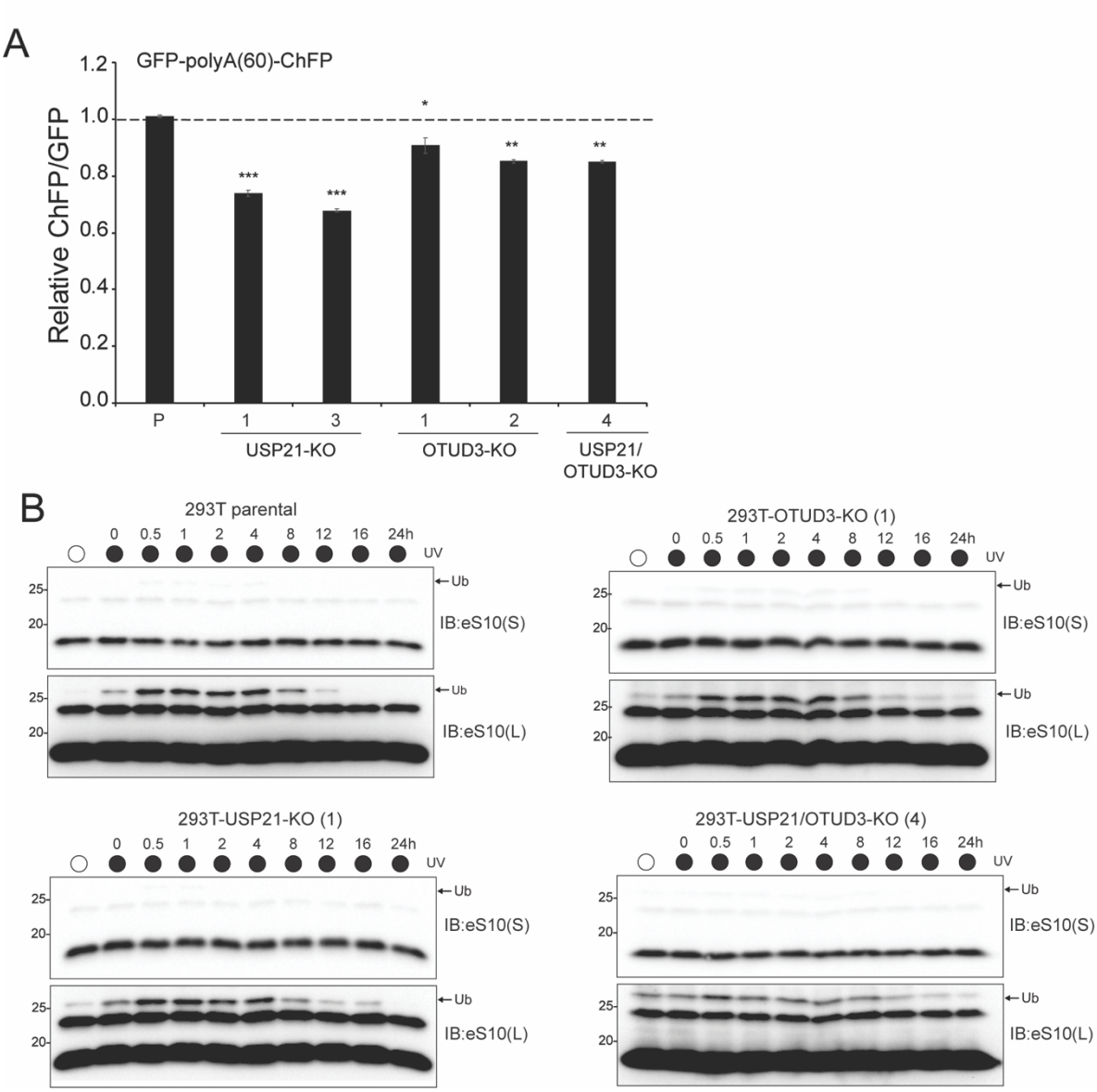

Figure 2.6. Loss of USP21 or OTUD3 expression results in enhanced ribosome stalling on poly(A) sequences and delayed eS10 ubiquitylation following RQC activation.
(A) Parental 293T cells (P), USP21 knock-out (KO) cells, OTUD3-KO cells and the combined double-KO cells were transfected with the poly(A)-stall reporter. Fluorescence intensities were measured by flow cytometry and the relative ChFP:GFP ratio is depicted. Numbers represent distinct knockout clones for OTUD3 or USP21. Error bars denote SEM for triplicate transfections. ***p<0.0001, **p<0.001, *p<0.05 using Student's t-test comparing the different KO clones to the parental control transfection.
(B) Parental 293T cells, USP21-KO (clone 1), OTUD3-KO (clone 1), and USP21/OTUD3 double-KO (clone 4) cells were exposed to UV and allowed to recover for the indicated times. Whole-cell extracts were analyzed by SDS-PAGE and immunoblotted with the indicated antibody. The ubiquitin-modified ribosomal protein is indicated by the arrow. S and L denote short and long exposures (representative immunoblots shown (n=2).

Figure 2.7. OTUD3 preferentially demodifies RQC RRub sites and is present within ribosome enriched fractions.
(A,B) Cells with stable inducible expression of wild type USP21 (A), or OTUD3 (B) were induced or uninduced with doxycycline (2μg/ml) for 16 hours and then treated with dithiothreitol (DTT, 5mM) or harringtonine (HTN, 2μg/mL). Whole-cell extracts were analyzed by SDS-PAGE and immunoblotted using the indicated antibodies. The ubiquitin-modified ribosomal protein is indicated by the arrow. S and L denote short and long exposures (n=1).
(C,D) Cells with stable inducible expression of wild type OTUD3 or USP21 were induced or uninduced and then treated with anisomycin (ANS, 5μg/ml) for the indicated times. Ribosomes were pelleted through a sucrose cushion and whole-cell extracts (input) and pelleted material were analyzed by SDS-PAGE and immunoblotted using the indicated antibodies. The ubiquitin-modified ribosomal protein is indicated by the arrow. S and L denote short and long exposures (n=1).
(E) Cells with stable inducible expression of wild type OTUD3 were induced for 16 hours followed by ANS (5μg/ml) treatment for 1 hour. Whole-cell extracts were separated by sucrose density gradient centrifugation and fractions were collected. The UV absorbance across the fractions is depicted above the immunoblots. Individual fractions were TCA precipitated and analyzed by SDS-PAGE and immunoblotted using the indicated antibodies. The ubiquitin-modified ribosomal protein is indicated by the arrow. S and L denote short and long exposures (n=1).

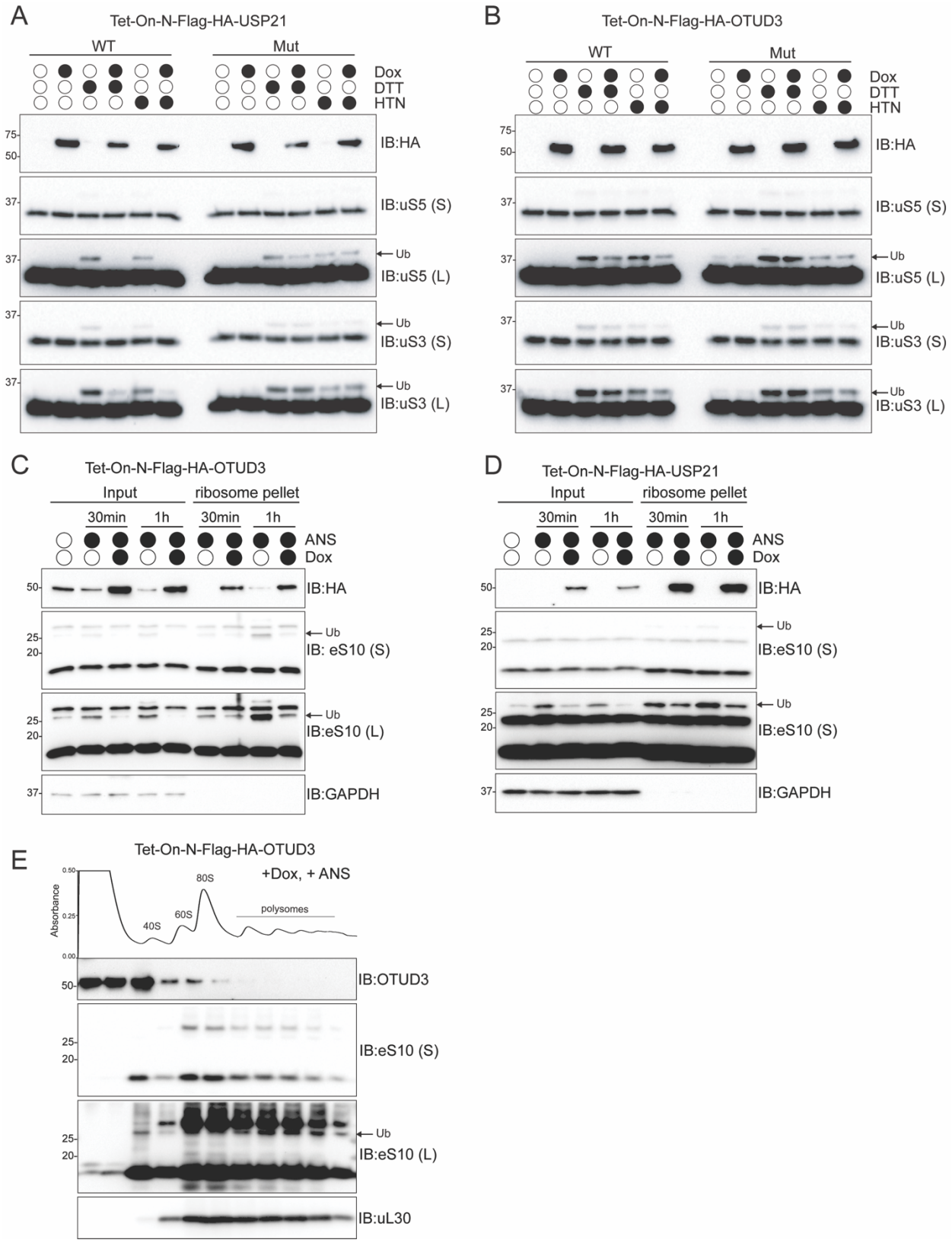
A
Tet-On-N-Flag-HA-USP21
WT
Mut
Dox
DTT
HTN
IB:HA
IB:uS5 (S)
Ub
IB:uS5 (L)
IB:uS3 (S)
IB:uS3 (L)
B
Tet-On-N-Flag-HA-OTUD3
C
Tet-On-N-Flag-HA-OTUD3
Input
ribosome pellet
30min
1h
ANS
IB: eS10 (S)
IB:eS10 (L)
IB:GAPDH
D
Tet-On-N-Flag-HA-USP21
E
Tet-On-N-Flag-HA-OTUD3
+Dox, + ANS
Absorbance
40S
60S
80S
polysomes
IB:OTUD3
IB:uL30

2.10 Supplemental Figures

Figure 2.8. Quantification of site-specific RRub demodification upon exposure to stress.
(A,B) The amount of ubiquitylated eS10 (red line) and uS10 (blue dashed line) and unmodified eS10 (black column) and uS10 (grey column) in the indicated cell lines after the indicated treatments compared to untreated cells quantified from immunoblots in Figure 2A,B.
(C,D) The amount of ubiquitylated uS3 (red line) and unmodified uS3 (black column) and uS5 (grey column) after the indicated treatments compared to untreated cells quantified from immunoblots in Figure 2C,D.
(E) Whole cell extracts from individual clones of HCT116 uS10 knock-in (KI) cells or control parental (par) HCT116 cells exposed to UV were analyzed by SDS-PAGE and immunoblotted with the indicated antibodies. The ubiquitin-modified ribosomal protein is indicated by the arrow (n=1).
(F) HCT116 eS10 knock-in cells or control parental (par) HCT116 cells were exposed to increasing doses of UV radiation. Whole cell extracts were analyzed by SDS-PAGE and immunoblotted with the indicated antibodies. The ubiquitin-modified ribosomal protein is indicated by the arrow. S and L denote short and long exposures (n=1).
(G) The ChFP:GFP ratio from HCT116 parental, eS10-KI, uS10-KI, uS5-KI and uS3-KI cells transfected with the poly(A)-stall reporter plasmid relative to parental cells. Error bars denote SEM for triplicate transfections.

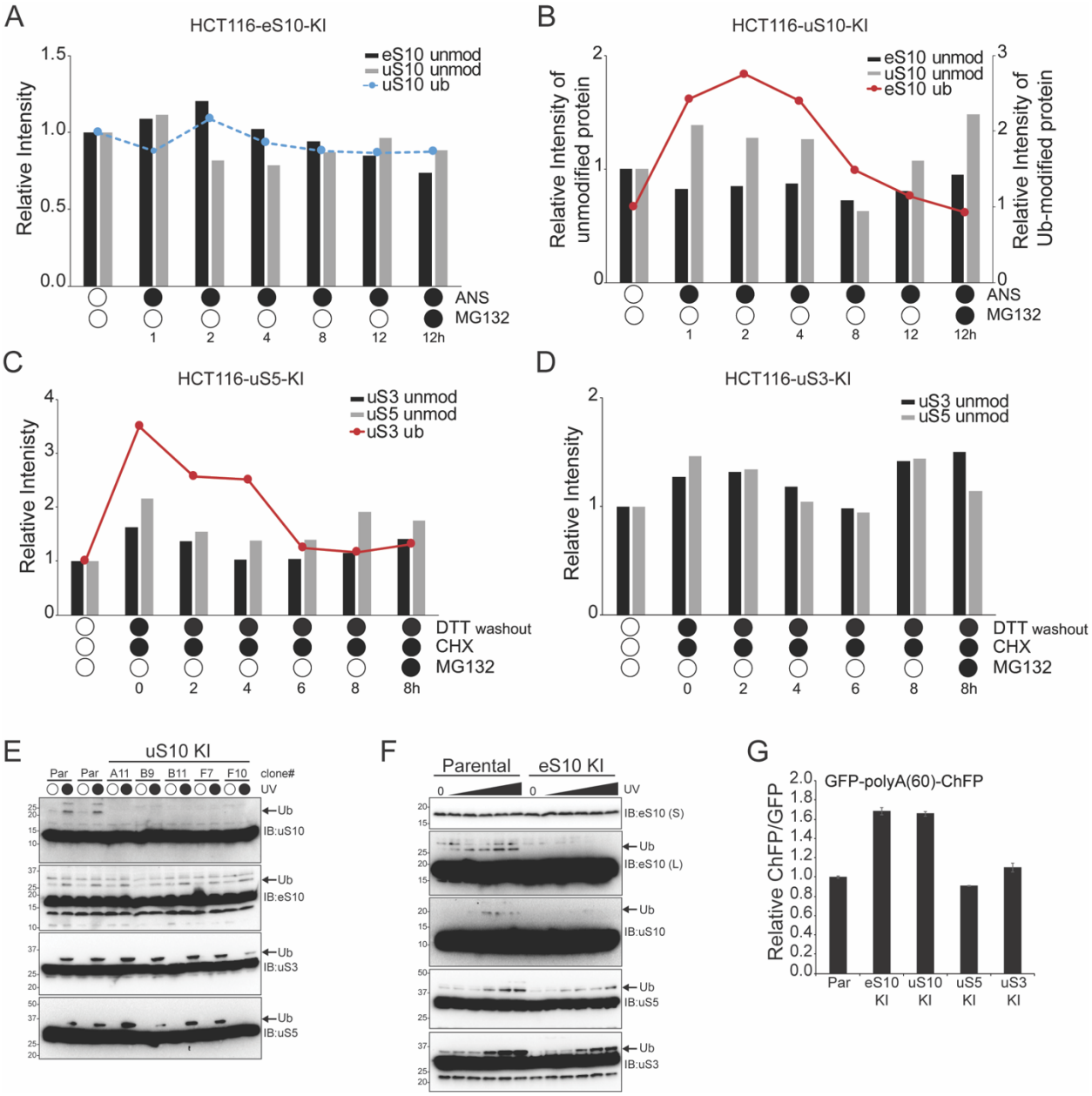
A
HCT116-eS10-KI
Relative Intensity
eS10 unmod
uS10 unmod
uS10 ub
ANS
MG132
1
2
4
8
12
12h
B
HCT116-uS10-KI
Relative Intensity of unmodified protein
Relative Intensity of Ub-modified protein
eS10 unmod
uS10 unmod
eS10 ub
ANS
MG132
C
HCT116-uS5-KI
Relative Intenisty
uS3 unmod
uS5 unmod
uS3 ub
DTT washout
CHX
MG132
0
2
4
6
8
8h
D
HCT116-uS3-KI
Relative Intensity
uS3 unmod
uS5 unmod
E
uS10 KI
Par
A11
B9
B11
F7
F10
clone#
UV
Ub
IB:uS10
IB:eS10
IB:uS3
IB:uS5
F
Parental
eS10 KI
IB:eS10 (S)
IB:eS10 (L)
G
GFP-polyA(60)-ChFP
Relative ChFP/GFP
Par
eS10 KI
uS10 KI
uS5 KI
uS3 KI

Figure 2.9. Validation of human Dub expression plasmids.
(A) Whole-cell extracts from cells transiently transfected with the indicated Myc-tagged Dub expression plasmids were analyzed by SDS-PAGE and immunoblotted with the indicated antibodies. S and L denote short and long exposures (representative immunoblots (n=2)).

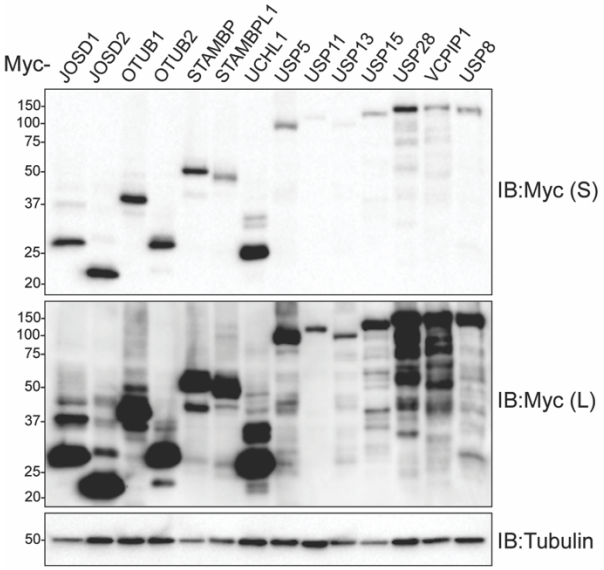
Myc-
JOSD1
JOSD2
OTUB1
OTUB2
STAMBP
STAMBPL1
UCHL1
USP5
USP11
USP13
USP15
USP28
VCPIP1
USP8
150
100
75
50
37
25
20
IB:Myc (S)
IB:Myc (L)
IB:Tubulin

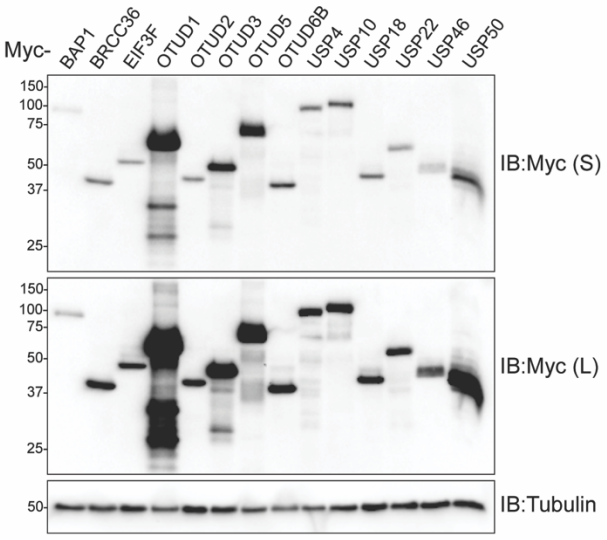
Myc-
BAP1
BRCC36
EIF3F
OTUD1
OTUD2
OTUD3
OTUD5
OTUD6B
USP4
USP10
USP18
USP22
USP46
USP50
150
100
75
50
37
25
IB:Myc (S)
IB:Myc (L)
IB:Tubulin

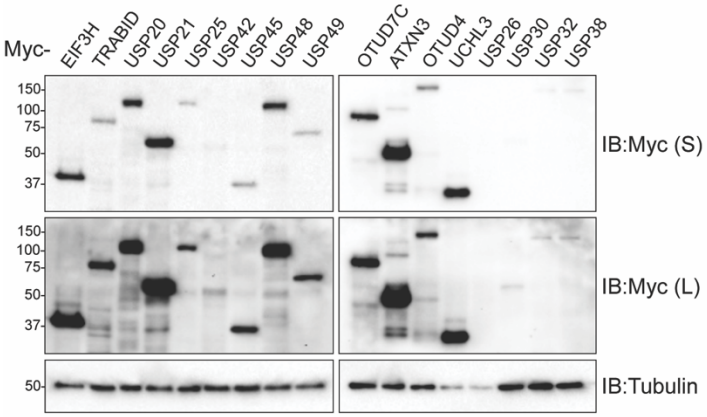
Myc-
EIF3H
TRABID
USP20
USP21
USP25
USP42
USP45
USP48
USP49
OTUD7C
ATXN3
OTUD4
UCHL3
USP26
USP30
USP32
USP38
150
100
75
50
37
IB:Myc (S)
IB:Myc (L)
IB:Tubulin

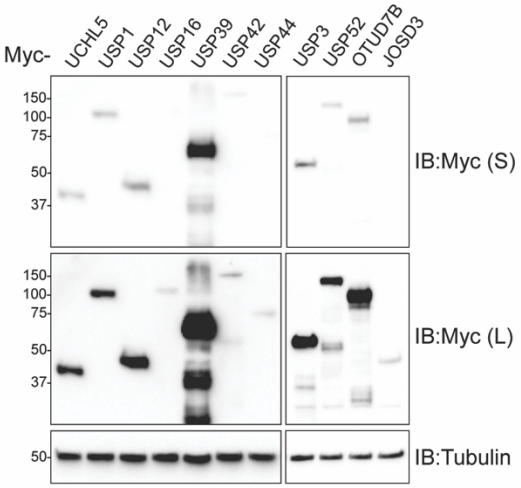
Myc-
UCHL5
USP1
USP12
USP16
USP39
USP42
USP44
USP3
USP52
OTUD7B
JOSD3
150
100
75
50
37
IB:Myc (S)
IB:Myc (L)
IB:Tubulin

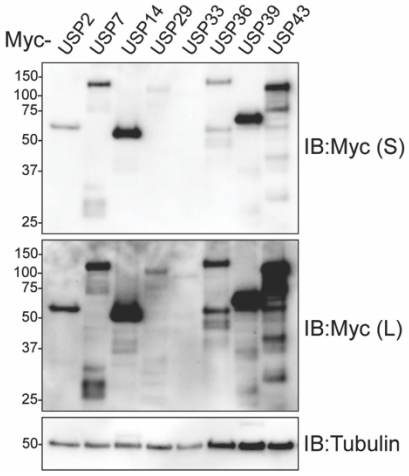
Myc-
USP2
USP7
USP14
USP29
USP33
USP36
USP39
USP43
150
100
75
50
37
25
IB:Myc (S)
IB:Myc (L)
IB:Tubulin

Figure 2.10. OTUD3 and USP21 enhance poly(A)-stall readthrough in a non-synergistic and ZNF598 dependent manner.
(A) The ChFP:GFP ratio from 293T cells transfected with the poly(A)-stall reporter plasmid and expression plasmids for USP21, OTUD3 or wild type ZNF598 alone (black circle) or with twice the amount of an individual expression plasmid (blue circle) relative to control transfection. Error bars denote SEM for triplicate transfections.
(B) The ChFP:GFP ratio from ZNF598 knock-out (KO) cells transfected with the indicated expression plasmids and the poly(A)-stall reporter. Wild type (black circles) or inactive (grey circles) versions of each candidate Dub, ZNF598 or control plasmid is indicated. Error bars denote SEM for triplicate transfections.
(C,D) Whole-cell extracts from cells transfected as indicated in Figure 4F and G were analyzed by SDS-PAGE and immunoblotted for the indicated.

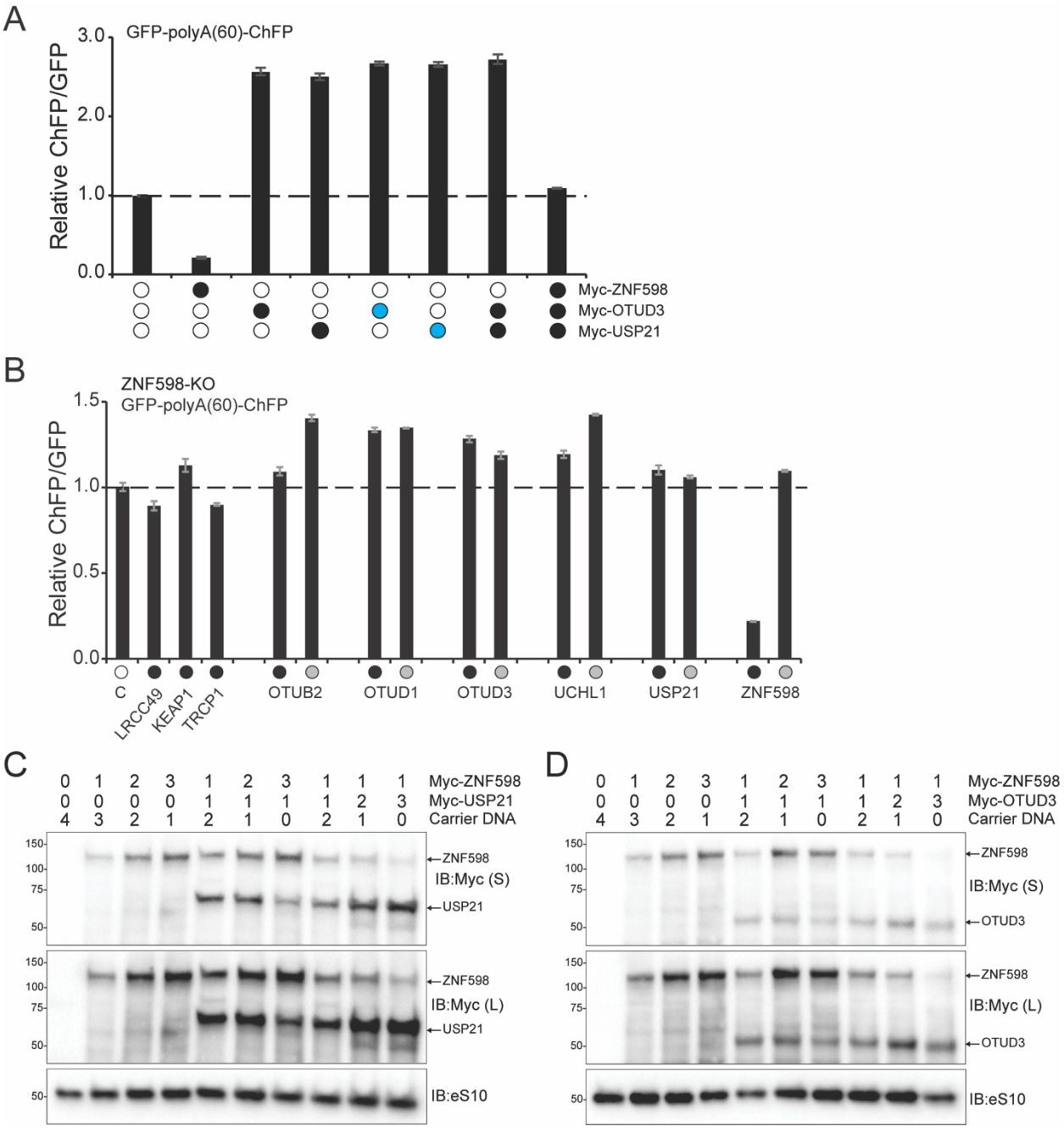
A
GFP-polyA(60)-ChFP
Relative ChFP/GFP
3.0
2.0
1.0
0.0
Myc-ZNF598
Myc-OTUD3
Myc-USP21
B
ZNF598-KO
GFP-polyA(60)-ChFP
Relative ChFP/GFP
1.5
1.0
0.5
0.0
C
LRCC49
KEAP1
TRCP1
OTUB2
OTUD1
OTUD3
UCHL1
USP21
ZNF598
C
Myc-ZNF598
Myc-USP21
Carrier DNA
IB:Myc (S)
IB:Myc (L)
IB:eS10
ZNF598
USP21
D
Myc-ZNF598
Myc-OTUD3
Carrier DNA
IB:Myc (S)
IB:Myc (L)
IB:eS10
ZNF598
OTUD3

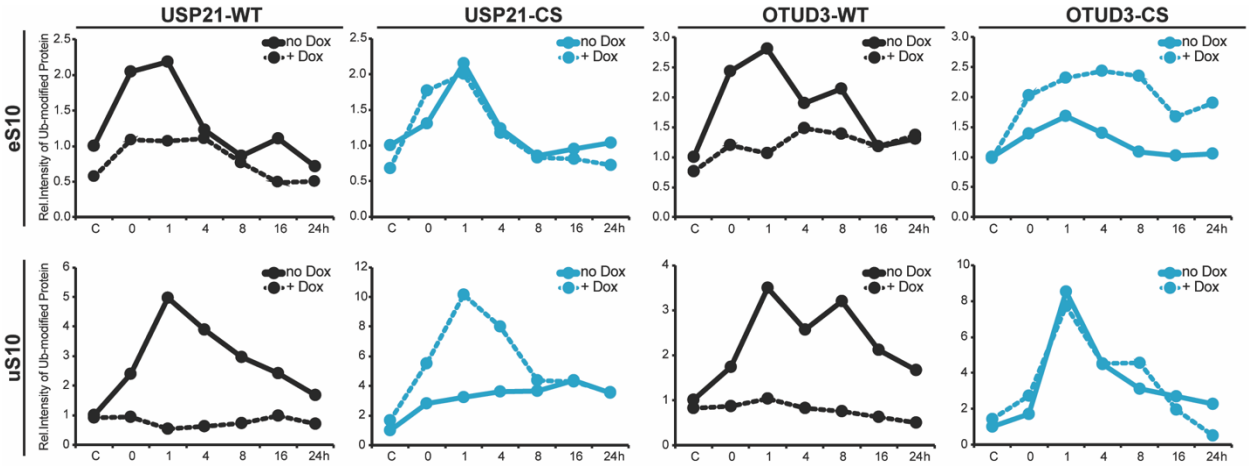

Figure 2.11. Quantification of site-specific RRub demodification upon Dub overexpression.
(A) Quantification of the relative amount of ubiquitylated eS10 and uS10 during the UV treatment time course from the immunoblots in Figure 5A-D.

Figure 2.12. **Knockdown of OTUD3 or USP21 does not result in enhanced resolution of poly(A)-induced RQC.**
(A) Whole-cell extracts from USP21 knockout (KO), OTUD3 KO, or USP21/OTUD3 double KO cell lines were generated and analyzed by SDS-PAGE and immunoblotted with the indicated antibodies. The numbers represent individual cell line clones. The band for USP21 is indicated by the arrow. S and L denote short and long exposures (representative immunoblots of n=2 independent experiments).
(B) Quantification of the percent modification of eS10 during the UV treatment time course from the immunoblots in Figure 6B.
(C) The ChFP:GFP ratio from cells transfected with either control siRNA oligos or siRNA oligos targeting OTUD3, USP21 or ZNF598 followed by poly(A)-stall reporter transfection. Numbers represent distinct siRNA oligos used to target OTUD3 or USP21. Error bars denote SEM for triplicate transfections.
(D) Parental 293T (top) or inducible 293 cells expressing Flag-HA-tagged USP21 (bottom) were transfected with either control siRNA oligos or three separate siRNA oligos targeting USP21 or OTUD3. Whole-cell lysates were analyzed by SDS-PAGE and immunoblotted with the indicated antibodies (n=1).
(E) The ChFP:GFP ratio from cells transfected with control siRNA oligos or siRNA oligos targeting USP21, OTUD3, or ZNF598 as indicated followed by poly(A)-stall reporter transfection. Error bars denote SEM for triplicate transfections. **p<0.001, *p<0.01, using Student's t-test comparing the different siRNA knockdowns or wild type ZNF598 overexpression to control siRNA.
(F) The ChFP:GFP ratio from cells transfected with control siRNA oligos or siRNA oligos targeting OTUB2, OTUD1, OTUD3, USP21 or ZNF598 individually or in combination followed by poly(A)-stall reporter transfection. Error bars denote SEM for triplicate transfections.
(G) The ChFP:GFP ratio from cells transfected with control siRNA oligos or pools of siRNA oligos (4 oligos each) targeting 24 individual Dubs or ZNF598 followed by poly(A)-stall reporter transfection. Error bars denote SEM for triplicate transfections.

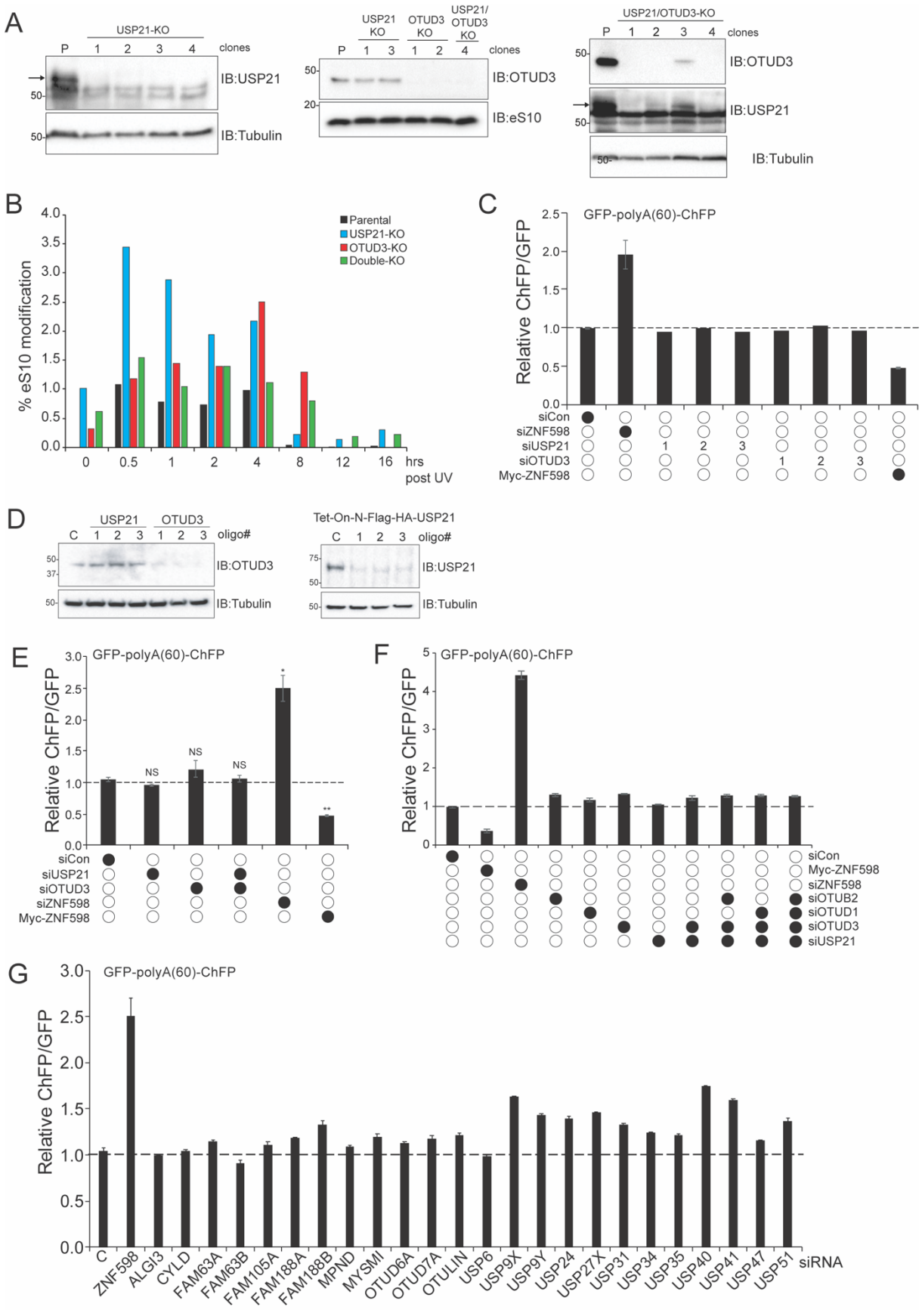
A
USP21-KO
P 1 2 3 4 clones
IB:USP21
IB:Tubulin
USP21 KO
OTUD3 KO
USP21/ OTUD3 KO
P 1 3 1 2 4 clones
IB:OTUD3
IB:eS10
USP21/OTUD3-KO
P 1 2 3 4 clones
IB:OTUD3
IB:USP21
IB:Tubulin
B
% eS10 modification
Parental
USP21-KO
OTUD3-KO
Double-KO
0 0.5 1 2 4 8 12 16 hrs post UV
C
GFP-polyA(60)-ChFP
Relative ChFP/GFP
siCon
siZNF598
siUSP21
siOTUD3
Myc-ZNF598
D
USP21 OTUD3
C 1 2 3 1 2 3 oligo#
IB:OTUD3
IB:Tubulin
Tet-On-N-Flag-HA-USP21
C 1 2 3 oligo#
IB:USP21
IB:Tubulin
E
GFP-polyA(60)-ChFP
Relative ChFP/GFP
NS
NS
NS
*
**
siCon
siUSP21
siOTUD3
siZNF598
Myc-ZNF598
F
GFP-polyA(60)-ChFP
Relative ChFP/GFP
siCon
Myc-ZNF598
siZNF598
siOTUB2
siOTUD1
siOTUD3
siUSP21
G
GFP-polyA(60)-ChFP
Relative ChFP/GFP
C ZNF598 ALG13 CYLD FAM63A FAM63B FAM105A FAM188A FAM188B MPND MYSM1 OTUD6A OTUD7A OTULIN USP6 USP9X USP9Y USP24 USP27X USP31 USP34 USP35 USP40 USP41 USP47 USP51
siRNA

Chapter 3

iRQC, a surveillance pathway for 40S ribosomal quality control during mRNA translation initiation

3.1 Summary

Post-translational modification of ribosomal proteins enables rapid and dynamic regulation of protein biogenesis. Site-specific ubiquitylation of 40S ribosomal proteins uS10 and eS10 plays a key role during ribosome-associated quality control. Distinct, and previously functionally ambiguous ubiquitylation events on the 40S proteins uS3 and uS5 are induced by diverse proteostasis stressors that impact translation activity. Here, we identify the ubiquitin ligase, RNF10, and the deubiquitylating enzyme, USP10, as the key enzymes that regulate uS3 and uS5 ubiquitylation. Prolonged uS3 and uS5 ubiquitylation results in 40S, but not 60S, ribosomal protein degradation in a manner independent of canonical autophagy. We show that blocking progression of either scanning or elongating ribosomes past the start codon triggers site-specific ribosome ubiquitylation events on uS5 and uS3. This study identifies and characterizes a distinct arm in the RQC pathway, initiation RQC (iRQC), that acts on 40S ribosomes during translation initiation to modulate translation activity and capacity.

3.2 Introduction

Translation is the critical process that decodes the genetic blueprint into functional proteins. While most translation events terminate in successful protein biogenesis, cis-acting features of the mRNA or nascent chain can result in abortive translation termination (Hinnebusch et al., 2016). Defects in either the emerging nascent polypeptide or translating mRNA can cause ribosomes to experience prolonged stalls during elongation which can subsequently result in 80S ribosome collisions and elicit a multifaceted ribosome-associated

quality control (RQC) pathway (Inada, 2020; Joazeiro, 2019; Yip and Shao, 2021). Components of the RQC act to degrade the truncated nascent chain, destroy the associated mRNA, and recycle the ribosomal subunits (Joazeiro, 2019; Meydan and Guydosh, 2020). Current models suggest that ribosome collisions are the integral first signal necessary to recruit factors that facilitate downstream RQC activities (D'Orazio and Green, 2021; Ikeuchi et al., 2019; Juszkiewicz et al., 2018b; Simms et al., 2017). Protein ubiquitylation plays two critical roles during mammalian RQC. The first involves conserved regulatory ribosomal ubiquitylation (RRub) of 40S proteins eS10 (RPS10) and uS10 (RPS20) mediated by the E3 ligase ZNF598 (Garzia et al., 2017; Juszkiewicz and Hegde, 2017; Sundaramoorthy et al., 2017). The second involves additional ligases, Listerin and the recently described CRL2/KLHDC10 and Pirh2 ligases, which are recruited to the 60S subunit, post-80S ribosome splitting, to catalyze nascent polypeptide chain ubiquitylation and subsequent degradation (Lyumkis et al., 2014; Shao and Hegde, 2014; Shao et al., 2013; Thrun et al., 2021). While these ubiquitylation events are well characterized, additional sites of ribosome ubiquitylation in mammals and other eukaryotes have been described that either play a direct role within the RQC (Ikeuchi et al., 2019; Saito et al., 2015) or operate outside of the RQC and have uncharacterized roles (Higgins et al., 2015; Montellese et al., 2020; Silva et al., 2015), suggesting ribosome ubiquitylation may regulate multiple steps during translation.

Dynamic feedback regulation between elongation and initiation meters ribosome traffic along mRNAs. Elevation in RQC activity due to increases in elongating ribosome collisions can indicate an overabundance of ribosome density on transcripts. Compensatory decreases in translation initiation rates can reduce ribosome collisions and RQC activity (Juszkiewicz et al., 2018b). Further, recent studies have defined a collision-induced feedback loop that downregulates translation initiation. Following ribosome collisions, in a ZNF598-independent manner, the collision-sensor EDF1 recruits the translation repressors GIGYF2 and 4EHP to inhibit translation of stall-inducing transcripts (Juszkiewicz et al., 2020a; Sinha et al., 2020). A

separate study also demonstrated that the same translation repressors, GIGYF2 and 4EHP, when deleted, increased translation of a stall-inducing reporter (Hickey et al., 2020). These studies highlight the requirement for dynamic coordination between elongation and initiation rates to regulate elongation collision frequency. While elongating ribosome collisions and the corresponding RQC pathway have been well-established, a quality control pathway that acts on ribosomes during the initiation phase of translation has not been described.

Here we identify a surveillance pathway, iRQC, in which regulatory ribosomal ubiquitylation of distinct residues within the 40S proteins uS3 (RPS3) and uS5 (RPS2) promotes 40S subunit degradation. We identify and characterize the ubiquitin ligase RNF10, and the deubiquitylating enzyme, USP10 as the key ubiquitin pathway enzymes that regulate uS5 and uS3 ribosomal ubiquitylation. Loss of USP10 function or RNF10 overexpression resulted in enhanced uS5 and uS3 ubiquitylation in the absence of exogenous stressors. We show that prolonged uS3 and uS5 ubiquitylation induces selective degradation of 40S, but not 60S ribosomal proteins in a manner that is independent of the canonical autophagy pathway. Several pharmacological agents that act to repress translation initiation, including integrated stress response activators, also induce RNF10-dependent uS3 and uS5 ubiquitylation. These results indicate that stalled or otherwise defective scanning preinitiation complexes may be targeted by RNF10-dependent ubiquitylation to mediate 40S destruction. Our results establish parallel, but distinct, RQC pathways that act on ribosomes during the elongation (eRQC) or initiation (iRQC) phases of translation.

3.3 Results

3.3.1 RNF10 catalyzes uS5 and uS3 ubiquitylation

Previous studies have documented dynamic ubiquitylation of a variety of ribosomal proteins suggesting the ubiquitylation may be used to regulate ribosome function beyond the

conical RQC pathway (Higgins et al., 2015; Montellese et al., 2020; Silva et al., 2015). We had previously demonstrated that either pharmacological translation inhibition or integrated stress response (ISR) activation results in robust uS3 (RPS3) and uS5 (RPS2) ubiquitylation (Higgins et al., 2015). Because these ubiquitylation events are not catalyzed by ZNF598 and do not function within the characterized RQC pathway (Garshott et al., 2020), how uS3 and uS5 ubiquitylation regulates ribosome function remained unknown.

In order to determine the molecular role(s) uS3 and uS5 ubiquitylation play during translation, we set out to identify the ubiquitin pathway enzymes that regulate uS3 and uS5 ubiquitylation. We utilized an siRNA-based loss-of-function screen targeting 18 known RNA-associated ubiquitin ligases and found that only depletion of RNF10 reproducibly prevented uS3 and uS5 ubiquitylation (Figures 3.1A and 3.8A-E). We then generated and verified RNF10 knockout cells using CRISPR-Cas9-based approaches and demonstrated that these cells completely lacked both ISR (DTT) or elongation inhibition (anisomycin, ANS)-induced uS3 and uS5 ubiquitylation (Figure 3.1B). To investigate the specificity of RNF10, we examined uS5, uS3, eS10, and uS10 ubiquitylation in 293 Flp-IN cells expressing inducible wild type RNF10. In the same manner that ZNF598 is specific in modifying eS10 and uS10 (Juszkiewicz and Hegde, 2017; Sundaramoorthy et al., 2017), RNF10 expression, in the absence of stress, resulted in enhanced uS3 and uS5 ubiquitylation but left eS10 and uS10 ubiquitylation largely unchanged (Figure 3.1C). Furthermore, in vitro ubiquitylation assays demonstrated that RNF10 maintains its ribosomal protein specificity when incubated with purified 40S subunits (Figures 3.1D and 3.8F). Collectively, these findings demonstrate that RNF10 is both necessary and sufficient to catalyze uS3 and uS5 ubiquitylation.

What is the fate of the ubiquitylated 40S? To begin to address this question, we utilized an RNF10 overexpression system where we transiently overexpressed either wild type RNF10, or a catalytically inactive mutant (C225S) in RNF10 knockout (KO) cells to enhance uS5 and uS3 ubiquitylation both at basal conditions and upon conditions that enhance uS3 and uS5

ubiquitylation. Expression of wild type, but not inactive RN10, rescued the ability to ubiquitylate uS3 and uS5 with or without DTT treatment (Figure 3.1E). Combining RNF10 overexpression with DTT treatment resulted in enhanced uS3 and uS5 ubiquitylation with more than 40% of total uS3 being ubiquitylated (Figures 3.1E,F). Notably, total uS3 and uS5 protein abundance was also reduced upon RNF10 overexpression with and without DTT treatment (Figures 3.1E,F). This result suggests the RNF10-catalyzed 40S ubiquitylation acts to reduce 40S protein levels. Utilizing a panel of ISR and elongation inhibitors, we observed that RNF10 overexpression further heightened uS3 and uS5 ubiquitylation while having no additional effect on eS10 or uS10 modification (Figures 3.1F and 3.8G). Because RNF10 overexpression, in the absence of stressors, induced uS5 and uS3 ubiquitylation, we hypothesized that the ribosomal species that is targeted by RNF10 is present under normal proliferative conditions and that the extent of ribosomal ubiquitylation may be limited by the cellular concentration of RNF10.

3.3.2 USP10 antagonizes RNF10-dependent uS3 and uS5 ubiquitylation

Our demonstration that RNF10 overexpression can stimulate uS3 and uS5 ubiquitylation at steady state argued that robust deubiquitylating activity antagonizes RNF10 ribosomal ubiquitylation. We serendipitously identified USP10 as the deubiquitylating enzyme responsible for removing ubiquitin from uS3 and uS5 while identifying and characterizing deubiquitylating enzymes that antagonize ZNF598 (Figure 3.9A) (Garshott et al., 2020). A recent study also identified USP10 as a ribosomal deubiquitylating enzyme (Meyer et al., 2020). Consistent with this previous work, USP10 knockout (KO) cells display constitutively high levels of not only ubiquitylated eS10 and uS10, but also ubiquitylated uS3 and uS5 (Figure 3.2A) (Meyer et al., 2020). These modifications were not further induced upon translation elongation inhibition (harringtonine, HTN), suggesting that loss of USP10 results in maximal uS3 and uS5 ubiquitylation which cannot be further augmented by the stressors used here (Figure 3.2A). Similarly, treatment with ISR agonists or high dose elongation inhibitors did not further elevate uS3 and uS5 ubiquitylation in USP10-KO cells (Figure 3.2B). These observations suggest that

excess levels of USP10 relative to RNF10 maintain low levels of ribosomal ubiquitylation at basal conditions. In agreement with this, exogenous USP10 overexpression resulted in a loss of observable ribosomal ubiquitylation that was largely dependent upon the deubiquitylating activity of USP10 (Figure 3.2A). Surprisingly, in USP10-KO cells, stress-induced uS3 and uS5 ubiquitylation decreased at later timepoints (Figure 3.2B). Because these cells lack the principle uS3 and uS5 deubiquitylating enzyme, the observed loss of ribosomal ubiquitylation was puzzling.

3.3.3 RNF10-mediated ribosome ubiquitylation acts post-translationally to reduce 40S abundance

We surmised that the observed loss in uS5 and uS3 ubiquitylation upon protein synthesis inhibition was due to protein degradation in the absence of new protein production. To examine this possibility, we overexpressed RNF10 in the presence and absence of USP10, followed by ISR activation (Figure 3.2C). RNF10 overexpression in parental cells resulted in robust uS3 and uS5 ubiquitylation and an obvious reduction in overall uS3 and uS5 protein levels in DTT-treated cells overexpressing RNF10 (Figure 3.2C). This reduction of protein levels was evident when summing the intestines of both the ubiquitylated and unmodified forms of uS3 and uS5 (which is what is reported as total levels in all figures) indicating that the loss in total protein levels was not merely due to the increase in the amount of ubiquitylated uS3 and uS5. These observations were further enhanced when we overexpressed RNF10 in USP10 knockout cells, both at steady state and following stress induction (Figure 3.2C). Additionally, total protein levels for both eS10 and uS10 are also reduced, as observed via immunoblotting, upon RNF10 overexpression (Figures 3.9B,C). In contrast, levels of the 60S subunit protein uL30 (RPL7) were unchanged upon RNF10 overexpression in either parental or USP10-KO cells (Figures 3.2C and 3.9C). To examine if RNF10 expression suppressed ribosomal gene transcription, we measured uS3, eS6 (RSP6), or uL30 mRNA abundance in cells overexpressing RNF10. RNF10

overexpression did not decrease mRNA abundance, consistent with a post-transcriptional mechanism underlying the observed reduction in 40S protein levels (Figure 3.9D). Taken together, these results suggest that the abundance of 40S, but not 60S, ribosomal proteins is decreased upon conditions that result in constitutively high levels of uS3 and uS5 ubiquitylation.

To determine if the observed reduction in 40S protein levels occurred due to lower mRNA translation, we used a metabolic pulse labeling approach: heavy SILAC-labeled cells were switched to the light label and ribosomal protein synthesis was followed over time by quantitative proteomics. Global protein synthesis rates were unaltered in USP10 KO cells whereas a small but significant increase occurred in the rate of 40S, but not 60S, protein synthesis (Figure 3.9E). RNF10 overexpression suppressed global protein synthesis rates, consistent with observations that RNF10 overexpression reduces cellular proliferation rates. Despite this decrease in overall protein synthesis, 40S protein synthesis rates were increased in cells overexpressing RNF10 relative to 60S or total protein synthesis rates (Figure 3.9E). These results indicate that the observed selective reduction in 40S compared to 60S protein levels when uS3 and uS5 ubiquitylation is enhanced is not due to a decrease in 40S protein synthesis.

3.3.4 Constitutive uS5 and uS3 ubiquitylation results in 40S protein degradation

To examine if enhanced uS3 and uS5 ubiquitylation more broadly impacts overall 40S ribosomal protein abundance, we used SILAC-based quantitative proteomics to compare ribosome protein levels between parental cells and RNF10-KO, USP10-KO, USP10/RNF10 double knockout cells, or cells overexpressing RNF10. RNF10-KO cells had comparable 40S and 60S protein levels to parental cells, whereas RNF10 overexpression resulted in a ~17% reduction in 40S ribosomal protein abundance while modestly increasing 60S protein levels (Figure 3.2D; Table S1). Consistent with a previous report, cells lacking USP10 have reduced 40S protein levels (Meyer et al., 2020). Furthermore, 60S protein levels were unchanged relative to parental cells in USP10-KO cells. RNF10 overexpression in USP10-KO cells further reduced 40S protein levels while slightly increasing 60S protein abundance (Figure 3.2D). The

observed decrease in 40S protein abundance in UPS10-KO cells was reversed in RNF10/USP10 double KO cells indicating that RNF10-dependent uS5 and uS3 ubiquitylation promotes 40S protein loss in USP10-KO cells. The abundance of the entire 40S subunit, rather than individual proteins, is reduced upon RNF10 overexpression or USP10 depletion suggesting that overall 40S protein stability is reduced by uS3 and uS5 ubiquitylation (Figure 3.2E; Table S1). These results are consistent with a model where ubiquitylated 40S ribosomal subunits that escape USP10-dependent ubiquitin removal can be targeted for degradation.

3.3.5 40S protein degradation is autophagy independent

Overall, our data indicate that RNF10 overexpression or loss of USP10 function results in 40S degradation. An autophagic mechanism seemed most plausible given that previous studies in *S. cerevisiae* have demonstrated that starvation conditions that inhibit mTOR signaling and stimulate autophagic flux result in enhanced ribosomal turnover by the autophagy pathway (Kraft et al., 2008). While mTOR-dependent degradation of ribosomes via autophagy does not appear to play a large role in regulating ribosomal abundance in mammalian cells (An and Harper, 2018; An et al., 2020), we directly evaluated if uS3 or uS5 ubiquitylation resulted in autophagy-dependent degradation of 40S ribosomal subunits. We first examined uS3 and uS5 protein levels upon RNF10 overexpression in parental or autophagy-deficient cells that are devoid of the critical ULK1 complex member, RB1CC1 (FIP200) (An et al., 2019). USP10 depletion or RNF10 overexpression alone or in combination resulted in the expected increase in uS3 and uS5 ubiquitylation and loss in 40S protein abundance in both parental and RB1CC1 knockout cells (Figure 3.3A). These results establish that cells deficient in canonical autophagy maintain the ability to degrade RNF10 targeted 40S proteins.

To confirm that RNF10-mediated ribosome ubiquitylation does not target 40S proteins for autophagy-dependent degradation, we utilized cell lines in which the genomic loci of uS3 or eL28 (RPL28) were tagged with the pH-sensitive fluorophore, Keima. Consistent with previous reports, inactivation of mTOR signaling enhanced both 40S and 60S flux to lysosomes as

indicated by an increase in the red to green Keima fluorescence (Figure 3.3B) (An and Harper, 2018). This observed enhanced 40S and 60S flux through the autophagy pathway upon mTOR inhibition was inhibited by co-incubation of either SAR405 or Bafilomycin A, both of which inhibit autophagy by distinct mechanisms (Figure 3.3B). Similar to a previous report, transient knockdown of USP10 also resulted in enhanced autophagic flux of both Keima-tagged uS3 and eL28 which was reversed upon BafA treatment (Figure 3.3C) (Meyer et al., 2020). This result was inconsistent with our observation that 40S but not 60S protein levels were reduced in USP10 knockout cells. We note that the observed increase in 40S and 60S flux upon mTOR inhibition observed here, and previously, accounts for a 3% decrease in total ribosome abundance (An and Harper, 2020). The increase in 40S and 60S autophagic flux observed upon transient knockdown of USP10 was less than that observed upon mTOR inhibition suggesting that this level of enhanced flux would be insufficient to reduce ribosome abundance by the ~15% we measured using quantitative proteomics. It is possible that loss of USP10 activity results in a general increase in autophagy that is independent of the ubiquitin-mediated degradation of 40S proteins demonstrated here upon RNF10 overexpression or USP10 depletion. Consistent with this hypothesis, RNF10 overexpression alone, or combined with USP10 knockdown, did not result in an increase in either 40S or 60S ribosomal flux to the lysosome (Figures 3.3D,E), further suggesting that the canonical autophagy pathway is not responsible for the observed robust degradation of ubiquitylated 40S subunits.

3.3.6 RNF10 mediated uS5 ubiquitylation accelerates 40S protein turnover

In order to quantitatively examine 40S and 60S protein degradation, we utilized previously characterized cell lines in which the genomic uS3, uL24 (RPL26), or eL29 (RPL29) loci were tagged with Halo (hereafter called Ribo-Halo) (An et al., 2020). These Ribo-Halo cell lines enable evaluation of ribosomal protein degradation kinetics through fluorescent pulse-chase experiments using fluorescently labeled Halo ligands (Figure 3.4A). Ribo-Halo cells overexpressing a control protein (LRRC49), wild type RNF10, or inactive RNF10 were red-

labeled with a tetramethylrhodamine (TMR) Halo ligand for 1 hour to mark the existing pool of uS3, uL24, or eL29. Following TMR labeling, excess label was washed out and the abundance of the TMR-labeled ribosomal pool was monitored over time by microscopy. Three days post-transfection, cells expressing wild type GFP-RNF10 but not inactive GFP-RNF10CS displayed a marked decrease in cellular uS3-Halo abundance while having no impact on uL24-Halo protein levels (Figure 3.4A). To directly evaluate uS3 protein turnover, we performed pulse-chase experiments upon RNF10 expression and quantified single-cell Ribo-Halo abundance by flow cytometry. Ribo-Halo abundance was initially measured 36 hours post transfection, and ribosome decay was observed following TMR washout for 24 hours. These experiments revealed an increased uS3 turnover rate in cells expressing wild type RNF10 that was not observed in cells expressing a control protein or inactive RNF10 (Figure 3.4B). Consistent with our proteomics results, RNF10 overexpression did not increase turnover of the 60S subunit protein eL29 (Figure 3.4B). Proteasome inhibition, but not autophagy inhibition, delayed the observed loss in uS3-Halo TMR signal 8 hours after TMR washout in cells with RNF10 overexpression (Figure 3.4C). These results indicate that constitutive uS3 and uS5 ubiquitylation enhances 40S, but not 60S, protein degradation.

Our previous studies delineated a hierarchical relationship among uS3 and uS5 ubiquitylation events such that eliminating uS3 ubiquitylation renders uS5 incompetent for ubiquitylation, whereas eliminating uS5 ubiquitylation did not prevent uS3 ubiquitylation (Garshott et al., 2020). Based on these results, we engineered uS3-Halo cell lines to express either wild type or a ubiquitylation deficient mutant version (K54R;K58R) of uS5. Consistent with previous results, stable expression of exogenous uS5 comprised 80% of total uS5 levels (Figure 3.10A). While uS5 ubiquitylation in cells expressing exogenous wild type uS5 remained intact following DTT treatment, uS5 ubiquitylation was absent upon expression of mutant uS5 (Figure 3.10A). We then performed Ribo-Halo pulse-chase experiments in the uS3-Halo cells containing wild type or ubiquitylation mutant uS5. Consistent with previous results, wild type RNF10

overexpression resulted in an 18% decrease in uS3-Halo levels 12 hours post TMR washout in cells expressing wild type uS5, compared to cells expressing a control protein, (Figure 3.4D). However, RNF10 overexpression failed to accelerate uS3 degradation in cells expressing the ubiquitylation deficient version of uS5 (Figure 3.4D). These experiments causally link RNF10-dependent enhanced 40S protein degradation to the observed increase in ribosome ubiquitylation and demonstrate that uS5 ubiquitylation is required for 40S turnover.

3.3.7 Translation initiation inhibition triggers 40S ribosomal ubiquitylation

Our previous observation that cells lacking uS5 or uS3 ubiquitylation sites retained RQC activity suggested that RNF10-mediated ubiquitylation targeted a distinct population of ribosomes than those targeted by ZNF598 during elongation collisions (Garshott et al., 2020). We had previously demonstrated that treating cells with a variety of translation elongation inhibitors effecting distinct steps during the elongation cycle induced uS3 and uS5 ubiquitylation (Higgins et al., 2015). We were particularly intrigued by our observation that Harringtonine, which blocks progression of 80S ribosomes at the start codon without impacting elongating or scanning ribosomes (Fresno et al., 1977), induces uS3 and uS5 ubiquitylation (Higgins et al., 2015). This result suggested that inhibition of either elongation immediately after start codon recognition, or a defect in the ability of scanning preinitiation complexes to transition to elongation competent 80S ribosomes triggered uS3 and uS5 ubiquitylation. Consistent with previous results, HTN treatment resulted in rapid and robust uS5 and uS3 ubiquitylation (Figures 3.5A) (Higgins et al., 2015). Treatment with either HTN or lactimidomycin (LTM), a functionally similar but mechanistically distinct compound (Lee et al., 2012; Schneider-Poetsch et al., 2010), induced uS5 and uS3 ubiquitylation that was detectable after 5 minutes and further increased over time (Figure 3.5B). We then utilized characterized inhibitors that impede the mRNA scanning step of translation initiation to examine if inhibiting progression of preinitiation complexes prior to start codon recognition induces ribosome ubiquitylation. Addition of rocaglates (RocA) (Iwasaki et al., 2016b) or pateamine A (PatA) (Low et al., 2005), which inhibit

the RNA helicase eIF4A and impair mRNA scanning, induced uS5 and uS3 ubiquitylation in a dose dependent manner (Figures 3.5C and 3.11A,B). Combined, these results suggest that impeding early events during the translation cycle generates a ribosomal subpopulation that is targeted by RNF10. One possibility is that terminally stalled preinitiation complexes that cannot transition into 80S elongation complexes are targeted for RNF10-dependend ribosome ubiquitylation. Alternatively, collisions between either multiple 43S preinitiation complexes scanning within the 5'UTR or between scanning preinitiation complexes and a stalled 80S trigger uS5 and uS3 ubiquitylation.

The demonstration that maximal elongation collisions and uS10 and eS10 ubiquitylation occur with low dose, rather than high dose treatment of elongation inhibitors was a critical result establishing that ribosome collisions are the key event leading to ribosomal ubiquitylation and RQC pathway activation (Juszkiewicz et al., 2018b; Simms et al., 2017). To further examine potential differences between ZNF598-targeted elongation collisions and RNF10-targeted ribosome ubiquitylation events that occur upon translation initiation inhibition, we treated cells with increasing concentrations of translation elongation inhibitors. As expected, the ubiquitylation of eS10 ubiquitylation was induced at low CHX concentrations and diminished at high concentrations (Figure 3.5D). In contrast, uS3 and uS5 ubiquitylation increased with increasing CHX concentration and uS3 and uS5 ubiquitylation remained induced at the highest doses of CHX which failed to stimulate eS10 ubiquitylation (Figure 3.5D). This observation that uS3 and uS5 ubiquitylation is stimulated by high concentrations of elongation inhibitors suggests that inhibition of elongation shortly after start codon recognition, which would be more prevalent at higher inhibitor concentrations, elevates the abundance of the ribosomal population targeted by RNF10. Taken together, our results demonstrate that impeding progression of scanning or elongating ribosomes near start codons induces site-specific uS3 and uS5 ribosome ubiquitylation.

3.3.8 ISR activation similarly elicits uS5 and uS3 ubiquitylation in a ternary-complex concentration manner

We previously demonstrated that uS3 and uS5 ubiquitylation occurs upon activation of the integrated stress response (ISR) in an eIF2α phosphorylation-dependent manner (Higgins et al., 2015). These findings are distinct from those observed with HTN, as HTN treatment enhances uS3 and uS5 ubiquitylation in cells with compromised eIF2α phosphorylation (Higgins et al., 2015). ISR stimulated eIF2α phosphorylation inhibits translation initiation through depletion of the ternary complex (TC), which consists of methionyl-initiator tRNA (Met-tRNAi) and guanosine triphosphate (GTP)–bound eIF2 (Costa-Mattioli and Walter, 2020b; Hinnebusch, 2014). It was initially puzzling why stressors that reduce translation initiation activity would result in uS3 and uS5 ubiquitylation if stalled preinitiation complexes or early elongating 80S ribosomes are needed to trigger ribosome ubiquitylation. One explanation would be that ISR activation also induces stalled preinitiation complexes or otherwise defective scanning ribosomes. We noticed that distinct ISR agonists increased uS3 and uS5 ubiquitylation to varying degrees, with those inducing low levels of eIF2α phosphorylation resulting in higher uS3 and uS5 ubiquitylation (Figures 3.6A and 3.10C). Notably, high concentration sodium arsenite (NaAsO2) treatment resulted in the greatest extent of eIF2α phosphorylation, but poorly stimulated uS3 or uS5 ubiquitylation (Figures 3.6A and 3.11C).

We reasoned that high stoichiometry eIF2α phosphorylation would reduce stalled preinitiation complexes by completely depleting GTP-bound ternary complexes and blocking translation initiation. In contrast, ISR agonists that induce low levels of eIF2α phosphorylation may allow for loading of scanning preinitiation complexes with GTP-bound ternary complexes that are unable to reacquire ternary complex due to reduced, but not ablated TC levels, upon encountering and translating upstream open reading frames (uORFs) (Hinnebusch et al., 2016). Thus, upon completion of uORF translation, scanning ribosomes that maintain engagement with

mRNAs after uORF termination that cannot reacquire ternary complex may progress past downstream start codons and become terminally stalled. To test if low stoichiometry eIF2α phosphorylation induces a ribosomal population that is targeted for RNF10-depedent ubiquitylation, we treated cells with a range of sodium arsenite concentrations and quantified uS3 and uS5 ubiquitylation and eIF2α phosphorylation. Arsenite concentrations that induced less than 5% eIF2α phosphorylation resulted in maximal uS3 and uS5 ubiquitylation whereas conditions in which eIF2α was phosphorylated in excess of 40% did not induce ubiquitylation (Figures 3.6B,C). These results are consistent with our hypothesis that ISR activation resulting in low stoichiometry eIF2α phosphorylation results in elevated stalled preinitiation complexes that are targeted for ubiquitylation. Our results demonstrate that distinct, conserved ribosomal ubiquitylation events operate within separate RQC pathways which we classify as elongation RQC (eRQC) and initiation RQC (iRQC).

3.3.9 Sucrose gradient analysis of preinitiation collisions

We next sought to determine if uS3 and uS5 ubiquitylation is enriched within ribosomal populations that may contain elevated levels of stalled translation preinitiation complexes. We initially examined ribosome protein abundance across sucrose gradients from lysates treated with RNaseA. We compared untreated and HTN treated cells and observed that HTN treatment resulted in a noticeable broadening of the canonical 80S monosome peak, with a skew toward the lower density fractions (Figure 3.7A). Immunoblotting revealed that ribosomes with maximal HTN-induced uS3 and uS5 ubiquitylation migrated within fraction 5 which is at the front edge of the traditional monosome peak (Figure 3.7B). Abundant ubiquitylation within the 40S peak, which may also contain individual 43S preinitiation complexes, was also observed. Examination of endogenous RNF10 sedimentation within sucrose gradients revealed RNF10 to be present in fractions containing peak 40S ubiquitylation upon HTN treatment (Figure 3.7B). This result

suggests that RNF10 associates with ribosomes in a manner that is stimulated upon conditions that enhance the abundance of stalled preinitiation complexes.

In addition to HTN treatment, the widening and skewing of the monosome peak was observed in fractionated lysates from cells treated with DTT, PatA, or a moderate dose of NaAsO2, all of which induce uS5 and uS3 ubiquitylation (Figure 3.7C). While the monosome peak presumably contains predominately individual 80S complexes, this peak may also contain mRNAs with multiple loaded preinitiation complexes. According to this hypothesis, we should observe more 40S ribosome proteins relative to 60S proteins within the monosome peak under conditions that stimulate uS3 and uS5 ubiquitylation. We utilized SILAC-based quantitative proteomics to compare the abundance of 40S relative to 60S proteins across the sucrose gradient. Heavy-labeled HTN treated cells were mixed with untreated cells prior to lysis and density centrifugation. Directly comparing ribosome protein ratios revealed the expected increase in both 40S and 60S proteins in monosome-containing sucrose fractions in HTN-treated cells (Figures 3.12A-B; Table S3). We observed a significant increase in the 40S protein ratio compared to 60S in fraction 5, at the leading edge of the monosome peak, when comparing the summed and molecular weight normalized ion intensities from all 40S or 60S ribosomal proteins (Figure 3.7D; Table S3). This result is consistent with the hypothesis that HTN-induces stalled preinitiation complexes which migrate within the canonical monosome fraction in sucrose gradients. RNase treatment also resulted in noticeable deviation from the expected 40S:60S ratio in polysome-containing fractions (Figure 3.7D). Because RNaseA-mediated rRNA degradation may be impacting the integrity of 40S or 60S subunits, we repeated the sucrose gradient analysis without RNase treatment. We observed robust uS3 ubiquitylation throughout the broad HTN-induced monosome peak that was absent in untreated samples (Figures 3.12C-D). Further, we observed an increase in 40S protein abundance relative to 60S only in fraction 5 from HTN-treated cells (Figures 3.7E and 3.12E-F, Table S3). These results

suggest that HTN increases the abundance of stalled preinitiation complexes, which stimulates iRQC pathway activation.

3.4 Discussion

We identify RNF10 and USP10 as the key ubiquitylation enzymes that regulate uS3 and uS5 ubiquitylation and demonstrate that persistent uS3 and uS5 ubiquitylation, surprisingly, triggers 40S but not 60S protein degradation. We further demonstrate that RNF10-dependent ubiquitylation is stimulated by a variety of distinct pharmacological agents that inhibit progression of ribosomes either during mRNA scanning, or shortly after the transition to elongating 80S ribosomes. One possible model is that terminally stalled preinitiation complexes, in isolation, are targeted by RNF10 to promote 40S degradation. However, and similar to early descriptions of how eRQC events are triggered, it is unclear how a terminally stalled preinitiation complex that requires iRQC activity can be differentiated from a slowly scanning or paused, but otherwise functional, preinitiation complex. This quandary was rectified by the demonstration that elongation collisions were the key trigger that stimulates eRQC pathway activation (Juszkiewicz et al., 2018b; Simms et al., 2017). Intriguingly, the uS5 and uS3 ubiquitylation sites are positioned in the vicinity of the uS10 (RPS20) and eS10 (RPS10) ubiquitylation sites that are required for RQC events during elongation collisions (Figure 3.13A) (Ikeuchi et al., 2019; Juszkiewicz et al., 2018b; Juszkiewicz and Hegde, 2017; Matsuo et al., 2017; Sundaramoorthy et al., 2017). As such, it is plausible that preinitiation complex collisions during the mRNA scanning phase of translation initiation trigger uS3 and uS5 ubiquitylation. However, despite similarities with elongation collisions, collisions between preinitiation complexes or between preinitiation complexes and stalled 80S ribosomes at the start codon would contain initiation factors which would likely constitute a unique collision interface.

Currently, our data cannot distinguish between whether isolated terminally stalled preinitiation complexes or preinitiation complex collisions trigger uS3 and uS5 ubiquitylation.

Further biochemical evidence is needed to establish if preinitiation complex collisions occur within cells and if those collisions are targeted by RNF10. However, rapid rates of preinitiation complex loading and scanning relative to translation start would generate queues of potentially collided 43S preinitiation complexes within 5'UTRs. Evidence for such queueing has been demonstrated using in vitro translation systems and translation complex profile sequencing (TCP-seq) in yeast and human cells (Bohlen et al., 2020b; Shirokikh et al., 2019; Sogorin et al., 2012; Wagner et al., 2020a). Further, generating queues of preinitiation complexes using cycloheximide or insertion of an upstream open reading frame (uORF) resulted in alternative start codon utilization and translation recoding (Ivanov et al., 2018; Kearse et al., 2019). Combined, these studies suggest the possibility that preinitiation ribosome collisions occur.

Because RNF10-catalyzed 40S degradation appears to be autophagy-independent, 40S degradation, in a presumably proteasome-dependent manner, would require 40S disassembly prior to degradation. Thus, iRQC-dependent ribosomal degradation appears distinct from the proteasomal degradation of unassembled ribosomal proteins mediated by either Huwe1 or Ube2O (Nguyen et al., 2017; Sung et al., 2016; Yanagitani et al., 2017). We note that while proteasome inhibition does reduce 40S Ribo-Halo decay upon TMR washout (Figure 3.4C), it does so in cells expressing wild type and inactive RNF10 as well as those expressing a control protein. It is possible that the inhibition in cell cycle progression observed upon proteasome inhibition may result in slower cell growth and thus reduced dilution of the Ribo-Halo signal. As such, further experiments are needed to examine possible proteosome-mediated degradation of RNF10-catalyzed ubiquitylated 40S ribosome subunits.

Interestingly, in cells lacking USP10, uS5 and uS3 ubiquitylation reaches 20% of total uS5 and uS3 protein. These levels approach and surpass what has been observed for histone ubiquitylation, the most abundantly, and originally identified, ubiquitylated protein in the cell (Goldknopf and Busch, 1977). The large extent of ribosome ubiquitylation in USP10-KO cells also suggests that preinitiation complexes stall at a high frequency in unstressed, albeit rapidly

dividing, cells and that USP10 rapidly reverses ubiquitylation of these stalled preinitiation complexes. The fact that uS3 and uS5 ubiquitylation is low in cells with USP10 argue that translation activity has evolved to allow for rapid translation initiation rates and the possible subsequent increase in stalled, and possibly collided preinitiation complexes by maintaining an excess of USP10 relative to RNF10 (Nusinow et al., 2020) (Figure 3.13B). Further, controlling the relative USP10:RNF10 ratio would set the threshold for the abundance of stalled scanning 40S ribosomes at steady state while enabling stress-sensitive stall responses. USP10 protein abundance is reported to be in 2-fold excess of RNF10 in HEK293 cells and is often in even greater excess, (e.g. 27-fold in HCT116 cells) in many cell lines and tissues with RNF10 abundance being below detection thresholds (Wang et al., 2015). This data suggests that, under normal growth conditions, deubiquitylation of stalled preinitiation complexes is favored over degradation in most cell types to avoid the energetically costly spurious degradation of 40S subunits. These observations also suggest that, with sufficient USP10 activity, stalled preinitiation complexes can eventually transition into elongating ribosomes (Figure 3.13B).

Similar to eRQC, the iRQC pathway appears to be conserved in single-celled eukaryotes as USP10 and RNF10 orthologs have been shown to regulate uS3 ubiquitylation in *S. cerevisiae* (Jung et al., 2017; Sugiyama et al., 2019). Not only are the enzymes conserved, but so too are the mechanistic requirements: yeast with inactivating mutations in the peptidyl transferase center of ribosomes that allow for scanning, but block elongation, trigger ribosomal RNA decay in a manner dependent upon uS3 ubiquitylation (Sugiyama et al., 2019). The previous study in *S. cerevisiae* concluded that damaged ribosomes were the target of ubiquitylation. It is possible that some of the pharmacological agents used within this study to stimulate uS5 and uS3 ubiquitylation result in damaged and nonfunctional ribosomes. However, given the breadth of stimuli used here, and the observation that loss of USP10 results in enhanced uS3 and uS5 ubiquitylation in the absence of stress, we propose that ribosomal ubiquitylation is triggered by preinitiation complex collisions or singular stalled preinitiation

complexes. Interestingly, and completely opposite to what we observed during mammalian iRQC, the USP10 homolog in *S. cerevisiae,* Ubp3, has also been implicated in regulating 60S, but not 40S, ribosome degradation in an autophagy-dependent manner upon starvation (Kraft et al., 2008). Future studies are needed to disentangle starvation-induced ribophagy from iRQC-mediated 40S degradation as they appear to utilize overlapping components.

We propose that conserved ribosomal ubiquitylation acts as a cellular rheostat to dynamically regulate translation dynamics during conditions that enhance collision frequencies. Accumulating evidence suggests that elongation collisions not only trigger ribosomal subunit recycling, but also reduce translation initiation rates (Meydan and Guydosh, 2020; Vind et al., 2020). Our data suggest a possible model wherein stalled preinitiation complexes trigger ubiquitylation of specific 40S ribosomal proteins and that persistent uS5 and uS3 ubiquitylation results in 40S degradation. It is possible that iRQC could be utilized to globally reset translation initiation rates. As cellular proliferation rates change, for example during cellular differentiation, translation capacity and ribosome abundance may also be altered to match metabolic needs. Our demonstration that ISR-stimulating conditions also induce conditions that stimulate RNF10-dependent uS5 and uS3 ubiquitylation suggests that chronic stress signaling may also reset translation capacity. These findings describe a previously uncharacterized, and likely conserved, distinct ribosome-associated quality control pathway that can be utilized to regulate 40S ribosomal levels.

3.5 Acknowledgments

We thank Jody Puglisi and Alex Johnson (Stanford University) for technical advice and for providing purified ribosomal submits. We also acknowledge Julie Monda, Xuezhen Ge, and Steven Wasserman (UCSD) for editing assistance during manuscript preparation. The graphical abstract and Figure 4A were created with BioRender.com. This research was

supported by funding from the National Institutes for Health (DP2GM119132 (E.J.B.), R01GM136994 (E.J.B.), R01AG011085 (J.W.H.), R01NS083524 (J.W.H.), T32GM007240 (D.M.G.), and the National Science Foundation (DGE-1650112 (D.M.G.)).

3.6 Author contributions

Conceptualization, D.M.G. and E.J.B.; Methodology, D.M.G., H.A., and E.J.B.; Investigation, D.M.G., H.A., E.S., M.L., A.V. and E.J.B.; Visualization, D.M.G., H.A. and E.J.B.; Funding Acquisition, E.J.B and J.W.H.; Supervision, J.W.H., and E.J.B.; Writing- original draft, D.M.G. and E.J.B.; Writing- Review & Editing, D.M.G., H.A., E.S., M.L., A.V., J.W.H. and E.J.B.

3.7 Declaration of interests

E.J.B. serves on the scientific advisory board of Plexium Inc.. J.W.H. is a consultant and founder of Caraway Therapeutics and is a founding board member of Interline Therapeutics.

3.8 Materials and methods

Plasmids

Using Gateway cloning (Invitrogen) all protein coding regions were cloned into Myc- of GFP-tagged CMV expression vectors. Mutations were introduced using QuickChange site-directed mutagenesis utilizing PCR-based approaches (primers 5’ to 3’: RNF10-C225S, CATGAAGTGCCATCTTCCCCAATATGCCTCTATC). Template DNA was digested by Dpn1 followed by transformation of the mutated plasmids into TOP10 E. coli cells. Plasmids were confirmed by sequencing and screened for expression by immunoblotting.

Cell lines, transfections and siRNA

All HEK293, HEK293T, HCT116 and 293Flp-In cells were grown in DMEM (high glucose, pyruvate and L-Glutamine) containing 10% fetal bovine serum (FBS) and 1%

penicillin/streptomycin and maintained in a 5% CO2 humidified incubator. Where indicated, before harvesting cells were treated with either 1uM Tg, 5mM DTT, 2ug/ml HTN, 100ug/ml CHX, 500uM NaAsO2, 150nM Torin1, 50-100nM Bafilomycin A, 1uM SAR405, 10uM MG132 or were exposed to 0.02J/cm2 UV radiation using a SpectorlinkerTM XL-1000 (Spectronics). Lentiviral transduction was used to generate stable cells lines expressing Flag-HA tagged USP10. Using Mirus TransIT 293 transfection reagent cells were transfected with five helper plasmids pHAGE-GAG-POL; pHAGE-VSVG; pHAGE-tat1b; pHAGE-rev and pHAGE-Flag-HA-USP10 (wild type or catalytic mutant), followed by the addition of fresh media after 24 hours. The supernatant was filtered using a 0.45 mm sterile syringe filter and mixed with 2ul of 6mg/ml polybrene. The viral mixture was then added to cells seeded at 50% confluency and infected for 24hours. Stable expression clones were selected with 1ug/ml Puromycin.

The Flp-In^{TM} system (Thermo Fisher) through single locus integration and hygromycin selection was used to generate stable doxycycline inducible cell lines expressing Flag-HA-tagged proteins. Flp-In 293 cells were transfected with Flp-In expression vectors for RNF10 using TransIT 293 transfection reagent (Mirus) according to manufacturer guidelines. Cells were seeded at 60% confluency, transfected for 24 hours followed by selection of stable expression clones with 100ug/mL Hygromycin. Treatment with 2ug/mL doxycycline for 16 hours prior to harvesting was used to induce protein expression.

All transient transfections were carried out using Lipofectamine 2000 (Thermo Fisher) and all siRNA knockdown transfections were performed using Lipofectamine RNAiMAX (Thermo Fisher) according to manufacturer instructions. A list of all RNAi oligonucleotides used in this study can be found in table below.

Immunoblotting

For all immunoblot analysis, cell pellets were resuspended in urea denaturing lysis buffer (8M urea, 50mM Tris-Cl, pH 8.0, 75mM NaCl, 1mM NaV, 1mM NaF, 1mM β-glycerophosphate,

40mM NEM in the presence of EDTA-free protease inhibitor cocktail) and kept on ice during preparation. Cell lysates were sonicated for 10 s (output of 3W on a membrane dismembrator model 100 (Fisher Scientific) with a microtip probe then centrifuged for 10 min at 15,000rpm at 4°C. Lysate protein concentrations were measured by BCA Protein Assay (23225, Thermo Scientific Pierce). Laemmli sample buffer with β-mercaptoethanol was then added to cell lysates and heated at 95°C for 10 min. Samples were then cooled to room temperature and centrifuged briefly. Lysates were resolved on 12% Tris-glycine SDS-PAGE gels, followed by transfer to PVDF membranes (1620177, BioRad) using Bjerrum semi-dry transfer buffer (48mMTris Base, 39mM Glycine-free acid, 0.0375% SDS, 20% MeOH, pH 9.2) and a semi-dry transfer apparatus (Bio-Rad Turbo Transfer) for 30 min at 25V. Immunoblots were blocked with 5% blotting grade nonfat dry milk (APEX Bioresearch) in TBST for 1 hour. Primary antibodies were diluted in 5% BSA and rocked overnight. Immunoblots were developed using Clarity Western ECL Substrate (1705061, BioRad) and imaged on a Bio-Rad Chemi-Doc XRS+ system. All blots were processed using Imagelab (BioRad) software, with final images prepared in Adobe Illustrator. All plots were prepared using GraphPad Prism.

Phos-Tag SDS-PAGE

For Phos-tag analysis, cell pellets were resuspended in 500ul of lysis buffer (8M urea, 50mM Tris-Cl, pH 8.0, 75mM NaCl, 1mM NaV, 1mM NaF, 1mM β-glycerophosphate in the presence of EDTA-free protease inhibitor cocktail). Lysates were sonicated for 10s (as described above) followed by centrifugation for 10 min at 15,000rpm at 4°C. 125ul of TCA was added to each sample, then incubated on ice for 2h at 4°C. Protein was collected by spinning tube in microcentrifuge at 15,000 rpm for 30min at 4°C. The TCA protein pellet was washed with 200ul cold acetone, followed by centrifugation at 15,000 rpm for 10min at 4°C. The acetone wash step was repeated two more times. Pellets were left to dry for 30min at room temperature to evaporate any remaining acetone, then resuspended in 50ul 8M urea/20mM DTT. Protein

concentrations were measured by Bradford Assay (protein assay dye reagent concentrate, 500-0006, BioRad). Laemmli sample buffer with β-mercaptoethanol was then added to protein samples and heated at 95°C for 10 min. Samples were resolved on 12.5% SuperSepTM Phos-tagTM gels (198-17981, Fujifilm), followed by Zn2+ ion elimination. Gel was soaked in 1X transfer buffer (25mM Tris, 192mM Glycine, 10% v/v methanol) with 10mM EDTA for 20min with gentle agitation. This step was repeated three times with buffer exchanges, followed by 10min without EDTA. Wet-tank transfer to PVDF membranes using Towbin transfer buffer (25mM Tris, 192mM Glycine, 20% v/v methanol) was done overnight (16h) at 30V. Immunoblots were blocked, developed, and imaged as described above.

Sucrose density gradient fractionation

Cell pellets were lysed in 500 ul of lysis buffer (20mM Tris-Cl, pH 8.0, 150mM NaCl, 15mM MgCl2, 1% Triton-X 100, 40U Turbo DNase I, 40mM NEM, 1mM DTT, EDTA-free protease inhibitor cocktail in DEPC treated water) followed by vigorous pipetting and incubated on ice for 15min. The cell lysates were centrifuged at 15,000 rpm for 10min at 4°C and the supernatant was transferred to a new microcentrifuge tube. Total RNA concentration of each lysate was determined using a nanodrop (Thermo Scientific). 500ug of total RNA was digested with 3.5ug/ml of RNaseA for 15min at 25°C on a thermomixer (Eppendorf) at 500rpm. The digestion was stopped with 166.5U of SUPERaseIn RNase Inhibitor. Samples were fractionated over a 10–30% sucrose gradient containing 150ug/ml cycloheximide (prepared on Gradient Master 108 (Biocomp): 1min 54s, 81.5 degrees, 16rpm). Samples were centrifuged at 41,000rpm for 2 hr at 4°C in an SW41i rotor. 1ml fractions were collected using a PGFip piston gradient fractionator (Biocomp). Protein fractions were precipitated overnight with 10% TCA at 4°C, followed by three ice-cold acetone washes. Pellets were dried in Vacufuge plus (Eppendorf) at room temperature for 5 min. Pellets were then resuspended in Laemmli sample buffer with β-mercaptoethanol, heated at 95°C for 10 min.

SILAC LC-MS-MS analysis

Cells were grown in a media containing dialyzed FBS (FB03, Omega Scientific) and either light (K0) lysine and arginine (R0) or 13C615N2-labeled (K8) lysine and (R10) arginine (Cambridge Isotopes). Cells were harvested and mixed 1:1 by cell count and were processed for mass spectrometry as described previously (Markmiller et al., 2019). Briefly, cells were lysed using 8M urea lysis buffer with 40mM fresh NEM and lysates were quantified for protein content using the BCA assay. 20µg of total cell extract was diluted to a final urea concentration of 1M and then digested overnight with trypsin (V5111, Promega) at a 1:100 (enzyme:protein) ratio. The digests were reduced with 1mM DTT for 30 min and then alkylated with 10mM NEM in a dark for 30min. The digests were desalted using Stage-Tip method and analyzed by LC-MS/MS as described below. Mixed SILAC lysates were fractionated over sucrose gradients as described. Fractions were TCA precipitated, followed by resuspension in 50mM ammonium bicarbonate and digested overnight with 500ng/ul of trypsin (V5111, Promega) at 37°C. Digests were reduced, alkylated and desalted as described above.

All the samples (1ug digested peptides) were analyzed in triplicate by LC-MS/MS using a Q-Exactive mass spectrometer (Thermo Scientific, San Jose, CA) with the following conditions. A fused silica microcapillary column (100 mmID, 20 cm) packed with C18 reverse-phase resin (XSELECT CSH 130 C18 2.5 mm, Waters Co., Wilford, MA) using an in-line nano-flow EASY-nLC 1000 UHPLC (Thermo Scientific) was used to resolve the peptides. Peptides were eluted over a 45 min 2%–30% ACN gradient, a 5 min 30%–60% ACN gradient, a 2 min 60%–95% gradient, with a final 8 min isocratic step at 0% ACN for a total run time of 60 min at a flow rate of 250 nl/min. All gradient mobile phases contained 0.1% formic acid. MS/MS data were collected in a data dependent fashion using a top 10 method with a full MS mass range from 300–1750 m/z, 70,000 resolution, and an AGC target of 3e6. MS2 scans were triggered when an ion intensity threshold of 1e5 was reached with a maximum injection time of 60 ms. Peptides were fragmented using a normalized collision energy setting of 25. A dynamic

exclusion time of 20 s was used, and the peptide match setting was disabled. Singly charged ions, charge states above 8 and unassigned charge states were excluded.

The resultant RAW files were analyzed using Andromeda/MaxQuant (version 1.6.12.0) using the combined UniProt reviewed only database for Homo sapiens (Dec 2020). The default parameters were used and 'match between the runs' and 'requantify' options were enabled in the MaxQuant settings. The proteingroups output table was imported into Microsoft Excel for subsequent data analysis. Normalized SILAC ratios and LFQ intensities were used for data analysis.

Purification of RNF10

Cells were seeded at 50% confluency in ten 10cm plates one day prior to transfection of a N-Flag-TEV-RNF10 expression plasmid using the calcium phosphate method. 20ug of total DNA was mixed with 2M CaCl2 in distilled water. The mixture was added in a dropwise manner to equal volumes 2XHBS (280mM NaCl, 10mM KCl, 1.5mM Na2HPO4, 12mM glucose and 50mM HEPES pH 7.05) solution at room temperature with continuous mixing, followed by incubation at room temperature for 30 minutes. Transfection mixture was added to each plate and incubated overnight at 37°C. 48 hours post transfection cells were collected by scrapping into cold 1X PBS and pelleted at 1,000 rpm for 5min at 4°C. Cells were lysed in 2mL of lysis buffer (50mM HEPES, pH 7.4, 100mM KAc, 5mM MgAc2, 0.5% NP40, 1 mM DTT (made fresh) and 1X EDTA-free Complete protease inhibitor cocktail) and incubated on ice for 20min. Lysates were clarified by centrifugation at 15,000 rpm for 10min at 4°C. 200ul of clarified lysate was added to a 1:1 slurry of pre-equilibrated (in lysis buffer with 0.1% NP40) anti-Flag M2 resin (A2220, Sigma) and incubated with rotation for 2 hours at 4°C. Resin was collected by centrifugation at 3,000 rpm for 1min at 4°C, while flow through was saved in a new tube. Resin was washed three times in 1ml of IP buffer (50mM HEPES, pH 7.4, 100mM KAc, 5mM MgAc2, 0.1% NP40, 1mM DTT (made fresh) and 1X EDTA-free Complete protease inhibitor cocktail) for 2min with rotation, followed by centrifugation. Resin was then washed three times with 1ml of

high salt buffer (50mM HEPES, pH 7.4, 400mM KAc, 5mM MgAc2, 0.1% NP40, 1mM DTT), followed by three washes with 1ml of elution buffer (50mM HEPES, pH 7.4, 100mM KAc, 5mM MgAc2, 1mM DTT). Following elution, 100U of His-TEV protease (Z03030-1K, GenScript) was added to the 1:1 slurry of resin in elution buffer and incubated at room temperature for 30min. Resin was washed with an additional 100ul of elution buffer and then pooled with the first elution. 50ul of pre-equilibrated NiNTA agarose resin (30210, Qiagen) was added to the pooled elution fractions and incubated with rotation for 1h at 4°C. Cleared elution was collected by centrifugation, followed by silver stain and immunoblotting for confirmation of protein purification.

In vitro ubiquitylation assay

All in vitro ubiquitylation reactions were carried out for 60min at 37°C. Single reactions consisted of 400nM recombinant human His6-Ubiquitin E1 enzyme Ube1 (E-304, BostonBiochem), 2uM recombinant human UbcH5c/UBE2D3 protein (E2-627, BostonBiochem), 200uM recombinant human ubiquitin no K (UM-NOK, BostonBiochem), 125nM 40S ribosomes (Purified from Hap1 cells, gift from Jody Puglisi and Alex Johnson, Stanford University), 50mM Tris-Cl pH 7.5, 50mM MgCl2, 20mM ATP, 6U/ml pyrophosphatase, 35U/ml creatine kinase and 100mM creatine phosphate, and 8uM RNF10. Reactions were inactivated with Laemmli buffer, then incubated for 10min at 95°C. Proteins were resolved by 12% SDS-PAGE and visualized by immunoblotting.

Generation of knockout and knockin cell lines

Using CRISPR/Cas9 genome engineering USP10 and RNF10 knockout was done in 293Flp-In and 293T cells. Three individual guide RNAs were designed for each gene using CHOPCHOP website (https://chopchop.cbu.uib.no). RNF10: 5'-GCCGGCGAGTCTAAACCCAA-3', 5'- GCCACGTTAGACTCGGGAAG-3', 5'- CCGTTGATGCCGCTGAGCTC-3', USP10: 5'-GACTCCTCGATCTTCAGTTG-3', 5'- CTTACCTCAACTGAAGATCG-3' and 5'-

GCCTGGGTACTGGCAGTCGA-3. Cells were transfected with the pSpCas9(BB)-2a-GFP plasmid containing individual guide RNAs using lipofectamine 2000. 48 hours post transfection, GFP positive cells were either single cell sorted on a BD FACSAria Fusion (BD BioSciences) cell sorter, or pooled cell sorts were clonally isolated by limiting dilution method. Cells were validated for loss of USP10 and RNF10 by immunoblotting and sequencing. For HaloTag7 knock-in, guide RNA (gRNA) targeting the C-terminal region of human RPL26 gene was designed using the CHOPCHOP website (http://chopchop.cbu.uib.no/). The guide sequence for RPL26 gene (5′- GAAACCATTGAGAAGATGC-3′) was assembled into a pX459 plasmid. Donor vector was constructed by assembling a HaloTag7 transgene with upstream and downstream homology arms (650 nucleotide each) into a digested pSMART plasmid by Gibson assembly. Wild type HCT116 cells were transfected with donor and gRNA vectors (1 to 1 ratio) by Lipofectamine 3000 (Invitrogen). Five days after the transfection, the pool of transfected cells was treated with 100 nM Halo-TMR ligand for 1h, followed by washing three times. Fluorescence-positive cells were sorted into 96-well plates by flow cytometry (MoFlo Astrios EQ, Beckman Coulter). Three weeks later, the expanded single-cell colonies were screened for the integration of the HaloTag7 transgene by immunoblotting with α-RPL26.

Ribo-Halo microscopy

HCT116 Ribo-HaloTag7 cells were transfected with either GFP-RNF10 WT or CS expression plasmid (2 ug/dish) using lipofectamine 3000 (Invitrogen). 24 hours post transfection, the cells were plated onto 35 mm-glass bottom dishes (No. 1.5, 14 mm glass diameter, MatTek) pre-treated with poly-L-lysine. 48 hours later, Halo-TMR containing medium (50 nM) was added to the cells and incubated for 1 hour. The medium was removed, and the cells were washed with warm DMEM for two times. DMEM was replaced by FluoroBrite™DMEM (Thermo Fisher) before the live cell imaging. The cells were imaged using a Yokogawa CSU-X1 spinning disk confocal with Spectral Applied Research Aurora Borealis modification on a Nikon Ti motorized microscope equipped with a Nikon Plan Apo 60×/1.40 N.A

objective lens. Pairs of images for TMR and GFP fluorescence were collected sequentially using 100 mW 488 nm and 100 mW 561 solid state lasers attenuated and controlled with an AOTF (Spectral Applied Research LMM-5), and emission collected with a 525/50 nm or 620/60 nm filter (Chroma Technologies), respectively. Confocal images were acquired with the Hamamatsu ORCA-ER cooled CCD camera and MetaMorph software. The images were analyzed using FiJi software.

Flowcytometry analysis for Ribo-Halo labeling

Ribo-Halo cells were seeded at 40% confluency in 12-well plates one day prior to transient transfections. 36 hours post transfection cells were treated with 100nM TMR-ligand (G8251, Promega) for 1-2 hours. After TMR-labeling, cells were washed with fresh warmed DMEM without the Halo-ligand three times with 10min incubations in between washes. Fresh warm DMEM was added to cells and cells were collected at various time points post washout. Cells were trypsinized then collected in fresh media. Following a short 3min centrifugation at 3,500rpm, cell pellets were resuspended in 800ul of FACS buffer (2% FBS in 1x DPBS) and passed through a nitex nylon mesh (Genesee Scientific). Samples were analyzed by flow-cytometry on a BD LSRFortessaTM X-20 cell analyzer (BD Biosciences). FACS data was analyzed using FlowJo (v10.6.2).

qPCR analysis

For qPCR analysis, cells were plated at 50-60% confluency prior to lipofectamine based transfection, as described previously. 48 hours post transfection cells were collected in TRIzol and RNA was isolated using Direct-zol RNA miniprep kit (11-331, Zymo Research). Using 2ug RNA template, cDNA was synthesized is SuperScript III First Strand Synthesis system (18080-051, Invitrogen). Five standards were prepared by making four-fold dilutions of a sample pool. cDNA samples were each diluted 1:5 in water prior to plating. 8ul of each standard or sample was plated into a 96-well thermocycler plate, followed by 12ul of master mix containing SYBR

green super mix (1725121, BioRad) and primers for gene of interest. The following primers were used in this study: RPS3: 5'-CAGAACAGAAGGGTGGGAAG-3', 5'-GCAACATCCAGACTCCAGAATA-3', RPS6: 5'-GAGCGTTCTCAACTTGGTTATTG-3', 5'-GCGGATTCTGCTAGCTCTTT-3', RPL7: 5'-GGCGAGGATGGCAAGAAA-3', 5'-CTTTGGGCTCACTCCATTGATA-3', GAPDH: 5'-AACGGGAAGCTTGTCATCAATGGAAA-3', 5'-GCAGGAGGCAGCTGATGATCTT-3'. The following PCR conditions were run on a C1000 Thermo Cycler (BioRad): 50°C for 10min, 95°C for 15min, 95°C for 10s, 60°C for 30s (repeat for 40 cycles). All relative quantifications were calculated using the delta delta Ct method.

Quantification and statistical analysis

All FACS-based assays were performed in triplicate (n = 3) as biologically distinct samples. The median 561nm/488nm ratio and SD were calculated. Transient overexpression experiments were compared to a transfection control. Immunoblot quantification of the relative % ubiquitylation and % phosphorylation was calculated by normalization of the individual intensities for each concentration to that of the no treatment control. Significance (p value) was calculated using an unpaired two-tailed Student's t test using GraphPad Prism 9.0.

Chapter 3, in full, is a reprint of the material as it occurs in Cell Reports, Garshott, D.M.; An, H.; Sundaramoorthy, E.; Leonard, M.; Vicary, A.; Harper, J.W.; Bennett, E.J.; Cell Press, 2021. I am the primary author.

3.9 Figures

Figure 3.1. RNF10 catalyzes uS3 and uS5 ubiquitylation, See also Figure 3.8.
(A) Cell lysates from 293T cells transfected with either control siRNA oligos or three separate siRNA oligos targeting RNF10, followed by treatment with dithiothreitol (DTT) for 2 hours were analyzed by SDS-PAGE and immunoblotted with the indicated antibodies. * indicates non-specific background signal. Arrow indicates RNF10-specific immunoreactivity. For all blots the ubiquitin-modified ribosomal protein is indicated by the arrow. S and L denote short and long exposures, respectively.
(B) Cell extracts from parental 293T or RNF10 knockout (KO) cells were either untreated or treated with DTT or anisomycin (ANS) then analyzed by SDS-PAGE and immunoblotted with the indicated antibodies.
(C) HEK293-FlpIn cells expressing tet-inducible Flag-HA tagged RNF10 were treated with doxycycline (Dox) and cell lysates were analyzed by SDS-PAGE and immunoblotted with the indicated antibodies.
(D) In vitro ubiquitylation assay utilizing purified 40S ribosomal subunits and RNF10. Samples were analyzed by SDS-PAGE and immunoblotted with the indicated antibodies.
(E) (top) RNF10 knockout (KO) cells were transfected with Myc-tagged wild type (WT) or inactive mutant (CS) RNF10 and parental 293T or RNF10-KO cells were either untreated or treated with DTT. Cell lysates were analyzed by SDS-PAGE and immunoblotted with the indicated antibodies. (bottom) Quantitative representation of percent ubiquitylated uS3 and uS5, and percent relative total abundance from immunoblots (bottom).
(F) (top) 293T cells with and without Myc-tagged wild type RNF10 expression were drug treated as indicated. UV indicates that cells were exposed to UV and were allowed to recover for 1 or 4 hours. Cell extracts were analyzed by SDS-PAGE and immunoblotted with the indicated antibodies. (bottom) Quantitative representation of percent ubiquitylated uS3 and uS5, and percent relative total abundance from immunoblots.

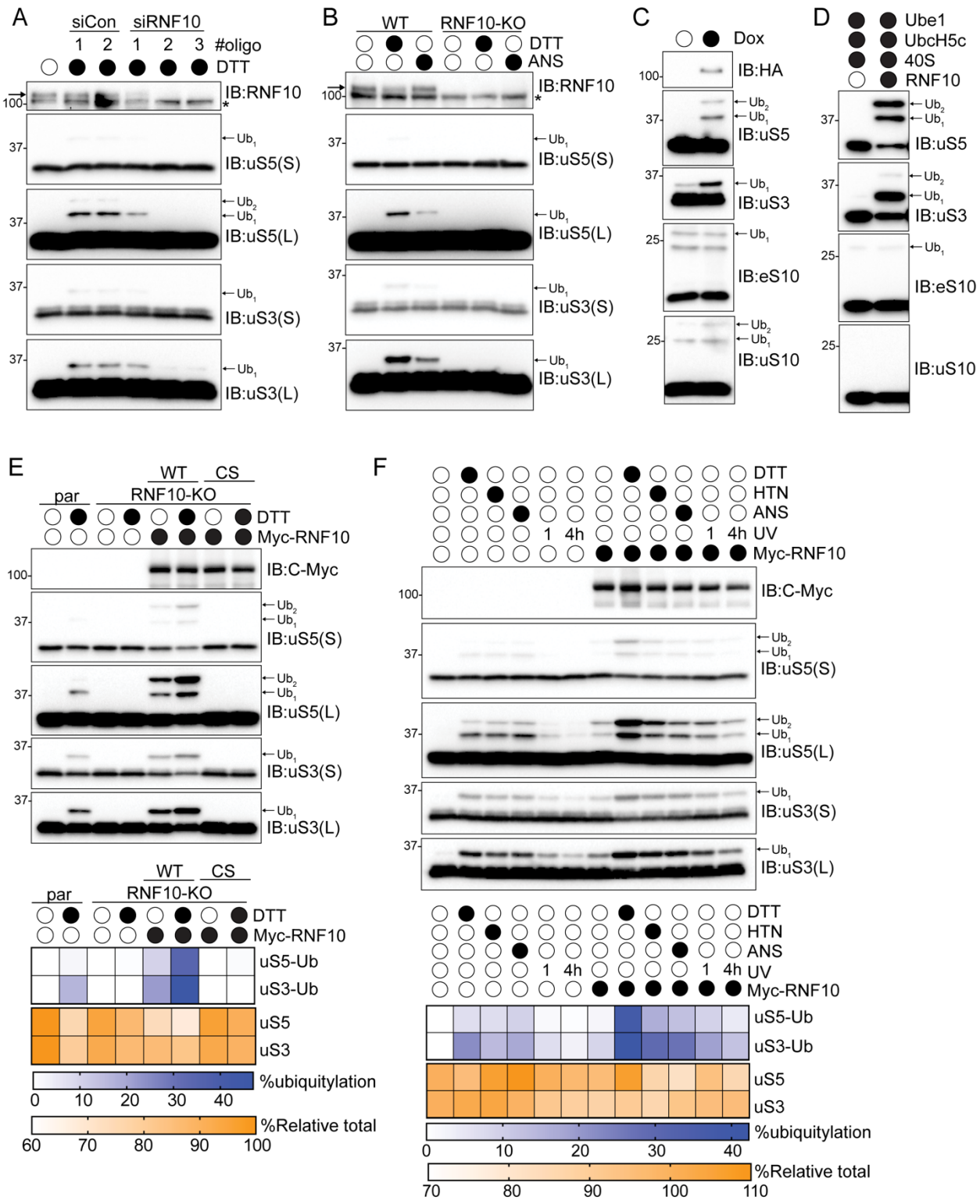
A
siCon
siRNF10
1 2 1 2 3 #oligo
DTT
IB:RNF10
IB:uS5(S)
IB:uS5(L)
IB:uS3(S)
IB:uS3(L)
B
WT
RNF10-KO
DTT
ANS
IB:RNF10
IB:uS5(S)
IB:uS5(L)
IB:uS3(S)
IB:uS3(L)
C
Dox
IB:HA
IB:uS5
IB:uS3
IB:eS10
IB:uS10
D
Ube1
UbcH5c
40S
RNF10
IB:uS5
IB:uS3
IB:eS10
IB:uS10
E
par
WT
CS
RNF10-KO
DTT
Myc-RNF10
IB:C-Myc
IB:uS5(S)
IB:uS5(L)
IB:uS3(S)
IB:uS3(L)
uS5-Ub
uS3-Ub
uS5
uS3
%ubiquitylation
%Relative total
F
DTT
HTN
ANS
1 4h 1 4h UV
Myc-RNF10
IB:C-Myc
IB:uS5(S)
IB:uS5(L)
IB:uS3(S)
IB:uS3(L)
uS5-Ub
uS3-Ub
uS5
uS3
%ubiquitylation
%Relative total

Figure 3.2. Persistent uS3 and uS5 ubiquitylation targets 40S ribosomal proteins for degradation, See also Figure 3.9.
(A) 293T USP10-knockout (KO) cells constitutively expressing wild type (WT) or inactive mutant (CS) USP10 were treated with HTN and cell lysates were analyzed by SDS-PAGE and immunoblotted with the indicated antibodies. For all blots the ubiquitin-modified ribosomal protein is indicated by the arrow. S and L denote short and long exposures, respectively.
(B) (top) USP10-KO cells were treated as indicated and cell extracts were analyzed by SDS-PAGE and immunoblotted with the indicated antibodies. (bottom) Percent ubiquitylated uS3 and uS5, and percent total relative abundance quantified from immunoblots
(C) (top) Parental 293T or USP10-KO cells expressing Myc-tagged wild type RNF10 were either untreated, treated as indicated and cell lysates were analyzed by SDS-PAGE and immunoblotted with the indicated antibodies. (bottom) Quantitative representation of uS3 and uS5 percent ubiquitylation, and percent relative total abundance for uS3, uS5 and uL30.
(D) The median normalized log2 SILAC ratio (H:L) for all quantified 40S and 60S ribosomal proteins comparing parental cells (light label) to cells of the indicated genotype (heavy label) with or without RNF10 overexpression (O/E). Each point represents a biological replicate, Bars denote mean value for replicate experiments with error bars displaying SEM. *=pvalue<0.05 by student's t test compared to parental controls.
(E) The median normalized log2 SILAC ratio (H:L) for individual 40S and 60S ribosomal proteins comparing parental cells (light label) to cells of the indicated genotype with or without RNF10 overexpression (O/E). Bars denote mean and error bars denote SD.

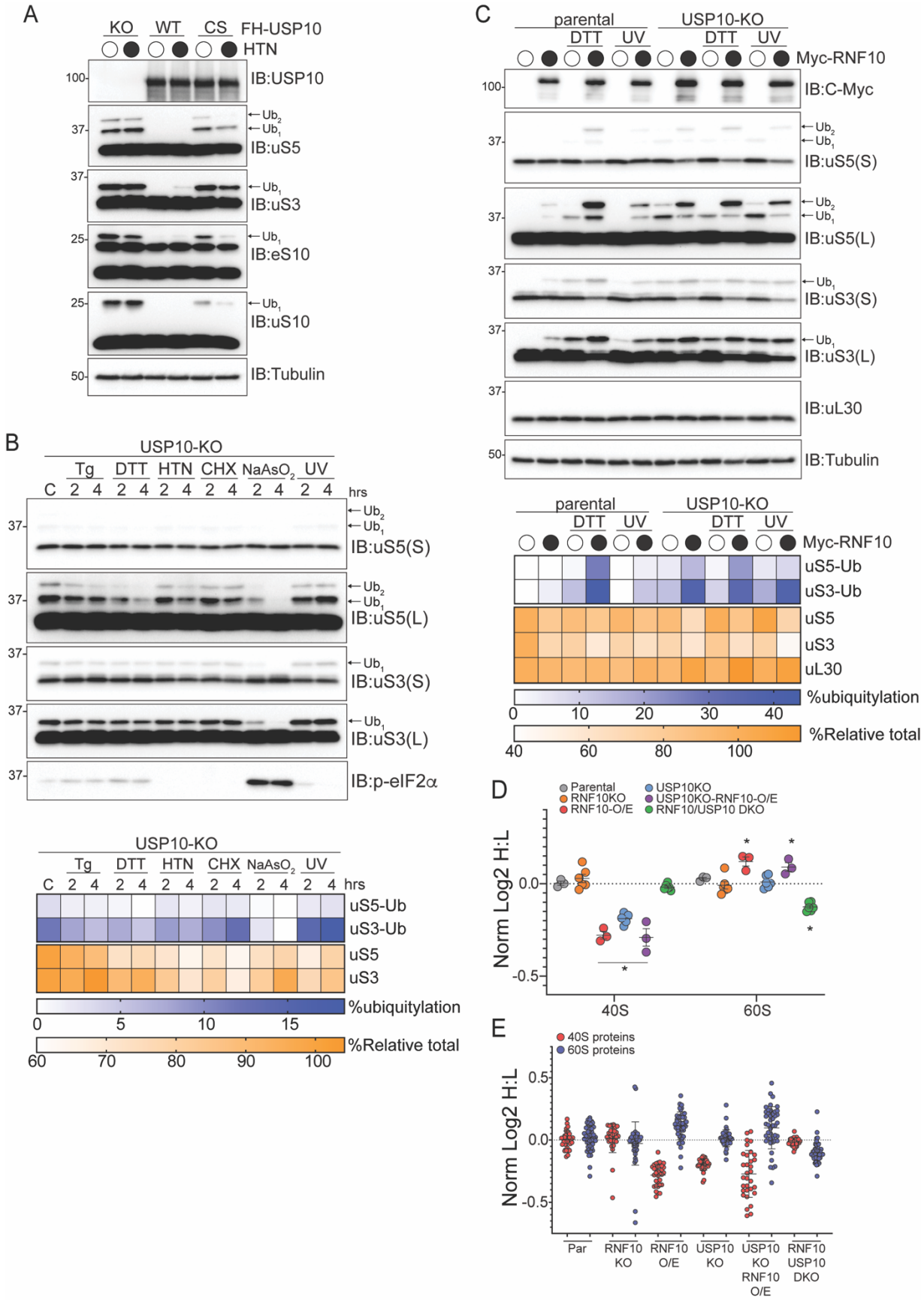
A
KO
WT
CS
FH-USP10
HTN
IB:USP10
IB:uS5
IB:uS3
IB:eS10
IB:uS10
IB:Tubulin
B
USP10-KO
Tg
DTT
HTN
CHX
NaAsO2
UV
hrs
IB:uS5(S)
IB:uS5(L)
IB:uS3(S)
IB:uS3(L)
IB:p-eIF2α
uS5-Ub
uS3-Ub
uS5
uS3
%ubiquitylation
%Relative total
C
parental
USP10-KO
Myc-RNF10
IB:C-Myc
IB:uS5(S)
IB:uS5(L)
IB:uS3(S)
IB:uS3(L)
IB:uL30
IB:Tubulin
D
Parental
RNF10KO
RNF10-O/E
USP10KO
USP10KO-RNF10-O/E
RNF10/USP10 DKO
Norm Log2 H:L
40S
60S
E
40S proteins
60S proteins
Par
RNF10 KO
RNF10 O/E
USP10 KO
USP10 KO RNF10 O/E
RNF10 USP10 DKO

Figure 3.3. Enhanced ubiquitylation results in turnover of 40S ribosomal proteins in an autophagy-independent manner.
(A) (top) Cell extracts from parental 293T or RB1CC1-KO cells transfected with either a control siRNA oligo or siRNA oligo targeting USP10, followed by transfection with Myc-tagged wild type RNF10 treated as indicated were analyzed by SDS-PAGE and immunoblotted with the indicated antibodies. (bottom) Quantitative representation of percent relative total abundance and uS3 and uS5 percent ubiquitylation.
(B) HEK293 uS3 or eL28 (RPL28) Keima-tagged cells were treated as indicated and frequency distributions of the red (561nm) to green (488nm) ratio are plotted.
(C) HEK293 uS3 or eL28 Keima-tagged cells were transfected with either a control siRNA oligo (black line), siRNA targeting USP10 (yellow line) or in combination with Bafilomycin A (50nM, 1h) treatment (green line). Frequency distributions of the red (561nm) to green (488nm) ratio are plotted.
(D) HEK293 uS3 or eL28 Keima-tagged cells expressing either a control plasmid (grey line), RNF10 wild type (blue line) or the catalytic mutant (red line) 48 hours post transfection were collected and analyzed via FACS. Frequency distributions of the red (561nm) to green (488nm) ratio are plotted.
(E) HEK293 uS3 or eL28 Keima-tagged cells transfected with either a control siRNA oligo (grey line), or siRNA targeting USP10 and expressing either a control plasmid (green line), RNF10 wild type (blue line) or the catalytic mutant (red line) 48 hours post transfection were collected and analyzed via FACS (bottom). All bar graphs denote median red:green ratio from triplicate experiments. N=3, error bars denote SD of triplicate experiments. *=pvalue<0.05, ns = non-significant by unpaired student's t test.

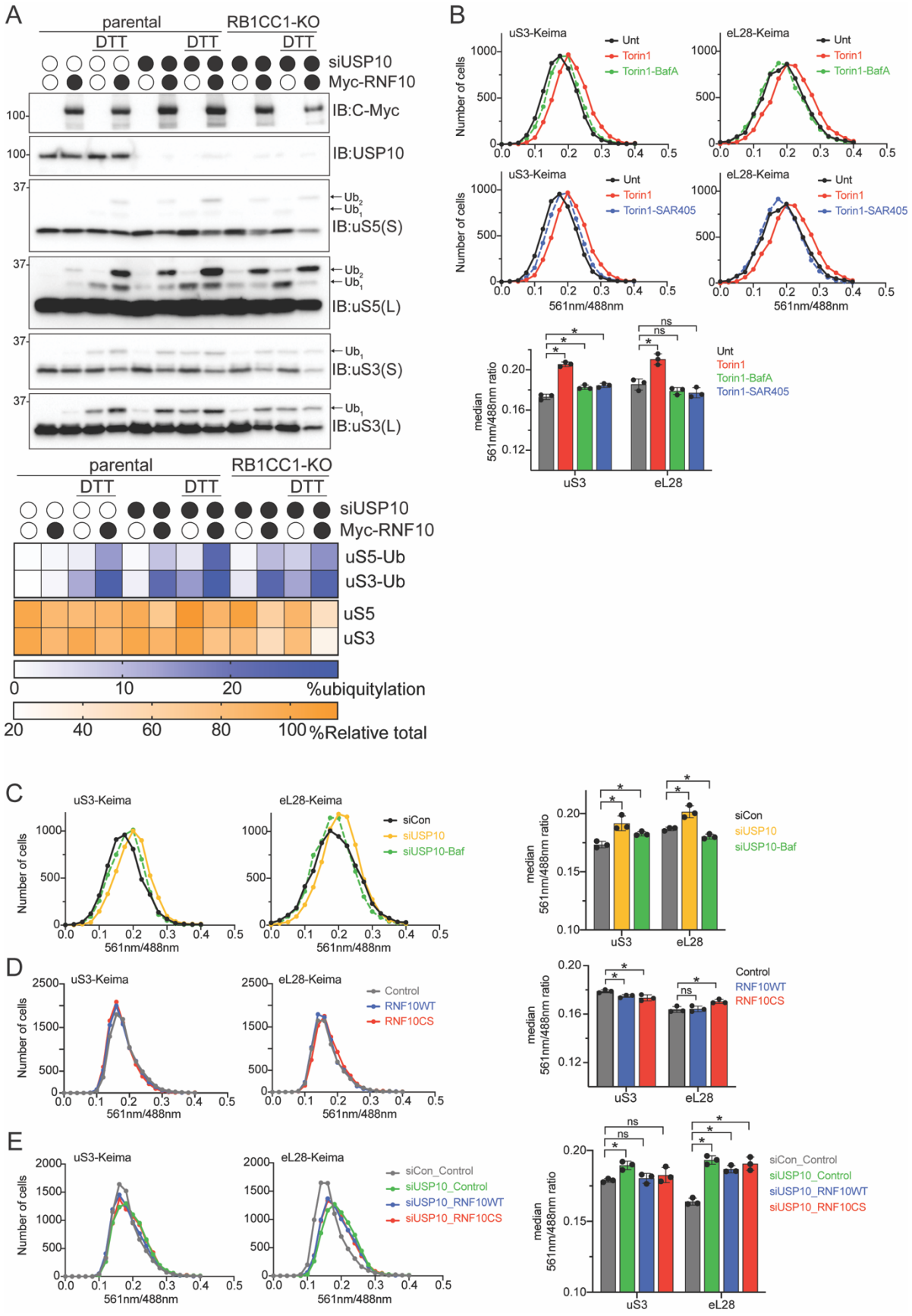
A
parental
RB1CC1-KO
DTT
siUSP10
Myc-RNF10
IB:C-Myc
IB:USP10
IB:uS5(S)
IB:uS5(L)
IB:uS3(S)
IB:uS3(L)
uS5-Ub
uS3-Ub
uS5
uS3
%ubiquitylation
%Relative total
B
uS3-Keima
eL28-Keima
Unt
Torin1
Torin1-BafA
Torin1-SAR405
Number of cells
561nm/488nm
median 561nm/488nm ratio
uS3
eL28
C
siCon
siUSP10
siUSP10-Baf
D
Control
RNF10WT
RNF10CS
E
siCon_Control
siUSP10_Control
siUSP10_RNF10WT
siUSP10_RNF10CS

Figure 3.4. RNF10-dependent uS5 ubiquitylation accelerates 40S protein turnover, See also Figure 3.10.
(A) Schematic of Ribo-Halo fluorescent pulse-chase assay (top). Microscopy images of HCT116 uS3 or uL24-Halo tagged cells expressing GFP-tagged wild type (WT) or inactive mutant (CS) RNF10. Ribosomes were labeled with TMR ligand for 2 hours prior to imaging. Arrows indicate the same cells across panels (bottom).
(B) The normalized (to control at 0h washout) TMR-fluorescence intensity for uS3 or eL29-Halo tagged cells expressing a control plasmid (grey bars), Myc-RNF10-WT (blue bars), or CS mutant (red bars) expression plasmid is depicted at the indicated time points post TMR washout (left). N=3, error bars denote SD of triplicate experiments. *=pvalue<0.05, ns = non-significant by multiple unpaired t tests compared to control protein. Frequency distribution of the normalized TMR signal at 24h is plotted (right).
(C) Normalized (to control at 0h washout) TMR-fluorescence intensities for uS3-Halo tagged cells expressing a control plasmid, Myc-RNF10-WT, or RNF10 mutant (CS) expression plasmid at time 0h (grey bars), 8h post TMR washout (blue bars) or with MG132 included during the 8h TMR washout (red bars) is depicted (left). TMR fluorescence intensities for cells expressing a control plasmid (grey bars), Myc-RNF10-WT (blue bars), or CS mutant (red bars) expression plasmid at 0 or 8h post TMR washout with or without BafA or SAR405 included in the TMR washout (right). N=3, error bars denote SD of triplicate experiments. *=pvalue<0.05 by unpaired student's t test.
(D) TMR fluorescence intensities 12h post washout from parental 293T uS3-Halo tagged cells alone or with stable expression of wild type (WT) or K54R/K58R mutant (Mut) uS5 and transfected with a control plasmid (grey bars), GFP-RNF10-WT (blue bars), or GFP-RNF10-CS mutant (red bars) expression plasmids are depicted. The normalized (to control at 0h washout) TMR intensities are depicted. N=3, error bars denote SD of triplicate experiments. *=pvalue<0.05, ns = non-significant by unpaired student's t tests compared to control protein.

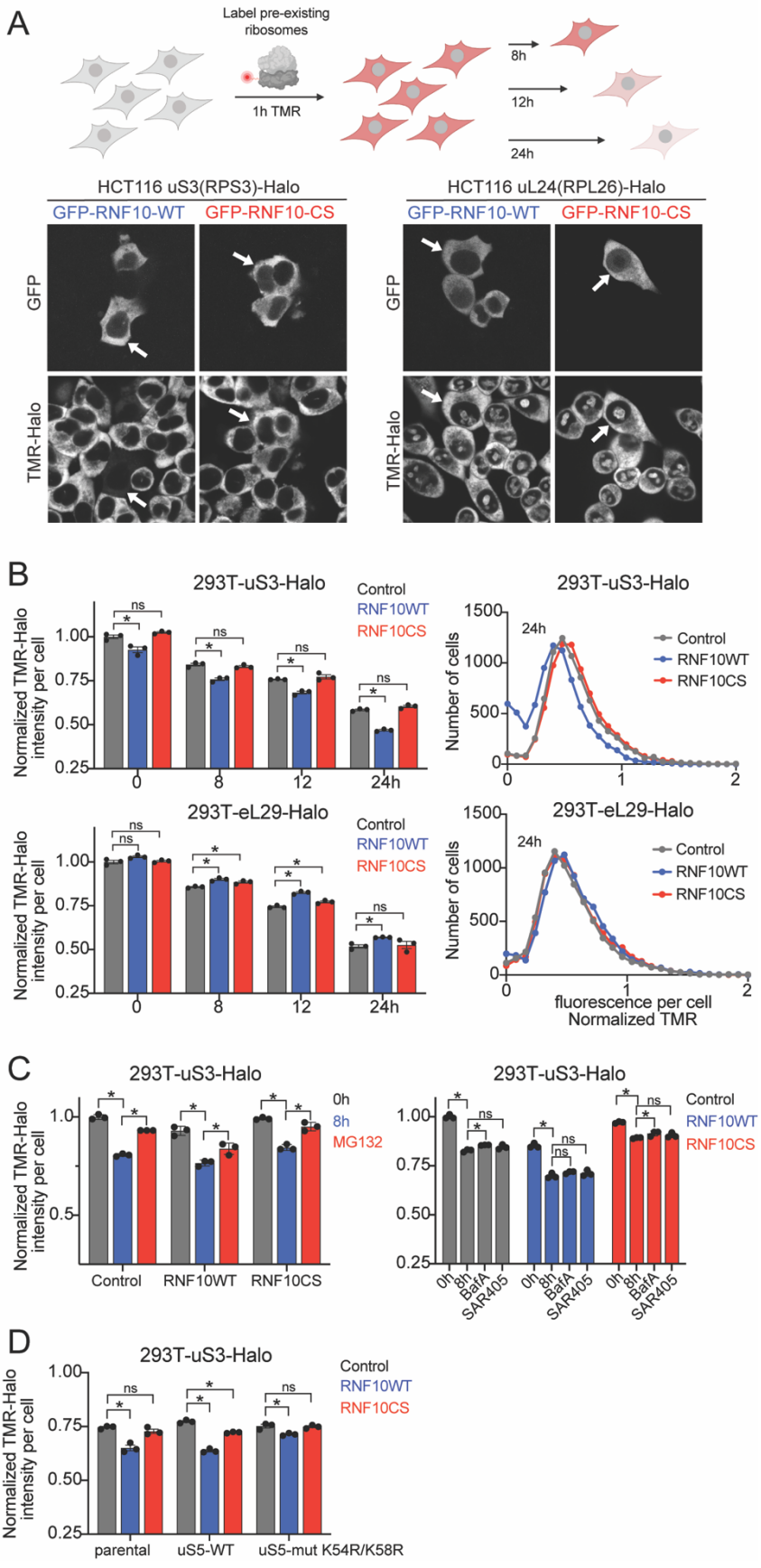
A
Label pre-existing ribosomes
1h TMR
8h
12h
24h
HCT116 uS3(RPS3)-Halo
HCT116 uL24(RPL26)-Halo
GFP-RNF10-WT
GFP-RNF10-CS
GFP
TMR-Halo
B
293T-uS3-Halo
293T-eL29-Halo
Control
RNF10WT
RNF10CS
Normalized TMR-Halo intensity per cell
Number of cells
fluorescence per cell
Normalized TMR
ns
C
0h
8h
MG132
BafA
SAR405
D
parental
uS5-WT
uS5-mut K54R/K58R

Figure 3.5. Translational initiation inhibition induces ribosomal ubiquitylation, See also Figure 3.11.
(A) (top) Cell extracts from 293T cells treated with increasing doses of HTN were analyzed by SDS-PAGE and immunoblotted (IB) with the indicated antibodies. For all blots, the ubiquitin-modified ribosomal protein is indicated by the arrow. S and L denote short and long exposures, respectively. (bottom) Percent ubiquitylated uS3 and uS5 quantified from immunoblots.
(B) Cell extracts from 293T cells treated with HTN or lactimidomycin (LTM) for the indicated times were analyzed by SDS-PAGE and immunoblotted with the indicated antibodies.
(C) Quantification of uS3 or uS5 percent ubiquitylation from 293T cells treated with increasing doses of either rocaglates (RocA) or patamineA (PatA) from blots in S4A,B.
(D) (top) Cell extracts from 293T cells treated with increasing concentration of cycloheximide (CHX) were analyzed by SDS-PAGE and immunoblotted with the indicated antibodies. (bottom) Quantitative representation of uS3, uS5, and eS10 percent ubiquitylation from immunoblots.

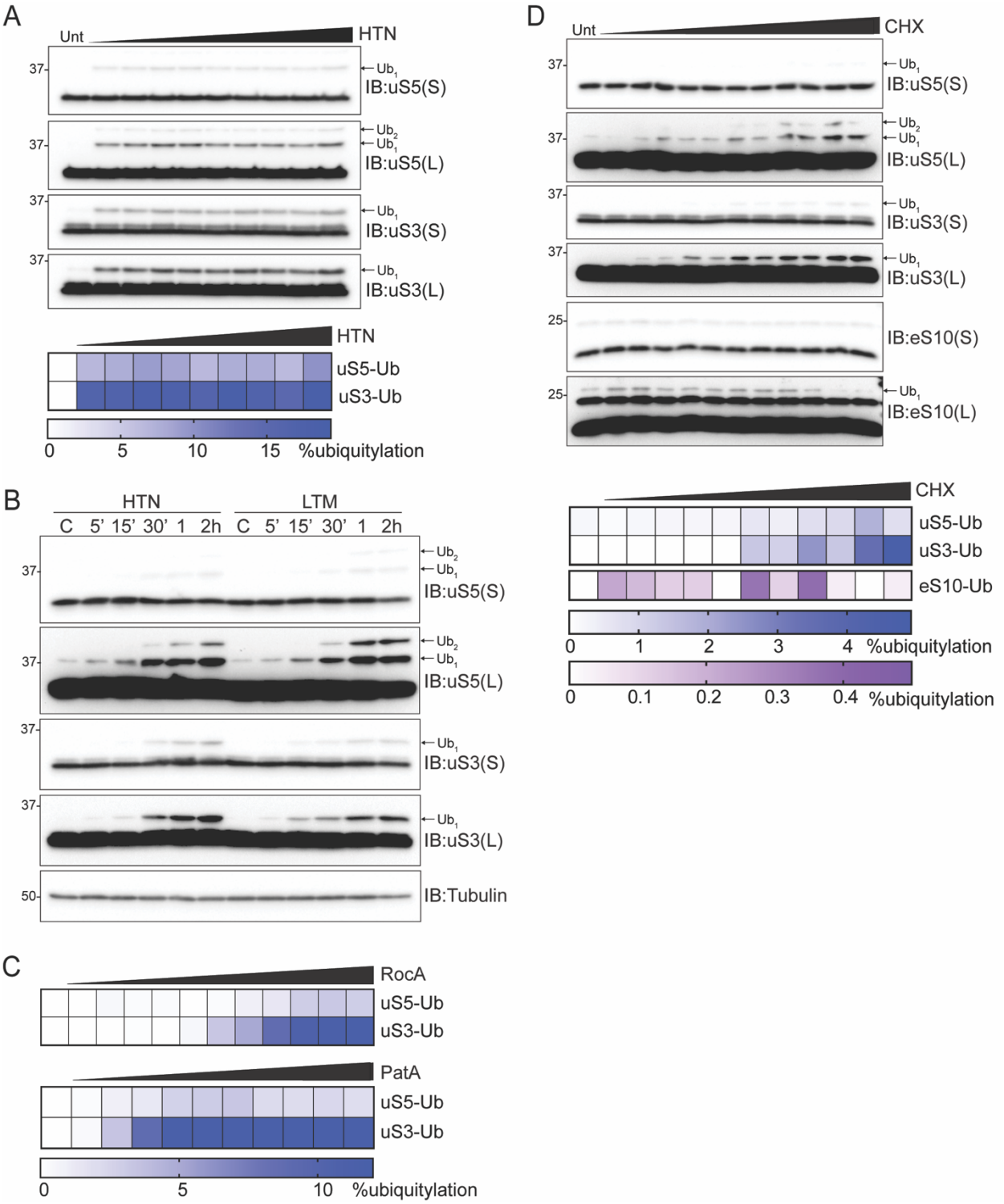
A
Unt
HTN
37
Ub1
IB:uS5(S)
37
Ub2
Ub1
IB:uS5(L)
37
Ub1
IB:uS3(S)
37
Ub1
IB:uS3(L)
HTN
uS5-Ub
uS3-Ub
0 5 10 15 %ubiquitylation
B
HTN
LTM
C 5' 15' 30' 1 2h C 5' 15' 30' 1 2h
37
Ub2
Ub1
IB:uS5(S)
37
Ub2
Ub1
IB:uS5(L)
37
Ub1
IB:uS3(S)
37
Ub1
IB:uS3(L)
50
IB:Tubulin
C
RocA
uS5-Ub
uS3-Ub
PatA
uS5-Ub
uS3-Ub
0 5 10 %ubiquitylation
D
Unt
CHX
37
Ub1
IB:uS5(S)
37
Ub2
Ub1
IB:uS5(L)
37
Ub1
IB:uS3(S)
37
Ub1
IB:uS3(L)
25
IB:eS10(S)
25
Ub1
IB:eS10(L)
CHX
uS5-Ub
uS3-Ub
eS10-Ub
0 1 2 3 4 %ubiquitylation
0 0.1 0.2 0.3 0.4 %ubiquitylation

Figure 3.6. Moderate integrated stress response activation induces uS3 and uS5 ubiquitylation, See also Figure 3.11.
(A) Cell extracts from 293T cells treated as indicated were analyzed by SDS-PAGE and immunoblotted with the indicated antibodies. For all blots, the ubiquitin-modified ribosomal protein is indicated by the arrow. S and L denote short and long exposures, respectively.
(B) Cell extracts from 293T cells treated with increasing concentrations of sodium arsenite (NaAsO2) were analyzed by SDS-PAGE and immunoblotted with the indicated antibodies.
(C) Quantification of uS3 percent ubiquitylation and eIF2α percent phosphorylation (from Phos-tag gels) following NaAsO2 treatment from B.

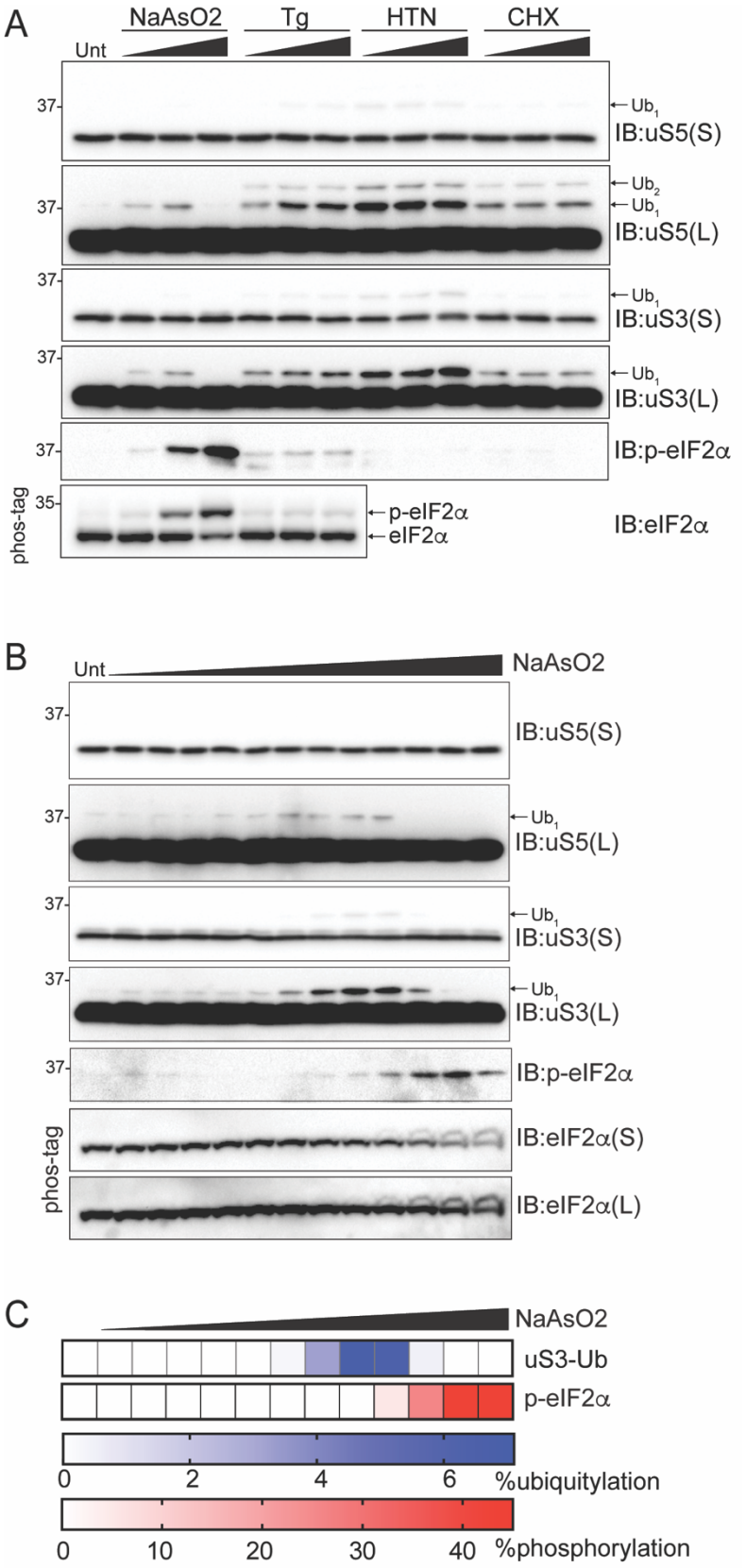
A
NaAsO2
Tg
HTN
CHX
Unt
37
Ub1
IB:uS5(S)
Ub2
Ub1
IB:uS5(L)
IB:uS3(S)
IB:uS3(L)
IB:p-eIF2α
phos-tag
35
p-eIF2α
eIF2α
IB:eIF2α
B
Unt
NaAsO2
IB:uS5(S)
IB:uS5(L)
IB:uS3(S)
IB:uS3(L)
IB:p-eIF2α
IB:eIF2α(S)
IB:eIF2α(L)
C
NaAsO2
uS3-Ub
p-eIF2α
0
2
4
6
%ubiquitylation
0
10
20
30
40
%phosphorylation

Figure 3.7. HTN induces 40S ubiquitylation in density gradient fractions with excess 40S relative to 60S ribosomal proteins, See also Figure 3.12.
(A) RNaseA treated cell extracts from untreated (black line) or HTN treated (red line) 293T cells were fractionated on 10-30% sucrose gradients. The 254nm absorbance trace is depicted.
(B) Fractions (designated in A) were analyzed by SDS-PAGE and immunoblotted with the indicated antibodies. The ubiquitin-modified ribosomal protein is indicated by the arrow. S and L denote short and long exposures respectively.
(C) RNaseA treated cell lysates 293T cells treated as indicated were fractionated on 10-30% sucrose gradients. The relative 254nm absorbance trace is depicted.
(D,E) The ratio of the summed molecular weight (MW) normalized LFQ intensities 40S proteins:60S proteins from untreated, light labeled (black bars) or HTN treated, heavy labeled (purple bars) 293T cells. Cell extracts with either untreated (E) or treated (D) with RNaseA prior to density gradient centrifugation. Bars denote mean value for replicate experiments (n=3) with error bars displaying SEM. *=pvalue<0.05 by unpaired two-tailed Student's t test.

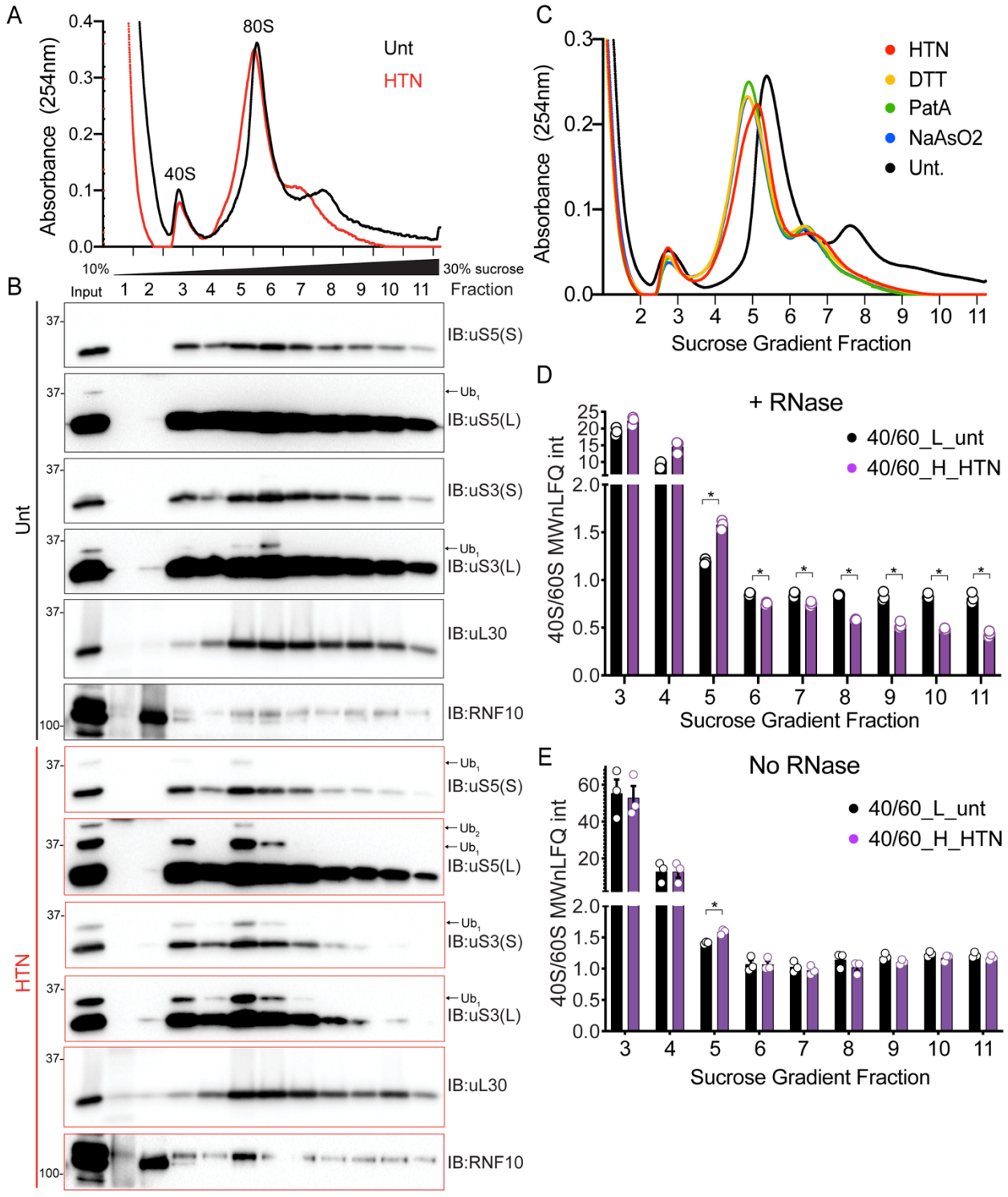
A
Absorbance (254nm)
0.4
0.3
0.2
0.1
0.0
40S
80S
Unt
HTN
10%
30% sucrose
B
Input 1 2 3 4 5 6 7 8 9 10 11
Fraction
Unt
HTN
37-
100-
IB:uS5(S)
IB:uS5(L)
IB:uS3(S)
IB:uS3(L)
IB:uL30
IB:RNF10
Ub1
Ub2
C
Absorbance (254nm)
HTN
DTT
PatA
NaAsO2
Unt.
Sucrose Gradient Fraction
D
+ RNase
40/60_L_unt
40/60_H_HTN
40S/60S MWnLFQ int
Sucrose Gradient Fraction
E
No RNase
40/60_L_unt
40/60_H_HTN
40S/60S MWnLFQ int
Sucrose Gradient Fraction

3.10 Supplemental Figures

Figure 3.8. Screening RNA-associated ubiquitin ligases identifies RNF10 as the uS3/uS5 ubiquitin ligase, Related to Figure 3.1.
(A-E) 293T cells were transfected with either a control siRNA oligo or three separate siRNA oligos targeting the indicated E3 ligase, followed by treatment with DTT (5mM) for two hours. Cell lysates were analyzed by SDS-PAGE and immunoblotted with the indicated antibodies. For all blots, the ubiquitin-modified ribosomal protein is indicated by the arrow. S and L denote short and long exposures, respectively.
(F) RNF10 immunoblot and silver stain of affinity purified wild type RNF10 expressed in 293T cells.
(G) 293T cells with and without Myc-tagged wild type RNF10 expression were drug treated as indicated. UV indicates that cells were exposed to UV (0.02J/cm^2) and were allowed to recover for 1 or 4 hours. Cell extracts were analyzed by SDS-PAGE and immunoblotted with the indicated antibodies.

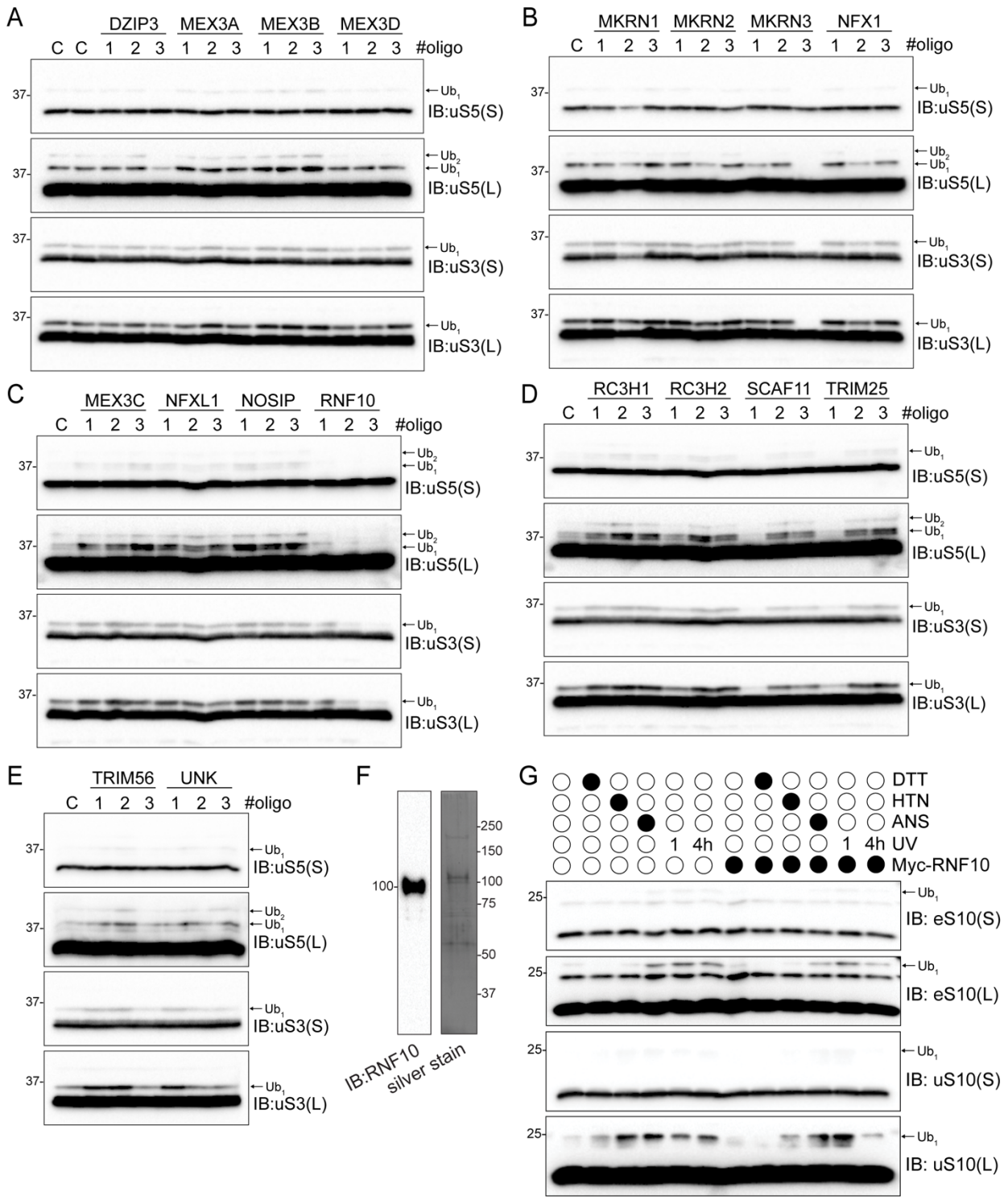
A
DZIP3
MEX3A
MEX3B
MEX3D
C C 1 2 3 1 2 3 1 2 3 1 2 3 #oligo
37
Ub1
IB:uS5(S)
Ub2
Ub1
IB:uS5(L)
IB:uS3(S)
IB:uS3(L)
B
MKRN1
MKRN2
MKRN3
NFX1
C 1 2 3 1 2 3 1 2 3 1 2 3 #oligo
C
MEX3C
NFXL1
NOSIP
RNF10
D
RC3H1
RC3H2
SCAF11
TRIM25
E
TRIM56
UNK
F
100
250
150
100
75
50
37
IB:RNF10
silver stain
G
DTT
HTN
ANS
1 4h UV
1 4h
Myc-RNF10
25
IB: eS10(S)
IB: eS10(L)
IB: uS10(S)
IB: uS10(L)

Figure 3.9. uS3 and uS5 ubiquitylation trigger 40S subunit turnover, Related to Figure 3.2.
(A) Cell extracts from parental 293T cells or USP21-KO, OTUD3-KO or USP10-KO cells were analyzed by SDS-PAGE and immunoblotted with the indicated antibodies. For all blots, the ubiquitin-modified ribosomal protein is indicated by the arrow. S and L denote short and long exposures, respectively.
(B) (top) Parental 293T or USP10-KO cells expressing Myc-tagged wild type RNF10 were either untreated, treated with DTT or exposed to UV. Cell lysates were analyzed by SDS-PAGE and immunoblotted with the indicated antibodies. (bottom) Quantitative representation of percent relative total abundance for eS10 and uS10.
(C) Quantitative representation of percent relative total protein abundance for uL30, uS3, uS5, eS10 and uS10 from immunoblots in 2C and S2B.
(D) Relative mRNA abundance measured by qPCR for uS3 (RPS3), eS6 (RPS6), and uL30 (RPL7) in parental cells, or parental cells expressing wild type (WT) or inactive mutant (CS) RNF10. N=3, error bars denote SEM.
(E) Total protein (black line), 40S (red line), or 60S (blue line) ribosomal protein synthesis rates from parental 293T, USP10-KO, and USP10-KO cells overexpressing wild type RNF10 were determined using SILAC label swap from cells collected at the indicated time point post label swap. Light to heavy ratios were determined by mass spectrometry. N=3, error bars denote SEM of triplicate experiments. *=pvalue<0.05 using unpaired, two-tailed Student's t-test comparing slope of best-fit line for replicate experiments.

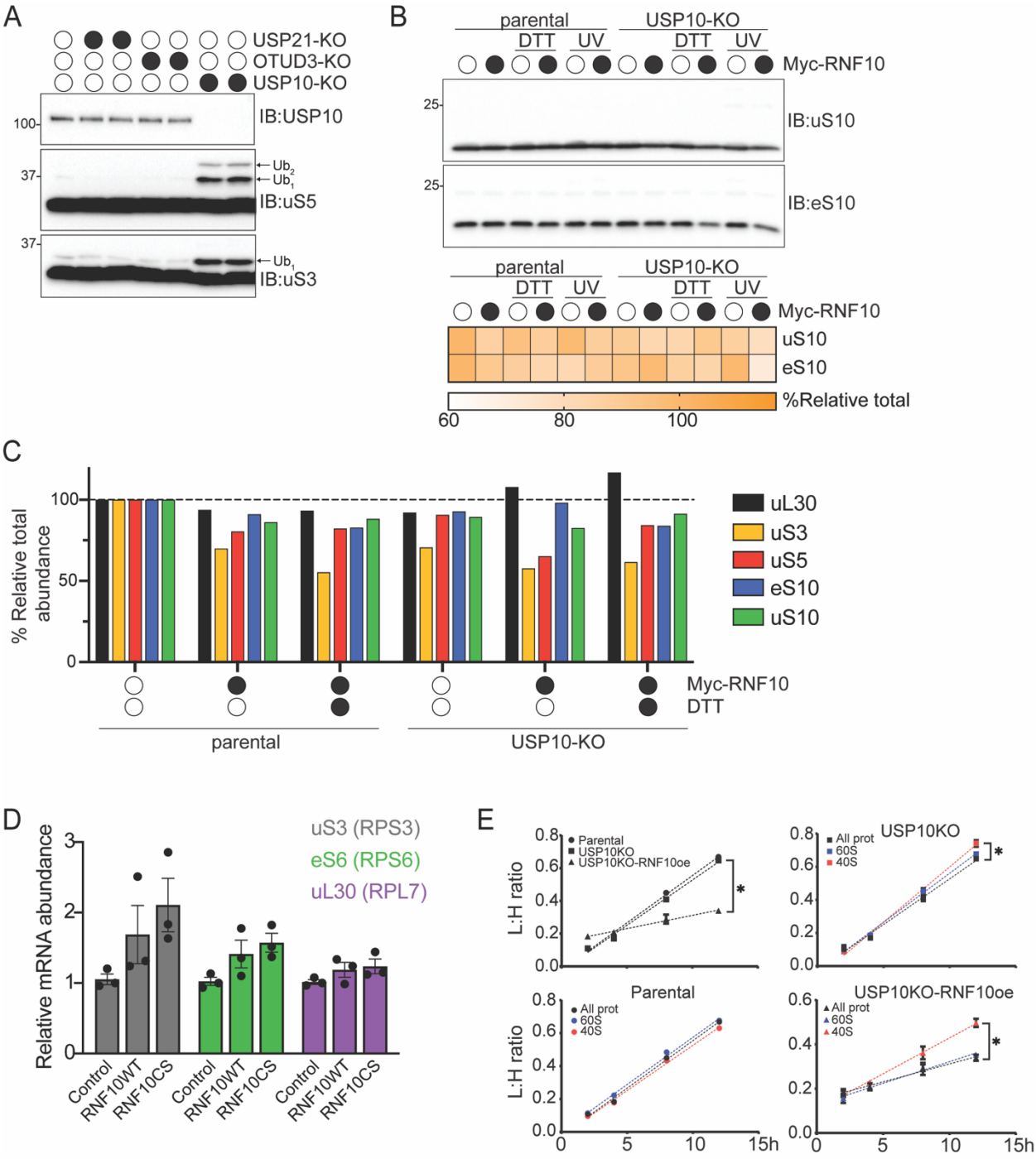
A
USP21-KO
OTUD3-KO
USP10-KO
100
IB:USP10
37
Ub2
Ub1
IB:uS5
37
Ub1
IB:uS3
B
parental
USP10-KO
DTT
UV
DTT
UV
Myc-RNF10
25
IB:uS10
25
IB:eS10
parental
USP10-KO
DTT
UV
DTT
UV
Myc-RNF10
uS10
eS10
%Relative total
60
80
100
C
% Relative total abundance
100
50
0
uL30
uS3
uS5
eS10
uS10
Myc-RNF10
DTT
parental
USP10-KO
D
Relative mRNA abundance
3
2
1
0
uS3 (RPS3)
eS6 (RPS6)
uL30 (RPL7)
Control
RNF10WT
RNF10CS
Control
RNF10WT
RNF10CS
Control
RNF10WT
RNF10CS
E
L:H ratio
Parental
USP10KO
USP10KO-RNF10oe
*
USP10KO
All prot
60S
40S
*
Parental
All prot
60S
40S
USP10KO-RNF10oe
All prot
60S
40S
*
0.8
0.6
0.4
0.2
0.0
0
5
10
15h

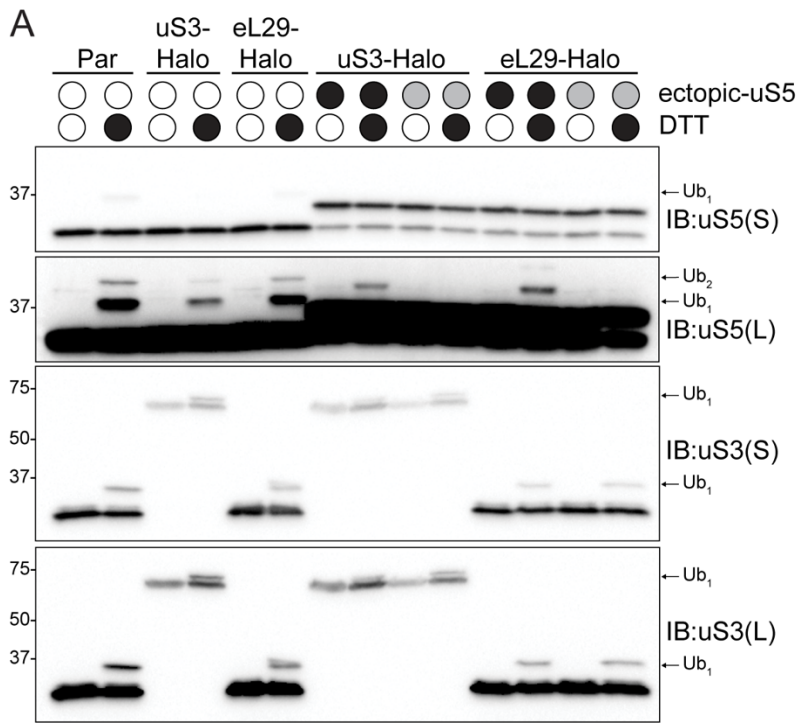

Figure 3.10. Loss of uS5 ubiquitylation blocks RNF10-mediated 40S protein turnover, Related to Figure 3.4.
(A) 293T parental cells (Par) or 293T-uS3-Halo or eL29-Halo cells alone or with constitutive wild type (black circles) or K54R/K58R mutant (grey circles) uS5 expression were either untreated or treated with DTT (5mM) for 2 hours. Cell lysates were analyzed by SDS-PAGE and immunoblotted with the indicated antibodies.

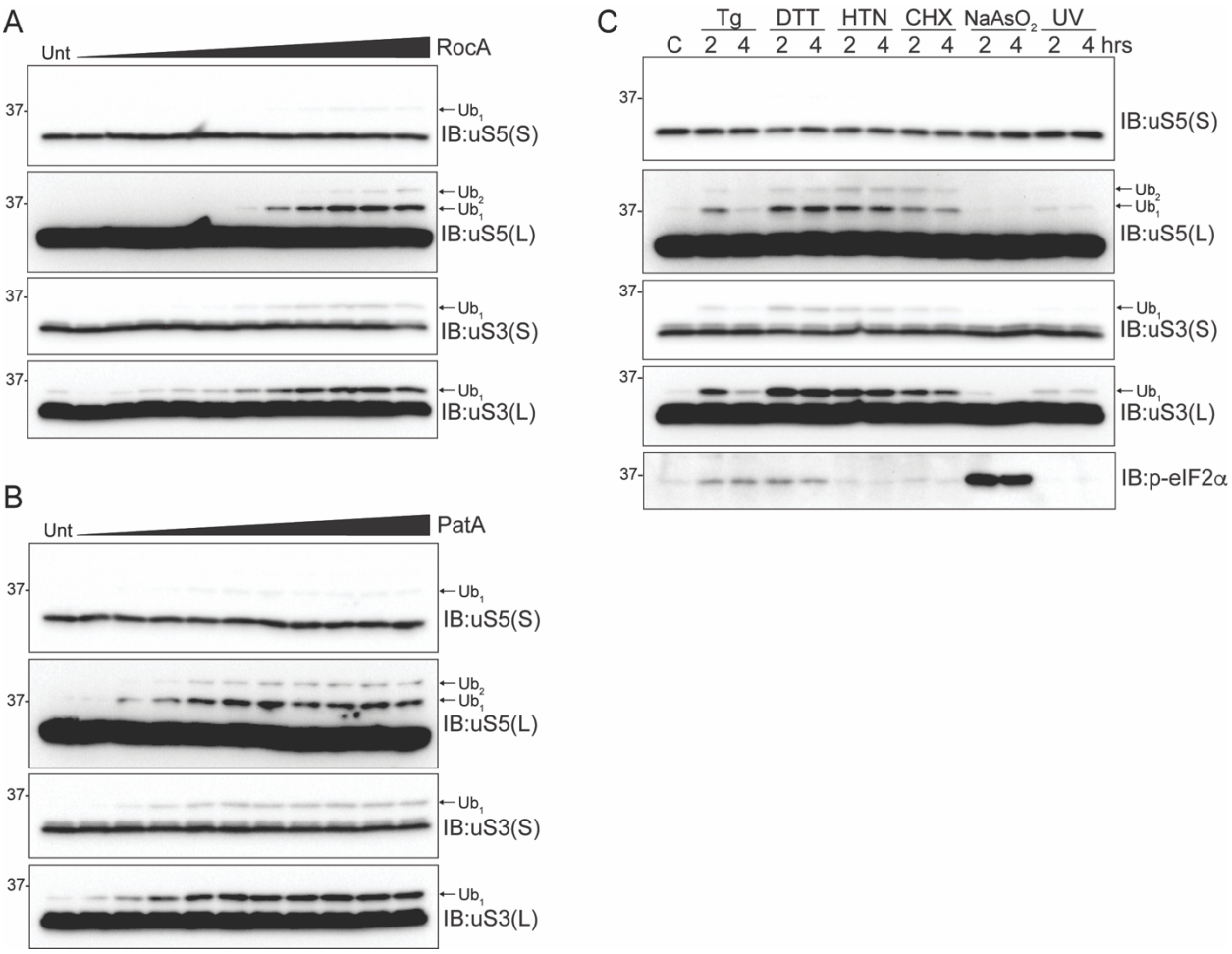

Figure 3.11. Translation initiation inhibition triggers ribosome ubiquitylation, Related to Figures 3.5 and 3.6.

(A,B) 293T cells were treated with increasing concentrations of either RocA (0.031-3.2uM) (A) or PatA (0.31-100nM) (B) for two hours. Whole-cell lysates were analyzed by SDS-PAGE and immunoblotted with the indicated antibodies. For all blots, the ubiquitin-modified ribosomal protein is indicated by the arrow. S and L denote short and long exposures, respectively.
(C) Cell extracts from cells treated with Tg (1uM), DTT (5mM), HTN (2ug/ml), CHX (100ug/ml), NaAsO2 (500uM) or UV (0.02J/cm^2) (washout) for two or four hours were analyzed by SDS-PAGE and immunoblotted with the indicated antibodies.

Figure 3.12. Ribosomal subunit imbalance is present in gradient fractions containing ubiquitylated ribosomes, Related to Figure 3.7.
(A-B) The normalized log2 SILAC ratio (H-HTN:L-untreated) of all quantified 40S (A, red circles) and 60S (B, blue circles) proteins within indicated sucrose gradient fractions from lysates treated with RNaseA prior to density gradient centrifugation. Each data point is an individual ribosomal protein, and the black bar denotes the median value.
(C-D) Cell extracts from untreated (C) or HTN (2ug/ml) treated (D) 293T cells were fractionated on 10-30% sucrose gradients. The 254nm absorbance trace is depicted. Fractions were analyzed by SDS-PAGE and immunoblotted with the indicated antibodies. The ubiquitin-modified ribosomal protein is indicated by the arrow. S and L denote short and long exposures respectively.
(E-F) The normalized log2 SILAC ratio (H-HTN:L-untreated) of all quantified 40S (E, red circles) and 60S (F, blue circles) proteins within indicated sucrose gradient fractions from untreated lysates prior to density gradient centrifugation. Each data point is an individual ribosomal protein, and the black bar denotes the median value.

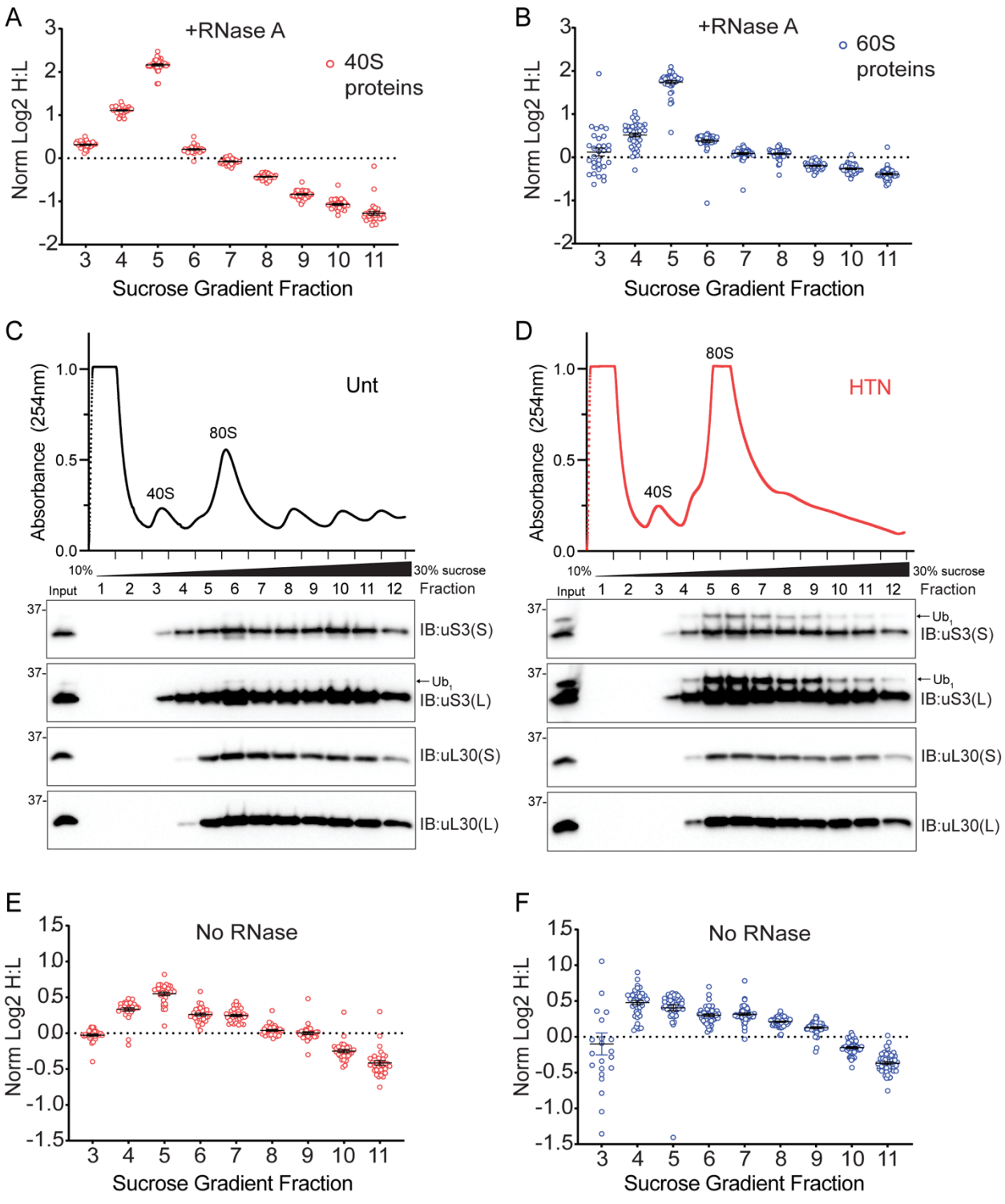
A
+RNase A
40S proteins
Norm Log2 H:L
Sucrose Gradient Fraction
B
+RNase A
60S proteins
Norm Log2 H:L
Sucrose Gradient Fraction
C
Unt
Absorbance (254nm)
40S
80S
10%
30% sucrose
Input
Fraction
IB:uS3(S)
IB:uS3(L)
IB:uL30(S)
IB:uL30(L)
D
HTN
Absorbance (254nm)
40S
80S
IB:uS3(S)
IB:uS3(L)
IB:uL30(S)
IB:uL30(L)
E
No RNase
Norm Log2 H:L
Sucrose Gradient Fraction
F
No RNase
Norm Log2 H:L
Sucrose Gradient Fraction

Figure 3.13. Model of iRQC activation, Related to Figure 3.7.
(A) Collided disome structure with ubiquitylated 40S proteins that function either within (uS10/RPS20, eS10/RP10 shown in orange) or outside (uS3/RPS3, uS5/RPS2 shown in magenta) the characterized RQC pathway. RACK1 (green) mRNA (blue), and P-site tRNA (blue) are indicated. Structure from PDB:6HCQ and 6HCM.
(B) Under normal homeostatic conditions, cap-dependent translation proceeds with 43S scanning of the 5' untranslated region, followed by start codon recognition, and 60S subunit joining to form an elongation competent 80S ribosome (indicated by yellow ribosomes). Stalled preinitiation complexes or collisions between 43S and 80S ribosomes (red ribosomal subunits) activate the iRQC pathway in which RNF10 is recruited to ubiquitylate uS5 and uS3 on specific lysine residues. Persistent ribosome ubiquitylation triggers 40S subunit destruction and recycling of initiation factors and the 60S subunit. Stalled and/or collided preintiation complexes can alternatively undergo USP10-dependent ribosome deubiquitylation to allow for translation initiation progression.

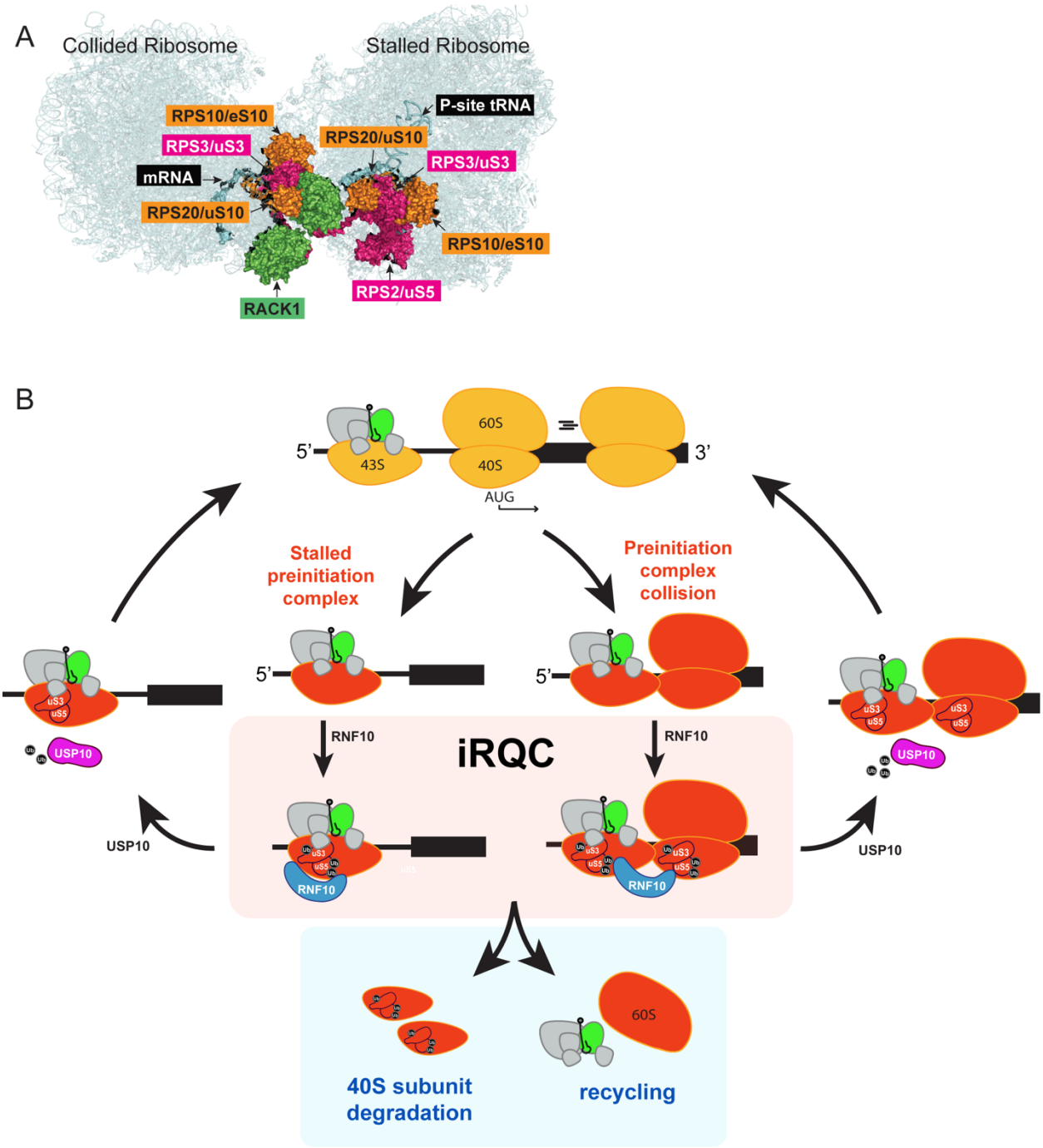
A
Collided Ribosome
Stalled Ribosome
RPS10/eS10
RPS3/uS3
mRNA
RPS20/uS10
RACK1
RPS2/uS5
P-site tRNA
RPS20/uS10
RPS3/uS3
RPS10/eS10
B
5'
43S
60S
40S
3'
AUG
Stalled preinitiation complex
Preinitiation complex collision
RNF10
iRQC
USP10
40S subunit degradation
recycling

Chapter 4

Future research directions aimed at understanding the role of regulatory ribosomal ubiquitylation

4.1 The effects of initiation factor loss-of-function on RRub

As discussed previously in chapter 3, we are currently unable to tell whether uS3 and uS5 ubiquitylation is triggered by isolated terminally stalled preinitiation complexes, or preinitiation complex collisions. We hypothesize that if a collision event is occurring between either a 43S/43S or 43S/80S then sucrose gradient fractionation should reveal an increase in the relative abundance of both 40S ribosomal proteins to 60S, as well as the initiation factors. To test this, we utilized SILAC-based quantitative proteomics to compare the abundance of these proteins across the sucrose gradient. Heavy-labeled HTN treated cells were mixed with untreated cells prior to lysis, followed by density centrifugation. We observed a slight increase in 40S protein abundance relative to 60S in fraction five from HTN-treated cells (Figure 4.1A). Fraction five corresponds to the leading edge of the 80S peak, which widens and skews towards the left in response to translation initiation inhibitors (Figure 3.7C). With the idea that this disequilibrium among ribosomal proteins indicates the presence of potentially collided 43S preinitiation complex collisions, then the relative abundance of the individual initiation factors should also increase within fraction five. We began by taking a closer look at the eIF3 complex, which is the largest initiation factor complex comprised of 13 subunits. We observed noticeable variance in the abundance of the individual eIF3 complex proteins across the gradient following HTN treatment (Figure 4.1B). Some proteins of the eIF3 complex (e.g. eIF3A) were not observed within every sucrose fraction, while others displayed decreased normalized abundance throughout the gradient (e.g. eIF3C). For the majority of eIF3 subunits, HTN treatment results in increased protein abundance in fraction five, with the exception of eIF3C

and eIF3K (Figure 4.1B). While the normalized log2 ratio (H:L-HTN:untreated) for the remaining subunits is not equivalent to that of the ribosomal proteins, their presence in this fraction does hint that 43S preinitiation complexes may be present within this fraction of the sucrose gradient. Fraction three has been shown to contain primarily 40S ribosomes, however a 10-30% sucrose gradient lacks the resolving power to distinguish a 40S subunit from an initiation factor decorated 43S preinitiation complex. The relative abundance of the individual eIF3 complex proteins is on par with 40S ribosomal proteins, suggesting that this fraction contains a mixture of 40S and 43S ribosomal complexes. To examine if the observed variability in protein abundance across the sucrose gradient was unique to the eIF3 complex, we looked at the abundance of additional initiation factors that comprise the 43S preinitiation complex (Figure 4.1C). The initiation factor eIF1AX, which is a paralog of eIF1A, appears to be enriched in fractions three, five and six, but then diminished in heavier fractions. Whereas EIF5A and eIF4A1 are enriched primarily in the heavier fractions. Interestingly, eIF6 was highly enriched throughout the entirety of the gradient. eIF6 is an integral initiation factor that binds the 60S ribosomal subunit to inhibit association of the 40S, and premature 80S formation. eIF6 enrichment within fractions five and six was expected with the potential presence of 43S complexes, however the presence of eIF6 throughout the heavier sucrose gradient fractions was puzzling, especially considering the drop in ribosomal protein abundance observed in fractions eight through eleven. We would have expected to see a gradual decrease in the heavier fractions as eIF6 abundance would be predicted to align with 60S ribosomal proteins. One possible explanation for the relative inconsistency in abundances across the gradient could be that the relative affinity between the 40S and the initiation factors may not be the same for each factor nor strong enough to withstand the density centrifugation step, ultimately leading to disassociation of the complex. To address this problem, crosslinking could be done either prior to or after cell lysis. Together these results suggest the potential presence of 43S preinitiation complexes within fraction five,

however further biochemical analysis is needed to confirm the existence of a collision event, as well as begin to elucidate the increased presence of eIF6 throughout the gradient.

Next, we wanted to understand the role of individual initiation factors in iRQC. We hypothesized that depletion of individual initiation factors would lead to induced or enhanced ubiquitylation of uS3 and uS5 through scanning inhibition. We utilized small interfering RNAs (siRNA) targeting ten initiation factors in the presence or absence of HTN. We found that only depletion of eIF6 resulted in increased basal ubiquitylation of uS3 and uS5, while loss of eIF4A1 resulted in complete ablation of HTN induced ubiquitylation (Figure 4.2A-E). In mammals the most abundant translation initiation factor is eIF4A; for which two paralogs with 90% identity exist, eIF4A1 (DDX2A) and eIF4A2 (DDX2B) (Nielsen et al., 1985). eIF4A is a DEAD-box RNA helicase that is responsible for recruitment of the 43S preinitiation complex to all mRNAs, irrespective of the structure of the 5' leader sequence (Pelletier and Sonenberg, 2019). Intriguingly, loss of eIF4A1 does not induce ubiquitylation of either uS3 or uS5 in otherwise untreated cells, nor upon HTN treatment (Figure 4.2A). The same loss of HTN induced ubiquitylation was not observed in cells knockdown for eIF4A2, however it should be noted that in 293T cells eIF4A1 is expressed ~7.5 fold higher than eIF4A2 (Pontén et al., 2008) which might account for the inconsistency. Based on our previous findings that eIF4A inhibitors like RocA and PatA enhance ubiquitylation of uS3 and uS5, we reasoned that depletion of eIF4A itself would also lead to uS3 and uS5 ubiquitylation. These findings suggest two possible explanations, first, eIF4A1 loss-of-function is most likely inhibiting the recruitment of the 43S to the mRNAs thus inhibiting translation initiation globally prior to commencement of 5'UTR scanning. Secondly, loss of eIF4A is fundamentally distinct from its inhibition with chemical compounds such as RocA, which has been shown to induce a physical block to scanning ribosomes by inducing eIF4A binding to polypurine motifs in an ATP-independent manner (Iwasaki et al., 2016a; Iwasaki et al., 2019).

We next examined eIF1A paralogs, 1AX and 1AY. The initiation factor eIF1A works synergistically with eIF1 to promote formation of the 43S preinitiation complex and scanning of the 5' leader sequence. Together these factors have been shown to assist in recognition of the correct start codon by stabilizing the 40S ribosome in an open-latch conformation (Passmore et al., 2007). Loss of either eIF1AX or 1AY did not induce uS5 or uS3 ubiquitylation. However, we did observe that two oligos targeting eIF1AX, when transfected into cells resulted in decreased ubiquitylation following HTN treatment (Figure 4.2B). Because HTN induced ubiquitylation of uS3 was detectable, this implies that scanning is still occurring, but suggests that depletion of eIF1AX results in a ribosome conformation that is inconducive to scanning, and thus promotes decreased AUG start codon recognition.

eIF5A was initially characterized as an initiation factor; however recent studies have shown that it serves a functional role during translation elongation as a ribosomal pause relief factor at difficult to translate motifs in the CDS (Manjunath et al., 2019). Additionally, a role in facilitating correct start codon selection has been shown using MYC expression, where eIF5A depletion resulted in translation initiation at an upstream non-cognate start codon yielding an N-terminal extension on the MYC1 protein (Manjunath et al., 2019). Depletion of eIF5A resulted in no induced uS3 and uS5 basal ubiquitylation, however there was a slight reduction in uS5 modification following HTN treatment (Figure 4.2C). Alternatively, eIF5B is a GTPase initiation factor that promotes the joining of the 60S ribosomal subunit and the 48S PIC to form an 80S ribosome (Lee et al., 2002; Pestova et al., 2000). Single-molecule studies in yeast have shown that eIF5B controls the transition from translation initiation to elongation (Wang et al., 2019). As a means to ensure proper selection of the start codon and to prevent ribosomal collisions in the 5'UTR, the transition time between initiation and elongation is comparatively slower in eukaryotes than bacteria (Juszkiewicz et al., 2018a; Wang et al., 2019). This prolonged entry to elongation was due to a sustained dwell time of eIF5B on the ribosome immediately after subunit 80S formation. Interestingly, loss of eIF5B showed no discernable increase in uS3 or

uS5 ubiquitylation in untreated cells, however two of the oligos did show decreased ubiquitylation following HTN treatment, which could correspond to reduced formation of 80S ribosomes (Figure 4.2C).

To allow for 43S ribosomal complex movement along the mRNA, RNA secondary structures need to be unwound by specialized RNA helicases. DDX3X and DDX3Y are variants for DDX3, an ATPase DEAD-box helicase that removes secondary structures found in the 5'UTR of transcripts directly at the site of the 5'-cap, to allow for attachment of the scanning 43S PIC. Furthermore, DDX3 is selective for specific mRNAs which contain stable hairpin loops in the 5' end of the transcript (Calviello et al., 2021; Soto-Rifo et al., 2012). While loss of DDX3Y did not induce ubiquitylation of uS3 or uS5, there is a very small amount of uS3 ubiquitylation following DDX3X depletion (Figure 4.2D). Furthermore, the reduction in HTN induced ubiquitylation that is observed for individual oligos of both paralogs suggests a decrease in 43S PIC engagement and thus overall scanning. Because the secondary structures that DDX3 is targeting are located immediately after the 5'-cap, we hypothesize that loss of the DDX3 helicase results in reduced HTN induced ubiquitylation and not induce the RRub in the absence of stress. Similar to eIF4A and DDX3, another DExH-box helicase, DHX29, is also required for cap-dependent formation of the 43S PIC on transcripts with highly structured 5'UTR leader sequences (Pisareva et al., 2008). Previous (^{35}S)-methionine metabolic labeling studies using both siRNA and shRNA targeting DHX29 showed a 2-fold reduction in incorporation, suggesting repressed protein translation (Parsyan et al., 2009). While neither uS3 nor uS5 was ubiquitylated upon reduction of DHX29 alone, the HTN induced ubiquitylation of uS3 appears to be slightly diminished, with a clear loss of the uS5 diubiquitin band (Figure 4.2E). While this suggests that scanning remains intact, the inability to unwind secondary structures appears to be limiting translation elongation.

Having observed an enrichment in eIF6 abundance across sucrose gradients following HTN treatment, we were intrigued to find that depletion of eIF6 alone induces ubiquitylation of

uS3 and uS5 in cells (Figure 4.2E). These findings suggest that loss of eIF6 is potentially increasing the chance for premature 80S formation, in which the 40S and 60S subunits join in the 5'UTR without AUG or non-cognate start recognition, thus inducing terminal stalling and thereby downstream collisions with trailing scanning 43S complexes. Further biochemical studies including combinatorial loss of multiple initiation factors needs to be carried out to better understand the relationship between the steps in translation initiation and regulatory ribosomal ubiquitylation.

4.2 Transcriptome wide alterations following enhanced ubiquitylation of uS3 and uS5

Our demonstration that DTT treatment can both induce uS3 and uS5 ubiquitylation and trigger phosphorylation of eIF2α suggests that specific transcripts are being targeted by the iRQC pathway, and these mRNA are probably escaping the global translational shutdown brought on by ISR activation. To try and identify these transcripts we performed poly(A) selected RNAseq on three comparison groups looking at varying degrees of uS3 and uS5 ubiquitylation. First, we compared HTN induced ubiquitylation in 293T parental cell to USP10KO cells which display constitutive uS3 and uS5 ubiquitylation (Figure 4.3A) to see if similar transcripts were differentially expressed upon uS3/uS5 modification. Next, we analyzed the effects of RNF10 overexpression by directly comparing wild-type RNF10 expression to that of a catalytically inactive mutant RNF10, or control plasmid (LRRC49) (Figure 4.3B). This comparison would identify transcripts that are differentially regulated based upon RNF10 overexpression and further stratify those transcripts that alter in an RNF10 ubiquitin ligase-dependent manner. Finally, utilizing a 293FlpIn cell line we compared untreated parental cells to those treated with HTN, or to RNF10KO cells either untreated or HTN treated (Figure 4.3C). This allowed us to see how loss of uS3 and uS5 ubiquitylation affects HTN induced transcriptional changes.

The eukaryotic cytoplasmic ribosome is made up of two subunits: the large 60S which is comprised of 46 proteins and 3 rRNAs (5S, 28S, and 5.8S) and the smaller 40S made up of 33 proteins and the 18S rRNA (Ben-Shem et al., 2011). Historically the relative integrity of RNA samples has been attributed to the 28S:18S ratio. In the process of determining RNA integrity across the sample groups we were able to obtain the 18S/28S ratio which demonstrated an inconsistency with 18S rRNA abundance and the associated decrease in 40S proteins known to some of our sample conditions. For instance, loss of USP10 results in constitutive uS3 and uS5 ubiquitylation and thereby a 15% decrease in total 40S protein abundance as seen via proteomic analysis. We would expect that with loss of ribosomal proteins, there would be an associated decrease in 18S rRNA abundance. Tapestation analysis of rRNA abundance prior to RNA sequencing revealed a 7% decrease in the 18S/28S ratio in samples derived from USP10 knockout cells compared to untreated controls, however this was not statistically significant (Figure 4.3D). A similar decrease was observed in two cell types treated with HTN but was reversed in cells null for RNF10, suggesting a link between RNF10 mediated ubiquitylation and rRNA degradation. Furthermore, overexpression of RNF10 resulted in a dramatic 60% decrease in 18S/28S ratio as compared to a control plasmid. Not only does this not equate to the 15% loss of protein abundance observed via proteomic analyses, but overexpression of a catalytically inactive mutant of RNF10 also resulted in a significant decrease in the 18S/28S rRNA ratio. The observed loss of 18S rRNA in the overexpression experiment could be the result of experimental error. It is necessary to repeat some of these comparisons and run agarose gel electrophoresis to further examine 18S and 28S rRNA levels upon RNF10 WT and inactive mutant overexpression.

We hypothesize that in response to enhanced uS3 and uS5 ubiquitylation, there may be specific mRNAs that are always up or down regulated. To identify mRNA transcripts whose abundance may be regulated by iRQC pathway activation, we used RNAseq and corresponding examination of differentially expressed genes in untreated cells or cells treated with HTN for two

hours. Roughly 8,500 genes were differentially expressed in cells treated with HTN. A majority of the most significantly up regulated genes were histone related transcripts (Figure 4.4A). Gene ontology analysis revealed numerous pathways upregulated in HTN treated cells, including apoptosis signaling (*ATF3, FOS, MAP3K1, MAP3K14, JUN*) and the p53 pathway (*NOXA, GADD45, PPM1D*). We directly interrogated any change in expression for both the small and large subunit ribosomal transcripts. Interestingly, all mRNAs encoding ribosomal proteins, large or small, displayed reduced abundance in response to HTN (Figure 4.4A). Why ribosomal gene expression is reduced by HTN treatment is still unclear. Further bioinformatic analysis is needed to identify specific pathways or stress response mechanisms that may be regulated in response to HTN treatment and whether any of these directly correlate to ubiquitylation of the ribosome.

Our next question was if loss of USP10 results in a similar set of differentially expressed genes as compared to HTN treatment. USP10 knockout cells display constitutively high levels of uS3 and uS5 ubiquitylation. Comparing USP10 knockout cells to untreated parental controls, approximately 6,400 genes were differentially expressed, of these 4,000 transcripts corresponded differentially expressed mRNAs following HTN treatment (Figure 4.4B). We next looked at the direction of expression of the individual ribosomal genes. Similar to our findings with HTN, loss of USP10 results in reduced mRNA abundance for the majority of large and small subunit ribosomal protein mRNAs. However, this is in direct contrast to our previous findings that RNF10 overexpression results in increased small ribosomal protein mRNA abundance suggesting a possible post-transcriptional mechanism underlying the observed reduction in 40S protein levels. Moreover, while we do not see a loss of 60S ribosomal protein abundance in USP10KO cells, we do observe a reduction in 60S ribosomal gene expression. This further demonstrates that the reduced 40S protein levels are in fact controlled via post-translational mechanism.

We then analyzed differences in ribosomal protein mRNAs between cells overexpressing wild-type RNF10, and those expressing the catalytically dead mutant (CS).

Wild-type overexpression produced approximately 4,200 differentially expressed genes, while RNF10CS had over 7,400 differentially expressed genes (Figures 4.4C and 4.4D). Of these roughly 3,000 transcripts matched to both comparison groups. Transcripts enriched above 2-fold in cells expressing wild-type RNF10 included both an HSP70 response as well as downstream effectors of the ISR. This correlates with our unpublished data demonstrating that overexpression of RNF10 results in increased eIF2α phosphorylation. Moreover, phospho-eIF2α was also induced upon expression of the inactive RNF10 mutant, which suggests that RNF10 ligase activity does not play a role in activating the ISR. What then is the role of RNF10's ligase activity in regulating gene expression? Comparing the 3,000 differentially expressed genes that corresponded to both wild-type and inactive RNF10 expression showed that greater than 90% of differentially expressed transcripts were altered similarly upon WT or inactive RNF10 overexpression (Figure 4.4E). While genes like *FOS, EGR1*, and *C11orf95* were upregulated in wildtype expressing cells, the same genes were down regulated in cells expressing the CS mutant. Alternatively, we found genes like *MYC, TUBB2B* and *RPL22* to be up regulated in CS mutant expressing cells, while being down regulated in cells expressing wild-type RNF10. These results suggest that RNF10 overexpression results in large alterations to the transcriptome that are largely independent of its ligase activity. RNF10 was originally identified as a transcription factor that regulates expression of Myelin-associated glycoprotein (MAG), as well as Schwann cell differentiation (Hoshikawa et al., 2008). Therefore RNF10's putative function as a transcription factor might be playing a significant role in altering the transcriptome upon overexpression. Consistent with our previous qPCR findings that overexpression of wild-type or catalytically inactive RNF10 resulted in increased mRNA abundance for ribosomal proteins uS3, eS6 and uL30 (Figure 3.9D). Consistent with this observation, mRNA levels for all small and large subunit proteins were increased following RNF10 overexpression regardless of ligase activity (Figure 4.4F). These findings would suggest

a post-transcriptional mechanism underlying the observed reduction in 40S proteins following RNF10 overexpression. However, the up regulation in the large subunit transcripts could explain the slight increase in 60S protein abundance we observed with RNF10 overexpression (Figures 3.2D and 3.2E). Interestingly, these findings do not align with the ribosomal gene expression in USP10KO cells which exhibited an overall reduced expression for all ribosomal genes (Figure 4.4B). Given RNF10 overexpression and loss of USP10 both result in constitutive uS3 and uS5 ubiquitylation, this result suggests that the observed changes in ribosomal transcript levels are not directly correlated to ubiquitylation of the 40S ribosome.

To better understand what fraction of the observed transcript abundance changes that occur upon HTN treatment are dependent upon RNF10, we compared the differentially expressed genes from 293FlpIn parental cells either untreated or treated with HTN, to RNF10 knockout cells. The parental cells showed roughly 7,600 transcripts whose abundance was altered in response to HTN (Figure 4.5A), whereas the RNF10 knockout cells had approximately 7,100 differentially expressed genes (Figure 4.5B). Cross comparison of all differently expressed genes in parental cells versus RNF10KO cells either untreated or treated with HTN showed nearly 5,800 overlapping genes. The question remained, is there a correlation between parental cells and those null for RNF10 among the common differentially expressed genes? The log2 fold change comparison between parental and RNF10KO cells of commonly expressed genes showed a near perfect linear correlation regarding directionality of mRNA transcript abundance change (Figure 4.5C). This suggests that the loss of RNF10 and subsequently loss of uS3/uS5 ubiquitylation does not have a dramatic effect on the transcriptional changes associated with HTN treatment.

While we know that enhanced ubiquitylation triggers targeted degradation of the 40S ribosomal subunit, we have yet to identify mRNAs that elicit the iRQC response in cis. Although RNAseq proved to be very informative with regards to the transcriptome-wide changes associated with enhanced ubiquitylation or harringtonine treatment, it was not likely the right

approach to distinguish iRQC targeted transcripts. The more precise method for identifying specific mRNAs that contain either terminally stalled or collided preinitiation complexes would be translation complex profiling (TCP-seq). Unlike conventional ribosome-profiling TCP-seq identifies all ribosome-mRNA complexes, not simply elongating 80S ribosomes, across the transcriptome (Archer et al., 2016; Shirokikh et al., 2017). Covalent crosslinking allows for RNAse footprinting that, combined with deep sequencing, can be used to map mRNAs within all three phases of translation. Utilizing this method will not only indicate if transcripts with uORFs are preferentially targeted by the iRQC, but it will also reveal if preinitiation collisions are taking place in the 5'UTR of mRNAs. Potential queuing events have already been suggested in previous mammalian-based TCP-seq studies. Wagner et al. demonstrated a range of protected fragment sizes (24-70 nucleotides) in the 5'UTR of transcripts which correspond either to two queued 40S subunits or lingering initiation factors bound near the mRNA exit channel (Wagner et al., 2020b). Performing these types of experiments in the presence of harringtonine or in USP10KO cells will be very informative as to whether preinitiation complex collisions are taking place in vivo.

4.3 Concluding remarks

In mammalian cells, the majority of translational scanning has been shown to be cap-tethered, meaning that the 5'cap remains associated with the scanning preinitiation complex until initiation transitions into elongation (Bohlen et al., 2020a). Using selective 40S footprinting of endogenous transcripts in human cell lines, Bohlen et al. demonstrate that 40S ribosomes are cap-tethered throughout translation initiation by performing translational arrests with harringtonine and capturing the number of 40S footprints in the 5'UTR. They show that over the course of harringtonine treatment the number of footprints diminishes indicative of a single round of initiation. Otherwise, no queuing events are observed upstream of the stalled 80S ribosome (Bohlen et al., 2020a). Additionally, they reveal that initiation factors remain

associated with the 40S subunit throughout the elongation phase of uORFs. In the case of uORF containing transcripts, reinitiation is critical to the downstream translation of additional uORFs or the main ORF. Selective initiation factor footprinting of uORFs showed that while factors like eIF3B, eIF4G1 and eIF4E are retained at short uORFs following termination, the 40S subunit lost eIF2α and must reacquire it before translating the next ORF (Bohlen et al., 2020a). These findings would suggest that iRQC preinitiation collisions cannot occur in the context of cap-dependent translation. One possible explanation is that uS3 and uS5 ubiquitylation takes place solely on terminally stalled preinitiation complexes. This would align with the data that Bohlen et al. presented, except that the target of RNF10 would in fact be a stalled 80S at the start codon. A second possibility is that preinitiation complexes can collide with other complexes or 80S ribosomes, but they do so in a cap-independent manner. Utilizing non-canonical routes like internal ribosome entry sites (IRES) would allow the cell to differentially regulate mRNA translation. Further examination is needed to uncover the potential for a cap-independent mode of translation and the role of regulatory ribosomal ubiquitylation.

While the use of selective TCP-seq appears to be the best approach to identifying endogenous transcripts targeted by the iRQC pathway, isolating them among a majority of cap-tether transcripts might prove to be difficult. Alternatively, sucrose density gradients combined with selective immunoprecipitation could be used to identify endogenous transcripts. Having already identified the fraction most likely associated with terminally stalled preinitiation complexes and/or collisions, either USP10KO cells or cells treated with an ISR agonist, like DTT, could be run across sucrose gradients. Cells would be covalently crosslinked first, followed by RNAse treatment prior to density centrifugation and fractionation. Serial tandem ubiquitin-associated domain (UBA) pulldowns using ubiquitin as the handle would isolate collision complexes which could then undergo poly(A) selection RNA sequencing to reveal endogenous iRQC transcripts. Additionally, following pulldowns, the isolated complexes could

be applied to a grid and analyzed by cryo-EM to determine the biomolecular structure of a 43S preinitiation complex collision.

Following the identification of target transcripts, a fluorescent-based reporter system can be constructed utilizing interchangeable 5' leader sequences. Variability in length and start codon strength, as well as strong secondary structures like G-quadraplexes and hairpins can begin to illuminate how scanning impediments will affect 40S ribosomal ubiquitylation. Additionally, loss of USP10 or RNF10 will demonstrate how overall protein output is altered when uS3/uS5 ubiquitylation is either constitutive or completely ablated. Utilizing a system in which the reporter can be pulled down using biotinylated tiling probes can further assist in understanding the composition of ribosomal complexes along the transcript. Proteomics can be employed to identify the relative abundance of all ribosomal proteins, which should show a disequilibrium among 40S versus 60S if queuing events or collisions are occurring. While none of these experimental designs are without complications, determining if collisions occur in the 5'UTR of mRNAs is essential to understanding the role of ubiquitylation of 40S ribosomal complexes during translation initiation.

4.4 Figures

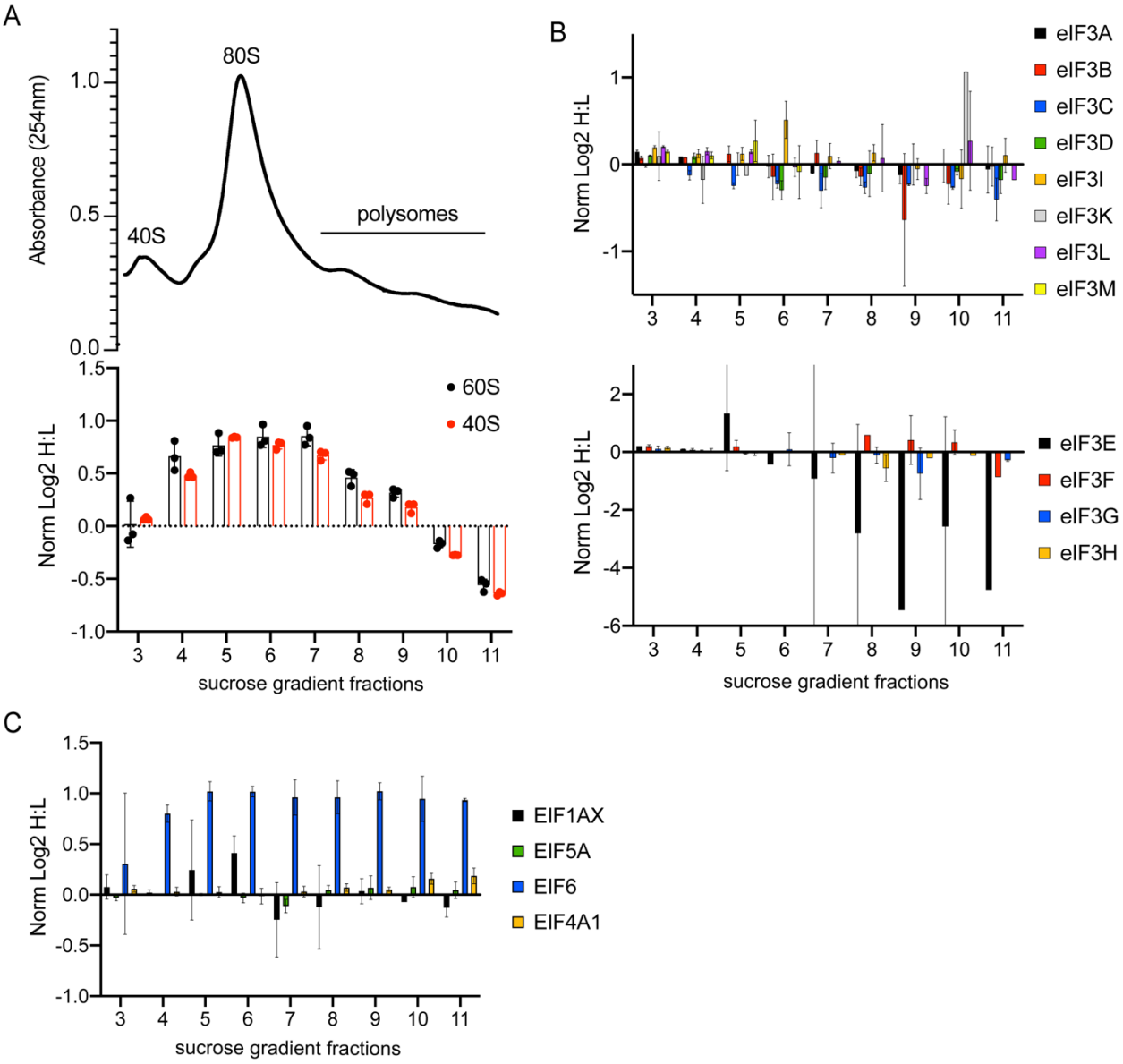

Figure 4.1. Enrichment for initiation factors across sucrose density gradient fractions.
(A) Top: equal amounts of 293T cells SILAC labeled (H-HTN (2ug/ml):L-untreated) we mixed together, lysed and fractionated on 10-30% sucrose gradients. The relative 254nm absorbance trace is depicted. Bottom: the normalized log2 SILAC ratio (H-HTN:L-untreated) of all quantified 40S (red bars) and 60S (black bars) proteins within indicated sucrose gradient fractions. Black bar denotes the median value from three biological replicates.
(B,C) The normalized log2 SILAC ratio (H-HTN:L-untreated) of the individual subunits of the eIF3 complex (B) or indicated initiation factors (C) within indicated sucrose gradient fractions following density gradient centrifugation. Bars denote the median value from three biological replicates.

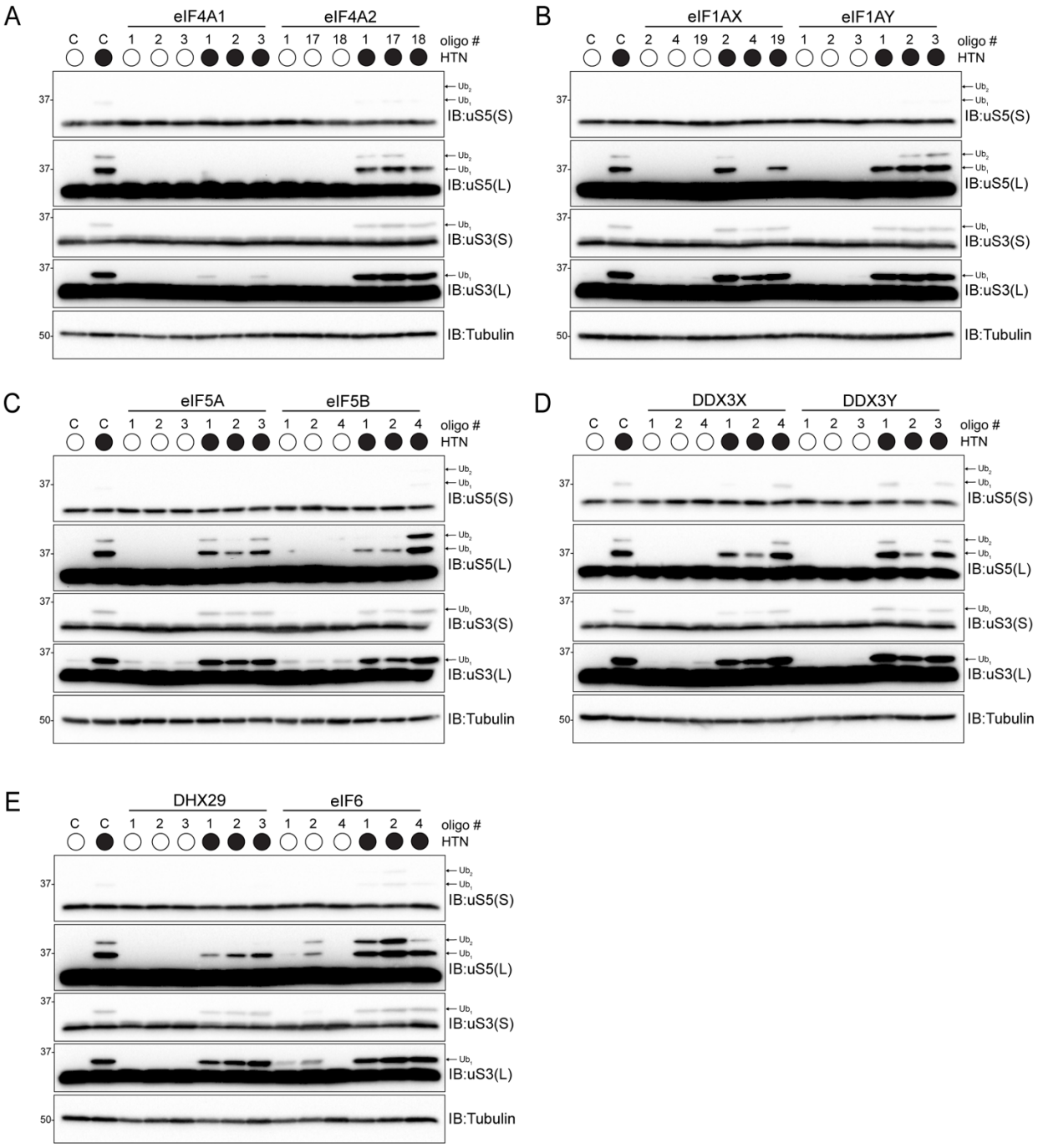

Figure 4.2. Depletion of translation initiation factors reduces ribosomal ubiquitylation. (A-E) 293T cells were transfected with either a control siRNA oligo or three separate siRNA oligos targeting the indicated initiation factor or helicase, followed by treatment with HTN (2ug/ml) for two hours. Cell lysates were analyzed by SDS-PAGE and immunoblotted with the indicated antibodies. For all blots, the ubiquitin-modified ribosomal protein is indicated by the arrow. S and L denote short and long exposures, respectively.

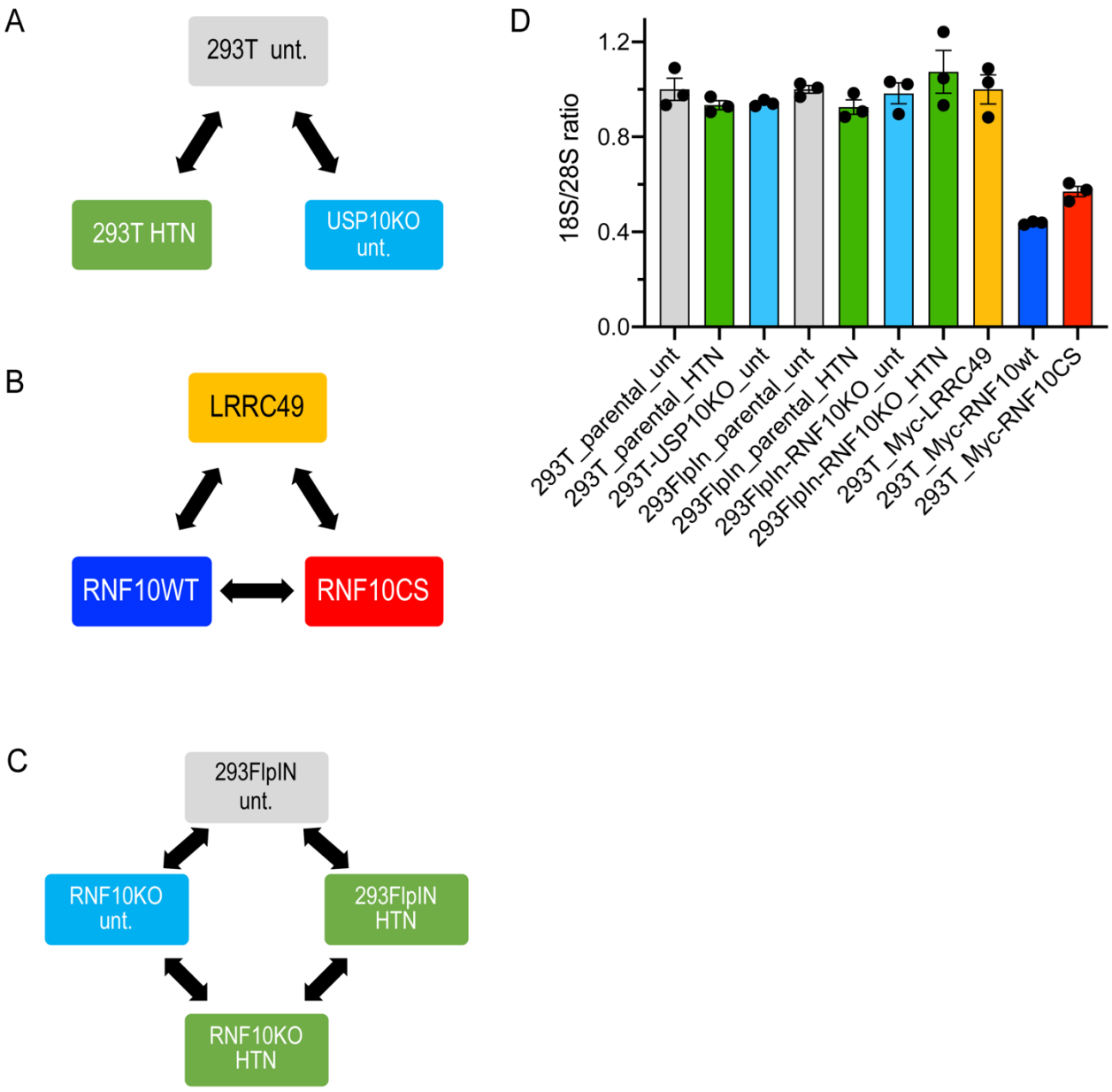

Figure 4.3. RNAseq analysis of induced uS3 and uS5 ubiquitylation.
(A-C) Schematic of different RNAseq comparison groups. 293T parental or USP10KO cells were either untreated or treated with HTN (2ug/ml) for two hours (A). 293T cells overexpressing either a control plasmid (LRRC49) or wild-type or catalytically inactive RNF10 (B). 293FlpIn parental or RNF10KO cells were either untreated or treated with HTN (2ug/ml) for two hours(C). (D) 18S/28S rRNA ratio for each of the different RNAseq comparison groups plotted based on the % integrated area calculated from the tapestation quality control RNA analysis. n=3, error bars denote SD.

Figure 4.4. Enhanced ubiquitylation of uS3 and uS5 trigger unique differential gene expression patterns.
(A,B) Left: volcano plot of the Log2 fold change (FC) for all differentially expressed genes for 293T parental cells either untreated or treated with HTN (2ug/ml) for two hours (A) or parental untreated cells compared to USP10KO untreated cells (B). Blue dots denote FC $\geq$ 1, red dots denote FC $\leq$ -1. Right: violin plot of the Log2 FC for all differentially expressed 60S (yellow) and 40S (purple) ribosomal proteins. Dashed line denotes median value.
(C,D) Volcano plot of the Log2 FC for all differentially expressed genes for 293T parental cells overexpressing either wild-type (C) or catalytically inactive (D) RNF10 compared to a plasmid control (LRRC49). Blue dots denote FC $\geq$ 1, red dots denote FC $\leq$ -1.
(E) Scatterplot of the Log2 FC of all differentially expressed genes in either cells overexpressing wild-type or CS mutant RNF10. Transcripts that are upregulated in RNF10CS expressing cells (red dots) or RNF10wt expressing cells (blue dots) are designated.
(F) Violin plot of the Log2 FC for all differentially expressed 60S (yellow) and 40S (purple) ribosomal proteins in cells overexpressing wild-type or catalytically inactive RNF10. Dashed line denotes median value.

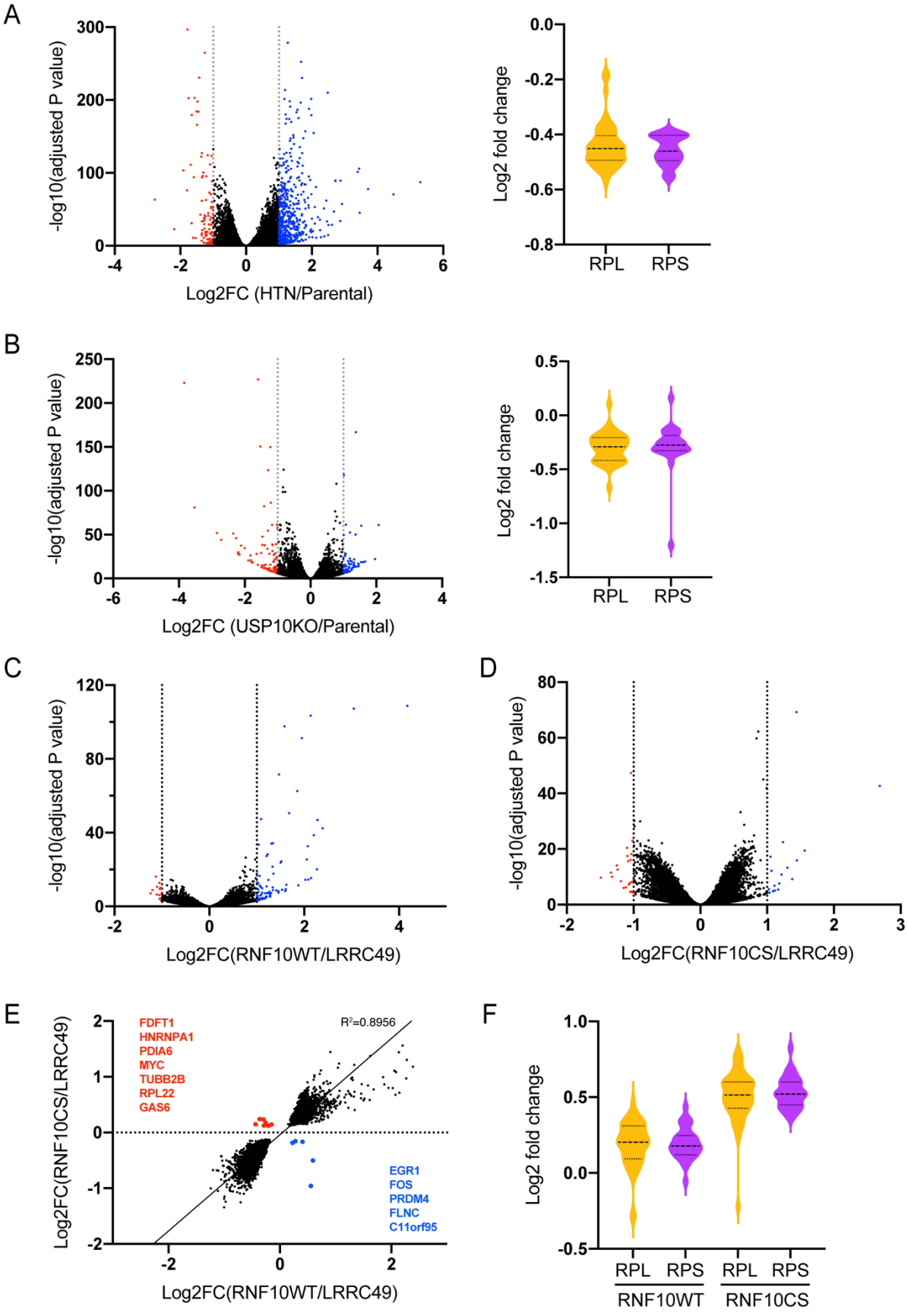
A
-log10(adjusted P value)
Log2FC (HTN/Parental)
Log2 fold change
RPL
RPS
B
-log10(adjusted P value)
Log2FC (USP10KO/Parental)
Log2 fold change
RPL
RPS
C
-log10(adjusted P value)
Log2FC(RNF10WT/LRRC49)
D
-log10(adjusted P value)
Log2FC(RNF10CS/LRRC49)
E
FDFT1
HNRNPA1
PDIA6
MYC
TUBB2B
RPL22
GAS6
R²=0.8956
EGR1
FOS
PRDM4
FLNC
C11orf95
Log2FC(RNF10CS/LRRC49)
Log2FC(RNF10WT/LRRC49)
F
Log2 fold change
RPL
RPS
RPL
RPS
RNF10WT
RNF10CS

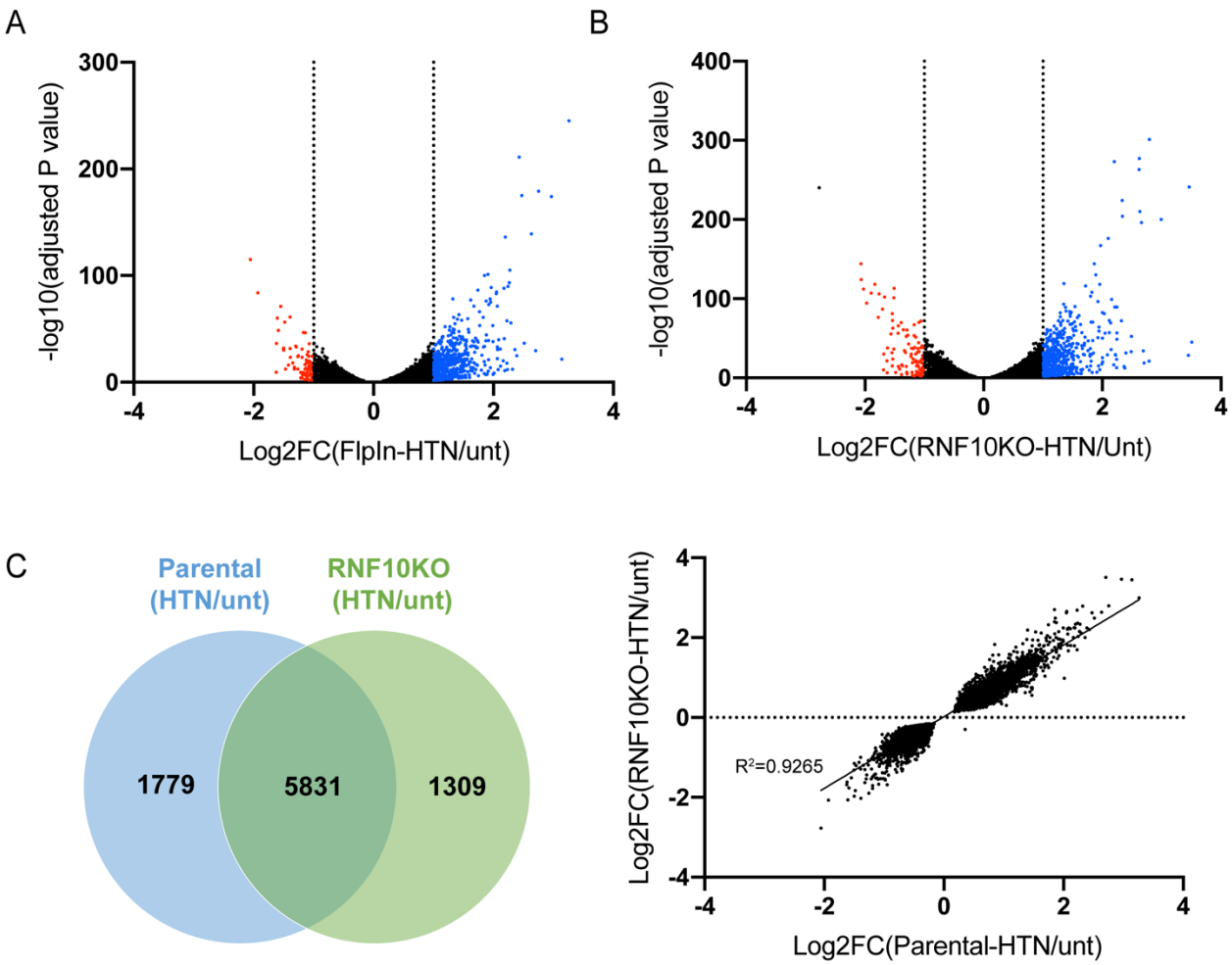

Figure 4.5. Loss of RNF10 exhibits no transcriptome wide changes.
(A,B) Volcano plot of the Log2 FC for all differentially expressed genes for either 293FlpIn parental (A) or RNF10KO (B) cells that were either untreated or treated with HTN (2ug/ml) for two hours. Blue dots denote FC ≥ 1, red dots denote FC ≤ -1.
(C) Left: Venn diagram of all differentially expressed genes in either 293FlpIn parental or RNF10KO cells comparing untreated to treatment with HTN for two hours. Right: Scatterplot of the Log2 FC of all the common differentially expressed genes.

References

Akutsu, M., Dikic, I., and Bremm, A. (2016). Ubiquitin chain diversity at a glance. J Cell Sci *129*, 875-880.

An, H., and Harper, J.W. (2018). Systematic analysis of ribophagy in human cells reveals bystander flux during selective autophagy. Nat Cell Biol *20*, 135-143.

An, H., and Harper, J.W. (2020). Ribosome Abundance Control Via the Ubiquitin-Proteasome System and Autophagy. J Mol Biol *432*, 170-184.

An, H., Ordureau, A., Korner, M., Paulo, J.A., and Harper, J.W. (2020). Systematic quantitative analysis of ribosome inventory during nutrient stress. Nature *583*, 303-309.

An, H., Ordureau, A., Paulo, J.A., Shoemaker, C.J., Denic, V., and Harper, J.W. (2019). TEX264 Is an Endoplasmic Reticulum-Resident ATG8-Interacting Protein Critical for ER Remodeling during Nutrient Stress. Mol Cell *74*, 891-908 e810.

Archer, S.K., Shirokikh, N.E., Beilharz, T.H., and Preiss, T. (2016). Dynamics of ribosome scanning and recycling revealed by translation complex profiling. Nature *535*, 570-574.

Balch, W.E., Morimoto, R.I., Dillin, A., and Kelly, J.W. (2008). Adapting Proteostasis for Disease Intervention. Science *319*, 916.

Barbosa, C., Peixeiro, I., and Romão, L. (2013). Gene expression regulation by upstream open reading frames and human disease. PLoS Genet *9*, e1003529.

Becker, T., Franckenberg, S., Wickles, S., Shoemaker, C.J., Anger, A.M., Armache, J.-P., Sieber, H., Ungewickell, C., Berninghausen, O., Daberkow, I., Karcher, A., Thomm, M., Hopfner, K.-P., Green, R., and Beckmann, R. (2012). Structural basis of highly conserved ribosome recycling in eukaryotes and archaea. Nature *482*, 501-506.

Ben-Shem, A., Garreau de Loubresse, N., Melnikov, S., Jenner, L., Yusupova, G., and Yusupov, M. (2011). The structure of the eukaryotic ribosome at 3.0 Å resolution. Science *334*, 1524-1529.

Bengtson, M.H., and Joazeiro, C.A. (2010). Role of a ribosome-associated E3 ubiquitin ligase in protein quality control. Nature *467*, 470-473.

Bohlen, J., Fenzl, K., Kramer, G., Bukau, B., and Teleman, A.A. (2020a). Selective 40S Footprinting Reveals Cap-Tethered Ribosome Scanning in Human Cells. Molecular Cell *79*, 561-574.e565.

Bohlen, J., Fenzl, K., Kramer, G., Bukau, B., and Teleman, A.A. (2020b). Selective 40S Footprinting Reveals Cap-Tethered Ribosome Scanning in Human Cells. Mol Cell *79*, 561-574 e565.

Bond, S., Lopez-Lloreda, C., Gannon, P.J., Akay-Espinoza, C., and Jordan-Sciutto, K.L. (2020). The Integrated Stress Response and Phosphorylated Eukaryotic Initiation Factor 2α in Neurodegeneration. Journal of Neuropathology & Experimental Neurology *79*, 123-143.

Brandman, O., and Hegde, R.S. (2016). Ribosome-associated protein quality control. Nat Struct Mol Biol *23*, 7-15.

Brandman, O., Stewart-Ornstein, J., Wong, D., Larson, A., Williams, C.C., Li, G.W., Zhou, S., King, D., Shen, P.S., Weibezahn, J., Dunn, J.G., Rouskin, S., Inada, T., Frost, A., and Weissman, J.S. (2012). A ribosome-bound quality control complex triggers degradation of nascent peptides and signals translation stress. Cell *151*, 1042-1054.

Calviello, L., Venkataramanan, S., Rogowski, K.J., Wyler, E., Wilkins, K., Tejura, M., Thai, B., Krol, J., Filipowicz, W., Landthaler, M., and Floor, Stephen N. (2021). DDX3 depletion represses translation of mRNAs with complex 5′ UTRs. Nucleic Acids Research *49*, 5336-5350.

Choe, Y.J., Park, S.H., Hassemer, T., Korner, R., Vincenz-Donnelly, L., Hayer-Hartl, M., and Hartl, F.U. (2016). Failure of RQC machinery causes protein aggregation and proteotoxic stress. Nature *531*, 191-195.

Ciechanover, A. (2015). The unravelling of the ubiquitin system. Nat Rev Mol Cell Biol *16*, 322-324.

Costa-Mattioli, M., and Walter, P. (2020a). The integrated stress response: From mechanism to disease. Science *368*, eaat5314.

Costa-Mattioli, M., and Walter, P. (2020b). The integrated stress response: From mechanism to disease. Science *368*.

D'Orazio, K.N., and Green, R. (2021). Ribosome states signal RNA quality control. Mol Cell *81*, 1372-1383.

D'Orazio, K.N., Wu, C.C., Sinha, N., Loll-Krippleber, R., Brown, G.W., and Green, R. (2019). The endonuclease Cue2 cleaves mRNAs at stalled ribosomes during No Go Decay. Elife *8*.

Defenouillere, Q., Zhang, E., Namane, A., Mouaikel, J., Jacquier, A., and Fromont-Racine, M. (2016). Rqc1 and Ltn1 Prevent C-terminal Alanine-Threonine Tail (CAT-tail)-induced Protein Aggregation by Efficient Recruitment of Cdc48 on Stalled 60S Subunits. J Biol Chem *291*, 12245-12253.

Deshaies, R.J., and Joazeiro, C.A.P. (2009). RING Domain E3 Ubiquitin Ligases. Annual Review of Biochemistry *78*, 399-434.

Douglas, P.M., and Dillin, A. (2010). Protein homeostasis and aging in neurodegeneration. J Cell Biol *190*, 719-729.

Dubnikov, T., Ben-Gedalya, T., and Cohen, E. (2017). Protein Quality Control in Health and Disease. Cold Spring Harb Perspect Biol *9*.

Elia, A.E., Boardman, A.P., Wang, D.C., Huttlin, E.L., Everley, R.A., Dephoure, N., Zhou, C., Koren, I., Gygi, S.P., and Elledge, S.J. (2015). Quantitative Proteomic Atlas of Ubiquitination and Acetylation in the DNA Damage Response. Mol Cell *59*, 867-881.

Faesen, A.C., Luna-Vargas, M.P., Geurink, P.P., Clerici, M., Merkx, R., van Dijk, W.J., Hameed, D.S., El Oualid, F., Ovaa, H., and Sixma, T.K. (2011). The differential modulation of USP activity

by internal regulatory domains, interactors and eight ubiquitin chain types. Chem Biol *18*, 1550-1561.

Fresno, M., Jimenez, A., and Vazquez, D. (1977). Inhibition of translation in eukaryotic systems by harringtonine. European journal of biochemistry *72*, 323-330.

Frolova, L., Le Goff, X., Zhouravleva, G., Davydova, E., Philippe, M., and Kisselev, L. (1996). Eukaryotic polypeptide chain release factor eRF3 is an eRF1- and ribosome-dependent guanosine triphosphatase. RNA (New York, N.Y.) *2*, 334-341.

Garshott, D.M., Sundaramoorthy, E., Leonard, M., and Bennett, E.J. (2020). Distinct regulatory ribosomal ubiquitylation events are reversible and hierarchically organized. Elife *9*.

Garzia, A., Jafarnejad, S.M., Meyer, C., Chapat, C., Gogakos, T., Morozov, P., Amiri, M., Shapiro, M., Molina, H., Tuschl, T., and Sonenberg, N. (2017). The E3 ubiquitin ligase and RNA-binding protein ZNF598 orchestrates ribosome quality control of premature polyadenylated mRNAs. Nat Commun *8*, 16056.

Gestwicki, J.E., and Garza, D. (2012). Protein quality control in neurodegenerative disease. Prog Mol Biol Transl Sci *107*, 327-353.

Gidalevitz, T., Ben-Zvi, A., Ho, K.H., Brignull, H.R., and Morimoto, R.I. (2006). Progressive disruption of cellular protein folding in models of polyglutamine diseases. Science *311*, 1471-1474.

Goldknopf, I.L., and Busch, H. (1977). Isopeptide linkage between nonhistone and histone 2A polypeptides of chromosomal conjugate-protein A24. Proc Natl Acad Sci U S A *74*, 864-868.

Green, R., and Noller, H.F. (1997). RIBOSOMES AND TRANSLATION. Annual Review of Biochemistry *66*, 679-716.

Gregersen, N. (2006). Protein misfolding disorders: pathogenesis and intervention. J Inherit Metab Dis *29*, 456-470.

Gregersen, N., Bross, P., Vang, S., and Christensen, J.H. (2006). Protein misfolding and human disease. Annu Rev Genomics Hum Genet *7*, 103-124.

Guan, B.J., van Hoef, V., Jobava, R., Elroy-Stein, O., Valasek, L.S., Cargnello, M., Gao, X.H., Krokowski, D., Merrick, W.C., Kimball, S.R., Komar, A.A., Koromilas, A.E., Wynshaw-Boris, A., Topisirovic, I., Larsson, O., and Hatzoglou, M. (2017). A Unique ISR Program Determines Cellular Responses to Chronic Stress. Mol Cell *68*, 885-900 e886.

Guydosh, N.R., and Green, R. (2017). Translation of poly(A) tails leads to precise mRNA cleavage. RNA *23*, 749-761.

Heideker, J., and Wertz, I.E. (2015). DUBs, the regulation of cell identity and disease. Biochem J *467*, 191.

Hershko, A., and Ciechanover, A. (1998). THE UBIQUITIN SYSTEM. Annual Review of Biochemistry *67*, 425-479.

Hershko, A., Heller, H., Elias, S., and Ciechanover, A. (1983). Components of ubiquitin-protein ligase system. Resolution, affinity purification, and role in protein breakdown. J Biol Chem *258*, 8206-8214.

Hickey, K.L., Dickson, K., Cogan, J.Z., Replogle, J.M., Schoof, M., D'Orazio, K.N., Sinha, N.K., Hussmann, J.A., Jost, M., Frost, A., Green, R., Weissman, J.S., and Kostova, K.K. (2020). GIGYF2 and 4EHP Inhibit Translation Initiation of Defective Messenger RNAs to Assist Ribosome-Associated Quality Control. Mol Cell *79*, 950-962 e956.

Higgins, R., Gendron, J.M., Rising, L., Mak, R., Webb, K., Kaiser, S.E., Zuzow, N., Riviere, P., Yang, B., Fenech, E., Tang, X., Lindsay, S.A., Christianson, J.C., Hampton, R.Y., Wasserman, S.A., and Bennett, E.J. (2015). The Unfolded Protein Response Triggers Site-Specific Regulatory Ubiquitylation of 40S Ribosomal Proteins. Mol Cell *59*, 35-49.

Hinnebusch, A.G. (2011). Molecular mechanism of scanning and start codon selection in eukaryotes. Microbiol Mol Biol Rev *75*, 434-467.

Hinnebusch, A.G. (2014). The scanning mechanism of eukaryotic translation initiation. Annu Rev Biochem *83*, 779-812.

Hinnebusch, A.G., Ivanov, I.P., and Sonenberg, N. (2016). Translational control by 5'-untranslated regions of eukaryotic mRNAs. Science *352*, 1413-1416.

Hoshikawa, S., Ogata, T., Fujiwara, S., Nakamura, K., and Tanaka, S. (2008). A novel function of RING finger protein 10 in transcriptional regulation of the myelin-associated glycoprotein gene and myelin formation in Schwann cells. PLoS One *3*, e3464.

Ikeuchi, K., Izawa, T., and Inada, T. (2018). Recent Progress on the Molecular Mechanism of Quality Controls Induced by Ribosome Stalling. Front Genet *9*, 743.

Ikeuchi, K., Tesina, P., Matsuo, Y., Sugiyama, T., Cheng, J., Saeki, Y., Tanaka, K., Becker, T., Beckmann, R., and Inada, T. (2019). Collided ribosomes form a unique structural interface to induce Hel2-driven quality control pathways. EMBO J *38*.

Inada, T. (2020). Quality controls induced by aberrant translation. Nucleic Acids Res.

Itzhak, D.N., Tyanova, S., Cox, J., and Borner, G.H. (2016). Global, quantitative and dynamic mapping of protein subcellular localization. Elife *5*.

Ivanov, I.P., Shin, B.S., Loughran, G., Tzani, I., Young-Baird, S.K., Cao, C., Atkins, J.F., and Dever, T.E. (2018). Polyamine Control of Translation Elongation Regulates Start Site Selection on Antizyme Inhibitor mRNA via Ribosome Queuing. Mol Cell *70*, 254-264 e256.

Iwasaki, S., Floor, S.N., and Ingolia, N.T. (2016a). Rocaglates convert DEAD-box protein eIF4A into a sequence-selective translational repressor. Nature *534*, 558-561.

Iwasaki, S., Floor, S.N., and Ingolia, N.T. (2016b). Rocaglates convert DEAD-box protein eIF4A into a sequence-selective translational repressor. Nature *534*, 558-561.

Iwasaki, S., Iwasaki, W., Takahashi, M., Sakamoto, A., Watanabe, C., Shichino, Y., Floor, S.N., Fujiwara, K., Mito, M., Dodo, K., Sodeoka, M., Imataka, H., Honma, T., Fukuzawa, K., Ito, T.,

and Ingolia, N.T. (2019). The Translation Inhibitor Rocaglamide Targets a Bimolecular Cavity between eIF4A and Polypurine RNA. Molecular Cell *73*, 738-748.e739.

Joazeiro, C.A.P. (2017). Ribosomal Stalling During Translation: Providing Substrates for Ribosome-Associated Protein Quality Control. Annu Rev Cell Dev Biol *33*, 343-368.

Joazeiro, C.A.P. (2019). Mechanisms and functions of ribosome-associated protein quality control. Nat Rev Mol Cell Biol *20*, 368-383.

Jung, Y., Kim, H.D., Yang, H.W., Kim, H.J., Jang, C.Y., and Kim, J. (2017). Modulating cellular balance of Rps3 mono-ubiquitination by both Hel2 E3 ligase and Ubp3 deubiquitinase regulates protein quality control. Exp Mol Med *49*, e390.

Juszkiewicz, S., Chandrasekaran, V., Lin, Z., Kraatz, S., Ramakrishnan, V., and Hegde, R.S. (2018a). ZNF598 Is a Quality Control Sensor of Collided Ribosomes. Mol Cell.

Juszkiewicz, S., Chandrasekaran, V., Lin, Z., Kraatz, S., Ramakrishnan, V., and Hegde, R.S. (2018b). ZNF598 Is a Quality Control Sensor of Collided Ribosomes. Mol Cell *72*, 469-481 e467.

Juszkiewicz, S., and Hegde, R.S. (2017). Initiation of Quality Control during Poly(A) Translation Requires Site-Specific Ribosome Ubiquitination. Mol Cell *65*, 743-750 e744.

Juszkiewicz, S., Slodkowicz, G., Lin, Z., Freire-Pritchett, P., Peak-Chew, S.Y., and Hegde, R.S. (2020a). Ribosome collisions trigger cis-acting feedback inhibition of translation initiation. Elife *9*.

Juszkiewicz, S., Speldewinde, S.H., Wan, L., Svejstrup, J.Q., and Hegde, R.S. (2020b). The ASC-1 Complex Disassembles Collided Ribosomes. Molecular Cell *79*, 603-614.e608.

Kaiser, S.E., Riley, B.E., Shaler, T.A., Trevino, R.S., Becker, C.H., Schulman, H., and Kopito, R.R. (2011). Protein standard absolute quantification (PSAQ) method for the measurement of cellular ubiquitin pools. Nature Methods *8*, 691-696.

Kapp, L.D., and Lorsch, J.R. (2004). The molecular mechanics of eukaryotic translation. Annu Rev Biochem *73*, 657-704.

Kashiwagi, K., Yokoyama, T., Nishimoto, M., Takahashi, M., Sakamoto, A., Yonemochi, M., Shirouzu, M., and Ito, T. (2019). Structural basis for eIF2B inhibition in integrated stress response. Science *364*, 495.

Kearse, M.G., Goldman, D.H., Choi, J., Nwaezeapu, C., Liang, D., Green, K.M., Goldstrohm, A.C., Todd, P.K., Green, R., and Wilusz, J.E. (2019). Ribosome queuing enables non-AUG translation to be resistant to multiple protein synthesis inhibitors. Genes Dev *33*, 871-885.

Kenner, L.R., Anand, A.A., Nguyen, H.C., Myasnikov, A.G., Klose, C.J., McGeever, L.A., Tsai, J.C., Miller-Vedam, L.E., Walter, P., and Frost, A. (2019). eIF2B-catalyzed nucleotide exchange and phosphoregulation by the integrated stress response. Science *364*, 491.

Kim, W., Bennett, E.J., Huttlin, E.L., Guo, A., Li, J., Possemato, A., Sowa, M.E., Rad, R., Rush, J., Comb, M.J., Harper, J.W., and Gygi, S.P. (2011). Systematic and quantitative assessment of the ubiquitin-modified proteome. Mol Cell *44*, 325-340.

Komander, D. (2010). Mechanism, specificity and structure of the deubiquitinases. Subcell Biochem *54*, 69-87.

Komander, D., Clague, M.J., and Urbe, S. (2009). Breaking the chains: structure and function of the deubiquitinases. Nat Rev Mol Cell Biol *10*, 550-563.

Komander, D., and Rape, M. (2012). The ubiquitin code. Annu Rev Biochem *81*, 203-229.

Kraft, C., Deplazes, A., Sohrmann, M., and Peter, M. (2008). Mature ribosomes are selectively degraded upon starvation by an autophagy pathway requiring the Ubp3p/Bre5p ubiquitin protease. Nat Cell Biol *10*, 602-610.

Lee, J.H., Pestova, T.V., Shin, B.-S., Cao, C., Choi, S.K., and Dever, T.E. (2002). Initiation factor eIF5B catalyzes second GTP-dependent step in eukaryotic translation initiation. Proceedings of the National Academy of Sciences *99*, 16689.

Lee, J.W., Beebe, K., Nangle, L.A., Jang, J., Longo-Guess, C.M., Cook, S.A., Davisson, M.T., Sundberg, J.P., Schimmel, P., and Ackerman, S.L. (2006). Editing-defective tRNA synthetase causes protein misfolding and neurodegeneration. Nature *443*, 50-55.

Lee, S., Liu, B., Lee, S., Huang, S.X., Shen, B., and Qian, S.B. (2012). Global mapping of translation initiation sites in mammalian cells at single-nucleotide resolution. Proc Natl Acad Sci U S A *109*, E2424-2432.

Low, W.K., Dang, Y., Schneider-Poetsch, T., Shi, Z., Choi, N.S., Merrick, W.C., Romo, D., and Liu, J.O. (2005). Inhibition of eukaryotic translation initiation by the marine natural product pateamine A. Mol Cell *20*, 709-722.

Lykke-Andersen, J., and Bennett, E.J. (2014). Protecting the proteome: Eukaryotic cotranslational quality control pathways. J Cell Biol *204*, 467-476.

Lyumkis, D., Oliveira dos Passos, D., Tahara, E.B., Webb, K., Bennett, E.J., Vinterbo, S., Potter, C.S., Carragher, B., and Joazeiro, C.A. (2014). Structural basis for translational surveillance by the large ribosomal subunit-associated protein quality control complex. Proc Natl Acad Sci U S A *111*, 15981-15986.

Manjunath, H., Zhang, H., Rehfeld, F., Han, J., Chang, T.-C., and Mendell, J.T. (2019). Suppression of Ribosomal Pausing by eIF5A Is Necessary to Maintain the Fidelity of Start Codon Selection. Cell Reports *29*, 3134-3146.e3136.

Markmiller, S., Fulzele, A., Higgins, R., Leonard, M., Yeo, G.W., and Bennett, E.J. (2019). Active Protein Neddylation or Ubiquitylation Is Dispensable for Stress Granule Dynamics. Cell Rep *27*, 1356-1363 e1353.

Matsuo, Y., Ikeuchi, K., Saeki, Y., Iwasaki, S., Schmidt, C., Udagawa, T., Sato, F., Tsuchiya, H., Becker, T., Tanaka, K., Ingolia, N.T., Beckmann, R., and Inada, T. (2017). Ubiquitination of stalled ribosome triggers ribosome-associated quality control. Nat Commun *8*, 159.

Matsuo, Y., Tesina, P., Nakajima, S., Mizuno, M., Endo, A., Buschauer, R., Cheng, J., Shounai, O., Ikeuchi, K., Saeki, Y., Becker, T., Beckmann, R., and Inada, T. (2020). RQT complex dissociates ribosomes collided on endogenous RQC substrate SDD1. Nature Structural & Molecular Biology *27*, 323-332.

Mevissen, T.E., Hospenthal, M.K., Geurink, P.P., Elliott, P.R., Akutsu, M., Arnaudo, N., Ekkebus, R., Kulathu, Y., Wauer, T., El Oualid, F., Freund, S.M., Ovaa, H., and Komander, D. (2013). OTU deubiquitinases reveal mechanisms of linkage specificity and enable ubiquitin chain restriction analysis. Cell *154*, 169-184.

Meydan, S., and Guydosh, N.R. (2020). A cellular handbook for collided ribosomes: surveillance pathways and collision types. Current genetics.

Meyer, C., Garzia, A., Morozov, P., Molina, H., and Tuschl, T. (2020). The G3BP1-Family-USP10 Deubiquitinase Complex Rescues Ubiquitinated 40S Subunits of Ribosomes Stalled in Translation from Lysosomal Degradation. Mol Cell *77*, 1193-1205 e1195.

Montellese, C., van den Heuvel, J., Ashiono, C., Dorner, K., Melnik, A., Jonas, S., Zemp, I., Picotti, P., Gillet, L.C., and Kutay, U. (2020). USP16 counteracts mono-ubiquitination of RPS27a and promotes maturation of the 40S ribosomal subunit. Elife *9*.

Mueller, P.P., and Hinnebusch, A.G. (1986). Multiple upstream AUG codons mediate translational control of GCN4. Cell *45*, 201-207.

Nakayama, K.I., and Nakayama, K. (2006). Ubiquitin ligases: cell-cycle control and cancer. Nature Reviews Cancer *6*, 369-381.

Nguyen, A.T., Prado, M.A., Schmidt, P.J., Sendamarai, A.K., Wilson-Grady, J.T., Min, M., Campagna, D.R., Tian, G., Shi, Y., Dederer, V., Kawan, M., Kuehnle, N., Paulo, J.A., Yao, Y., Weiss, M.J., Justice, M.J., Gygi, S.P., Fleming, M.D., and Finley, D. (2017). UBE2O remodels the proteome during terminal erythroid differentiation. Science *357*.

Nielsen, P.J., McMaster, G.K., and Trachsel, H. (1985). Cloning of eukaryotic protein synthesis initiation factor genes: isolation and characterization of cDNA clones encoding factor eIF-4A. Nucleic Acids Research *13*, 6867-6880.

Nusinow, D.P., Szpyt, J., Ghandi, M., Rose, C.M., McDonald, E.R., 3rd, Kalocsay, M., Jane-Valbuena, J., Gelfand, E., Schweppe, D.K., Jedrychowski, M., Golji, J., Porter, D.A., Rejtar, T., Wang, Y.K., Kryukov, G.V., Stegmeier, F., Erickson, B.K., Garraway, L.A., Sellers, W.R., and Gygi, S.P. (2020). Quantitative Proteomics of the Cancer Cell Line Encyclopedia. Cell *180*, 387-402 e316.

Ogle, J.M., Brodersen, D.E., Clemons, W.M., Tarry, M.J., Carter, A.P., and Ramakrishnan, V. (2001). Recognition of Cognate Transfer RNA by the 30S Ribosomal Subunit. Science *292*, 897.

Pakos-Zebrucka, K., Koryga, I., Mnich, K., Ljujic, M., Samali, A., and Gorman, A.M. (2016a). The integrated stress response. EMBO Rep *17*, 1374-1395.

Pakos-Zebrucka, K., Koryga, I., Mnich, K., Ljujic, M., Samali, A., and Gorman, A.M. (2016b). The integrated stress response. EMBO reports *17*, 1374-1395.

Parsyan, A., Shahbazian, D., Martineau, Y., Petroulakis, E., Alain, T., Larsson, O., Mathonnet, G., Tettweiler, G., Hellen, C.U., Pestova, T.V., Svitkin, Y.V., and Sonenberg, N. (2009). The helicase protein DHX29 promotes translation initiation, cell proliferation, and tumorigenesis. Proceedings of the National Academy of Sciences *106*, 22217.

Passmore, L.A., Schmeing, T.M., Maag, D., Applefield, D.J., Acker, M.G., Algire, Mikkel A., Lorsch, J.R., and Ramakrishnan, V. (2007). The Eukaryotic Translation Initiation Factors eIF1 and eIF1A Induce an Open Conformation of the 40S Ribosome. Molecular Cell *26*, 41-50.

Pelletier, J., and Sonenberg, N. (2019). The Organizing Principles of Eukaryotic Ribosome Recruitment. Annual Review of Biochemistry *88*, 307-335.

Pestova, T.V., Lomakin, I.B., Lee, J.H., Choi, S.K., Dever, T.E., and Hellen, C.U.T. (2000). The joining of ribosomal subunits in eukaryotes requires eIF5B. Nature *403*, 332-335.

Pickart, C.M. (2004). Back to the Future with Ubiquitin. Cell *116*, 181-190.

Pilla, E., Schneider, K., and Bertolotti, A. (2017). Coping with Protein Quality Control Failure. Annu Rev Cell Dev Biol *33*, 439-465.

Pisarev, A.V., Hellen, C.U.T., and Pestova, T.V. (2007). Recycling of Eukaryotic Posttermination Ribosomal Complexes. Cell *131*, 286-299.

Pisareva, V.P., Pisarev, A.V., Komar, A.A., Hellen, C.U.T., and Pestova, T.V. (2008). Translation Initiation on Mammalian mRNAs with Structured 5′UTRs Requires DExH-Box Protein DHX29. Cell *135*, 1237-1250.

Pontén, F., Jirström, K., and Uhlen, M. (2008). The Human Protein Atlas--a tool for pathology. J Pathol *216*, 387-393.

Saito, K., Horikawa, W., and Ito, K. (2015). Inhibiting K63 polyubiquitination abolishes no-go type stalled translation surveillance in Saccharomyces cerevisiae. PLoS Genet *11*, e1005197.

Scheffner, M., Nuber, U., and Huibregtse, J.M. (1995). Protein ubiquitination involving an E1-E2-E3 enzyme ubiquitin thioester cascade. Nature *373*, 81-83.

Schneider-Poetsch, T., Ju, J., Eyler, D.E., Dang, Y., Bhat, S., Merrick, W.C., Green, R., Shen, B., and Liu, J.O. (2010). Inhibition of eukaryotic translation elongation by cycloheximide and lactimidomycin. Nature chemical biology *6*, 209-217.

Schuller, A.P., and Green, R. (2018). Roadblocks and resolutions in eukaryotic translation. Nat Rev Mol Cell Biol.

Shao, S., and Hegde, R.S. (2014). Reconstitution of a minimal ribosome-associated ubiquitination pathway with purified factors. Mol Cell *55*, 880-890.

Shao, S., von der Malsburg, K., and Hegde, R.S. (2013). Listerin-dependent nascent protein ubiquitination relies on ribosome subunit dissociation. Mol Cell *50*, 637-648.

Shirokikh, N.E., Archer, S.K., Beilharz, T.H., Powell, D., and Preiss, T. (2017). Translation complex profile sequencing to study the in vivo dynamics of mRNA–ribosome interactions during translation initiation, elongation and termination. Nature Protocols *12*, 697-731.

Shirokikh, N.E., Dutikova, Y.S., Staroverova, M.A., Hannan, R.D., and Preiss, T. (2019). Migration of Small Ribosomal Subunits on the 5' Untranslated Regions of Capped Messenger RNA. Int J Mol Sci *20*.

Shoemaker, C.J., Eyler, D.E., and Green, R. (2010). Dom34:Hbs1 promotes subunit dissociation and peptidyl-tRNA drop-off to initiate no-go decay. Science *330*, 369-372.

Shoemaker, C.J., and Green, R. (2011). Kinetic analysis reveals the ordered coupling of translation termination and ribosome recycling in yeast. Proceedings of the National Academy of Sciences *108*, E1392.

Shoemaker, C.J., and Green, R. (2012). Translation drives mRNA quality control. Nature Structural & Molecular Biology *19*, 594-601.

Silva, G.M., Finley, D., and Vogel, C. (2015). K63 polyubiquitination is a new modulator of the oxidative stress response. Nat Struct Mol Biol *22*, 116-123.

Simms, C.L., Yan, L.L., and Zaher, H.S. (2017). Ribosome Collision Is Critical for Quality Control during No-Go Decay. Mol Cell *68*, 361-373 e365.

Sinha, N.K., Ordureau, A., Best, K., Saba, J.A., Zinshteyn, B., Sundaramoorthy, E., Fulzele, A., Garshott, D.M., Denk, T., Thoms, M., Paulo, J.A., Harper, J.W., Bennett, E.J., Beckmann, R., and Green, R. (2020). EDF1 coordinates cellular responses to ribosome collisions. Elife *9*.

Sogorin, E.A., Shirokikh, N.E., Ibragimova, A.M., Vasiliev, V.D., Agalarov, S., and Spirin, A.S. (2012). Leader sequences of eukaryotic mRNA can be simultaneously bound to initiating 80S ribosome and 40S ribosomal subunit. Biochemistry (Mosc) *77*, 342-345.

Sontag, E.M., Samant, R.S., and Frydman, J. (2017). Mechanisms and Functions of Spatial Protein Quality Control. Annu Rev Biochem *86*, 97-122.

Soto-Rifo, R., Rubilar, P.S., Limousin, T., de Breyne, S., Décimo, D., and Ohlmann, T. (2012). DEAD-box protein DDX3 associates with eIF4F to promote translation of selected mRNAs. The EMBO Journal *31*, 3745-3756.

Sugiyama, T., Li, S., Kato, M., Ikeuchi, K., Ichimura, A., Matsuo, Y., and Inada, T. (2019). Sequential Ubiquitination of Ribosomal Protein uS3 Triggers the Degradation of Non-functional 18S rRNA. Cell Rep *26*, 3400-3415 e3407.

Sundaramoorthy, E., Leonard, M., Mak, R., Liao, J., Fulzele, A., and Bennett, E.J. (2017). ZNF598 and RACK1 Regulate Mammalian Ribosome-Associated Quality Control Function by Mediating Regulatory 40S Ribosomal Ubiquitylation. Mol Cell *65*, 751-760 e754.

Sung, M.K., Porras-Yakushi, T.R., Reitsma, J.M., Huber, F.M., Sweredoski, M.J., Hoelz, A., Hess, S., and Deshaies, R.J. (2016). A conserved quality-control pathway that mediates degradation of unassembled ribosomal proteins. Elife *5*.

Taylor, R.C., Berendzen, K.M., and Dillin, A. (2014). Systemic stress signalling: understanding the cell non-autonomous control of proteostasis. Nature Reviews Molecular Cell Biology *15*, 211-217.

Taylor, R.C., and Dillin, A. (2011). Aging as an event of proteostasis collapse. Cold Spring Harb Perspect Biol *3*.

Thrun, A., Garzia, A., Kigoshi-Tansho, Y., Patil, P.R., Umbaugh, C.S., Dallinger, T., Liu, J., Kreger, S., Patrizi, A., Cox, G.A., Tuschl, T., and Joazeiro, C.A.P. (2021). Convergence of mammalian RQC and C-end rule proteolytic pathways via alanine tailing. Mol Cell *81*, 2112-2122 e2117.

Varshavsky, A. (2005). Regulated protein degradation. Trends in biochemical sciences *30*, 283-286.

Vendruscolo, M. (2012). Proteome folding and aggregation. Curr Opin Struct Biol *22*, 138-143.

Verma, R., Oania, R.S., Kolawa, N.J., and Deshaies, R.J. (2013). Cdc48/p97 promotes degradation of aberrant nascent polypeptides bound to the ribosome. Elife *2*, e00308.

Vind, A.C., Genzor, A.V., and Bekker-Jensen, S. (2020). Ribosomal stress-surveillance: three pathways is a magic number. Nucleic Acids Res *48*, 10648-10661.

Wagner, S., Herrmannova, A., Hronova, V., Gunisova, S., Sen, N.D., Hannan, R.D., Hinnebusch, A.G., Shirokikh, N.E., Preiss, T., and Valasek, L.S. (2020a). Selective Translation Complex Profiling Reveals Staged Initiation and Co-translational Assembly of Initiation Factor Complexes. Mol Cell *79*, 546-560 e547.

Wagner, S., Herrmannová, A., Hronová, V., Gunišová, S., Sen, N.D., Hannan, R.D., Hinnebusch, A.G., Shirokikh, N.E., Preiss, T., and Valášek, L.S. (2020b). Selective Translation Complex Profiling Reveals Staged Initiation and Co-translational Assembly of Initiation Factor Complexes. Mol Cell *79*, 546-560.e547.

Wang, J., Johnson, A.G., Lapointe, C.P., Choi, J., Prabhakar, A., Chen, D.-H., Petrov, A.N., and Puglisi, J.D. (2019). eIF5B gates the transition from translation initiation to elongation. Nature *573*, 605-608.

Wang, M., Herrmann, C.J., Simonovic, M., Szklarczyk, D., and von Mering, C. (2015). Version 4.0 of PaxDb: Protein abundance data, integrated across model organisms, tissues, and cell-lines. Proteomics *15*, 3163-3168.

Wethmar, K., Smink, J.J., and Leutz, A. (2010). Upstream open reading frames: molecular switches in (patho)physiology. Bioessays *32*, 885-893.

Wittmann, J., Hol, E.M., and Jäck, H.-M. (2006). hUPF2 Silencing Identifies Physiologic Substrates of Mammalian Nonsense-Mediated mRNA Decay. Molecular and Cellular Biology *26*, 1272-1287.

Yanagitani, K., Juszkiewicz, S., and Hegde, R.S. (2017). UBE2O is a quality control factor for orphans of multiprotein complexes. Science *357*, 472-475.

Ye, Y., and Rape, M. (2009). Building ubiquitin chains: E2 enzymes at work. Nat Rev Mol Cell Biol *10*, 755-764.

Yewdell, J.W. (2001). Not such a dismal science: the economics of protein synthesis, folding, degradation and antigen processing. Trends in Cell Biology *11*, 294-297.

Yip, M.C.J., and Shao, S. (2021). Detecting and Rescuing Stalled Ribosomes. Trends in biochemical sciences.

Yonashiro, R., Tahara, E.B., Bengtson, M.H., Khokhrina, M., Lorenz, H., Chen, K.C., Kigoshi-Tansho, Y., Savas, J.N., Yates, J.R., Kay, S.A., Craig, E.A., Mogk, A., Bukau, B., and Joazeiro, C.A. (2016). The Rqc2/Tae2 subunit of the ribosome-associated quality control (RQC) complex marks ribosome-stalled nascent polypeptide chains for aggregation. Elife *5*, e11794.

Zheng, N., and Shabek, N. (2017). Ubiquitin Ligases: Structure, Function, and Regulation. Annual Review of Biochemistry *86*, 129-157.